A Study On The Use Of Neuber's Rule In Fatigue Crack Initiation Predictions

by

SANJEEV K. VISVANATHA, B.Eng.

A thesis submitted to

the Faculty of Graduate Studies and Research

in partial fulfillment of

the requirements for the degree of

Master of Engineering in Aerospace Engineering

Department of Mechanical and Aerospace Engineering

The Ottawa-Carleton Institute for Mechanical and Aerospace Engineering

Carleton University

Ottawa, Ontario, Canada

September 1998

National Library
of Canada

Acquisitions and
Bibliographic Services

395 Wellington Street
Ottawa ON K1A 0N4
Canada

Bibliothèque nationale
du Canada

Acquisitions et
services bibliographiques

395, rue Wellington
Ottawa ON K1A 0N4
Canada

Your file Votre référence

Our file Notre référence

0-612-36898-X

Canada

Abstract

The local strain approach to fatigue life prediction contains a number of assumptions which can lead to considerable error in the prediction of crack initiation life. One assumption is the use of an approximate relationship known as Neuber's rule to estimate the stress and strain at the notch root of a component. The applicability of Neuber's rule in the local strain method was examined for two coupon geometries through a finite element analysis. In addition, the ability of the local strain method to predict the lives of the coupons subjected to spectrum loading was assessed by comparing local strain predictions for the two coupons with results from a coupon test program. The findings of this study verified the applicability of Neuber's rule in plane stress situations. A method of estimating multiaxial elastic-plastic notch stresses and strains was verified to be an effective means of accounting for notch root multiaxiality. A method of estimating total life, composed of crack initiation and crack propagation, was proposed which accounts for the notch size effect displayed in sharply notched coupons.

Acknowledgements

A mentor once told me that choosing a graduate school is similar to choosing real estate, where the three most important criteria are "Location, Location, Location". He went on to say that it was the supervisor alone who would either "make or break" the two-year experience, leading to the parallel rule for graduate school: "Supervisor, Supervisor, Supervisor". My two supervisors, Professor Paul V. Straznicky and Dr. Roy L. Hewitt, confirmed this rule and were instrumental in making my graduate degree an experience to remember! Their sage advice inspired me to find, and in many cases, construct the roads which led to here.

Several others were extremely helpful throughout the duration of this thesis. Thanks go to Mr. Jan Weiss for always taking the time out of his busy schedule to discuss the finer points of C_CI89, Ms. Pascale Affre for her assistance in the experimental program, and Mr. Luc Lafleur for coaching me on the use of the MTS rig.

Sincere gratitude is expressed to The Natural Sciences and Engineering Research Council (NSERC) for the award of a Post Graduate Scholarship, The Canadian Space Agency for the award of a supplement to the NSERC scholarship, Carleton University for the award

of a teaching and research assistantship, and to the Institute for Aerospace Research at the National Research Council of Canada for the generous use of their facilities.

Thanks go to my friends for the stimulating discussions and meaningless jokes which helped to keep insanity at bay through the years. Cheers!

Finally, gratitude is expressed to my parents, my siblings and their families. You have been supportive throughout my academic career. Thank you.

Table of Contents

List of Tables

List of Figures

List of Appendices

Nomenclature

CIL	Crack Initiation Life
D	Damage sum
D_i	Increment of damage
DLS	Design Limit Stress
E, E_σ	Elastic modulus, Secant modulus
EP1, EP2, EP3	Principal strains, ABAQUS naming system
F	Dimensionless function of geometry (Equation 8-1)
K'	Cyclic hardening coefficient (Equation 2-4)
K_f	Fatigue concentration factor
K_t	Theoretical stress concentration factor
K_{tq}	Equivalent stress concentration factor (Equation 7-3)
K_ε	Local strain concentration
K_σ	Local stress concentration
N, N_f	Cycles to failure of smooth specimen
$N_{f,i}$	Number of cycles to failure at load level *i* (Equation 2-1)
N_i	Number of load excursions at load level *i* (Equation 2-1)
N_A	Test result for sequence A (Equation 2-2)
N_B	Improved prediction for sequence B (Equation 2-2)

$N_{pred.\ A}$, $N_{pred.B}$	Predicted lives for sequences A and B (Equation 2-2)
R_ε	Strain ratio
R_σ	Stress ratio
S	Net-section nominal stress
SP1, SP2, SP3	Principal stresses, ABAQUS naming system
S_e	Fatigue strength
Z_d	Damage parameter (Equation 2-13)
a	Petersons's material constant (Equation 2-23)
a_e, b_e	Elastic stress ratios (Equations 7-1 and 7-2)
b	Fatigue strength exponent (Equation 2-9)
c	Fatigue ductility exponent (Equation 2-9)
c	Notch depth (Equation 8-1)
e	Net section nominal strain
l'	Size of crack at initiation (Equation 8-1)
n	Number of load levels (Equation 2-1)
n'	Cyclic hardening exponent (Equation 2-4)
r	Notch radius
x,y,z	Coordinate directions
α	Principal strain ratio
$d\varepsilon^p_i$	Principal plastic strain increment, i = 1,2,3 (Equation 2-19)
$d\varepsilon^p_q$	Equivalent plastic strain increment (Equation 2-19)
ε	Notch root strain

ε'_f	Fatigue ductility coefficient (Equation 2-9)
$\varepsilon_1, \varepsilon_2, \varepsilon_3$	Principal strains
ε^p_i	Principal plastic strains, i =1,2,3 (Equation 2-20)
ε^p_q	Equivalent plastic strains, i =1,2,3 (Equation 2-20)
ν, ν'	Poisson's ratio and modified Poisson's ratio (Equation 7-7)
σ	Notch root stress
$\sigma_{e1}, \sigma_{e2}, \sigma_{e3}$	Principal elastic stresses
σ'_i	Deviatoric stress, i = 1,2,3 (Equation 2-19)
σ'_f	Fatigue strength coefficient (Equation 2-9)
$\sigma_1, \sigma_2, \sigma_3$	Principal stresses
$[p\mathbf{I}]$	Hydrostatic stress tensor
$[\sigma]$	Stress tensor
$[\sigma']$	Deviatoric stress tensor

Prefixes:

Δ	range

Subscripts:

U	ultimate
Y	yield
eff	effective
eq, q	equivalent

max	maximum or peak
o	mean
pl	plastic

Superscripts:

(notched)	notched specimen
(smooth)	smooth specimen

Units

In keeping with the practices of the North American aerospace industry and the Institute for Aerospace Research (IAR) at the National Research Council of Canada (NRC), the British Imperial system of units is employed in this thesis. Système International d'Unités (SI) equivalents are provided in brackets within the text where practical. The following conversion factors are useful:

1 inch = 25.4 mm

1 lbf = 4.4482 N

1 ksi = 6.8948 MPa

1 kip = 1000 lbf

Chapter 1 - Introduction

Metal fatigue is a process which causes the failure of an engineering component subjected to repeated loading. Typical engineering structures are complex, and are subjected to irregular load histories. This, added with the complex nature of the fatigue process, makes it difficult to accurately predict the life of a structure. Nevertheless, fatigue analysis methods have been developed over the years to aid the design engineer. Today, fatigue life prediction is a fundamental undertaking in the design of many components and structures used in the automotive, aerospace and offshore industries.

Fatigue is a primary mode of failure for airframes. In general, fatigue cracks initiate within the airframe at points of stress concentration which can occur due to a material flaw, or a geometric feature such as a cutout or a rivet hole. Unless detected by an inspection program, these cracks may progress through the structure until failure occurs. Thus, for convenience, the fatigue process is often divided into two phases: crack initiation and crack propagation.

Fatigue life prediction methods in use today are based on the Nominal Stress (NS), Local Strain (LS), and Fracture Mechanics approaches. The NS approach uses constant amplitude stress-life curves to calculate the fatigue damage based on the nominal stress in

the component. A total life (initiation + propagation) prediction results from the use of the NS approach. The LS approach differs from the NS approach in that the stress and strain state at the notch is considered. The use of the LS approach results in a prediction of life to crack initiation. Finally, the fracture mechanics approach predicts the growth of a small crack to one which will cause failure of the component. An advantage to using the fracture mechanics approach is that damage is quantified in terms of a visible parameter, the crack length. This is in contrast to the NS and LS approaches where damage is quantified in terms of a numerically calculated damage sum.

The local strain approach is typically used in situations where life is defined as the onset of detectable flaws. One example is in the design of the CF-18 aircraft. The local strain approach is also being used in analysis work for the International Follow-On Structural Test Program (Simpson, 1997). IFOSTP, as the project is known, is a full scale fatigue test of the CF-18 airframe being conducted by the Canadian Forces (CF) and the Royal Australian Air Force (RAAF). The aft fuselage and empennage tests are the responsibility of the Australians, while the wing and centre fuselage are Canada's responsibility. The centre fuselage test is currently underway at Bombardier Inc., Canadair Defense Systems Division (BI/CDSD). Preparations are being made for the wing test at the Structures, Materials and Propulsion Laboratory of the Institute for Aerospace Research (SMPL-IAR) at The National Research Council of Canada (NRC).

The full scale test is performed by applying a representative load history to the test article through a system of hydraulic actuators. IFOSTP has adopted a load spectrum, derived from flight test data, which represents 279 flights of combined CF and RAAF usage.

To reduce the testing time, a process known as truncation is adopted whereby small load cycles which do not contribute to fatigue damage are removed from the load spectrum applied to the test article. The SMPL-IAR is currently performing spectrum truncation sensitivity studies to determine the level of truncation to apply to the wing load spectrum. A local strain based computer program, C_CI89 (Klohr, 1990), has been adopted by IFOSTP for use in the spectrum truncation sensitivity tests being conducted at SMPL-IAR. Variants of the C_CI89 program were used in the design of the CF-18, and are currently used by the CF for fleet management purposes.

The local strain method contains a number of assumptions which can cause considerable error in predictions. One assumption is the use of Neuber's rule to estimate the stress and strain at the notch root of a component. Neuber's rule was derived for a specific geometry and loading, but is generally used unconditionally in the LS method. The objective of this thesis is to analyze the applicability of Neuber's rule in the local strain approach.

The layout of the thesis is as follows. Chapter 2 contains a review of research regarding the prediction of fatigue crack initiation, including a review of Neuber's rule and its limitations. Having established the background, Chapter 3 presents the project definition.

Chapters 4 through 7 describe the analyses performed in support of the project definition. A discussion of the results of the study is given in Chapter 8. Conclusions and recommendations for future research are given in Chapter 9.

Chapter 2 - Review of Fatigue Crack Initiation Prediction

2.1 Introduction

This chapter gives an overview of the prediction of fatigue crack initiation. A review of the Nominal Stress method will be given first to make clearer the discussions which follow. The Local Strain method will then be reviewed and areas of concern will be discussed.

2.2 Aspects of Fatigue Crack Initiation

Since the "initiation" of a fatigue crack is not a single physical phenomenon, it must be arbitrarily defined by the user. The definition of fatigue crack initiation therefore varies in the literature. For instance, it is defined as the number of cycles to grow a crack 2-3 mm long in (SAE, 1988). However, most aerospace related literature quote the crack length at initiation equal to 0.01" (0.254 mm), e.g. (Baotong and Xiulin, 1993). The definition of a crack length at initiation is limited by the ability of non destructive inspection (NDI) techniques to reliably find cracks in a structure.

A useful criterion for the assessment of fatigue life prediction concepts is the ratio of "test results/prediction" obtained from a large number of predictions. The perfect prediction method would give a ratio of 1.0 every time. This is not achievable due to the complex nature of the fatigue process and the large number of simplifying assumptions present in fatigue life prediction methods. According to Buch (1980), a prediction concept works sufficiently well if the ratio for all predictions lies within the rage of 0.5 to 2.0.

2.3 Nominal Stress (NS) Approach

The NS approach was the first fatigue life prediction method and is still used even though more complex methods have been developed. Although the NS approach yields a total life (initiation + propagation) estimate, a review of this method will make clearer the discussion of the LS approach which follows.

The basis for the method is the stress-life, or S-N curve. The S-N curve is usually generated by rotating bending tests which are performed for a number of stress ratios to account for mean stress effects. The tests are run until the specimen ruptures. Stress concentrations are taken into account by using S-N curves which are obtained for different values of the theoretical stress concentration factor, K_t.

The Palmgren-Miner Rule (Miner's rule) is used to account for the variability of loading with time. Miner's rule assumes that failure of the component occurs when the damage sum equals unity. The damage sum, D, is defined as the fraction of life used up by a series of damaging load excursions. The rule is expressed as:

$$D = \sum_{i=1}^{n} \frac{N_i}{N_{f,i}} \cong 1.0 \tag{2-1}$$

where n is the number of load levels in the spectrum, i is the current load level, N_i is the number of load excursions at level i, and $N_{f,i}$ is the number of cycles to cause specimen failure at load level i.

If the results of variable amplitude loading tests are available, an improved prediction can be made using the "Relative-Miner" approach (Heuler and Schütz, 1986). The Relative Miner approach suggests that it is not necessary for the damage sum at failure to be unity, but only that the damage sum at failure be the same for spectra which are similar. Consider two spectra labelled "A" and "B". The rule is expressed as:

$$N_B = \frac{N_A}{N_{pred,A}} N_{pred,B} \tag{2-2}$$

where N_A and $N_{pred,A}$ are the test result and prediction for spectrum A, $N_{pred,B}$ is the prediction for spectrum B, and N_B is the improved prediction for spectrum B. The definition of the similarity of the spectra is open to interpretation, but can include similar peak values and global stress ratios.

The NS approach has several weaknesses which led to the development of the local strain and fracture mechanics approaches. The weaknesses outlined by Bannantine *et al.* (1990) are:

1. The NS method is completely empirical in nature and lacks the physical insights into the mechanisms of fatigue demonstrated by other methods.
2. The actual stress-strain response of materials is ignored, thus mean residual stresses resulting from sequential loading effects cannot be modelled. This implies that the NS approach may have problems dealing with spectra which are not "close" to constant amplitude.

Even though the NS approach has serious shortcomings, it is still used since there is a large amount of fatigue data available.

2.4 Local Strain (LS) Approach

2.4.1 Principle of LS Method

The LS approach was developed to overcome some of the problems inherent in the NS approach. The principle behind the LS approach, depicted in Figure 2-1, is that smooth specimens tested under strain-control can simulate the fatigue damage at the notch root of an engineering component. Equivalent fatigue damage is assumed to occur at the notch root and in the smooth specimen when both are subjected to identical stress-strain histories. This is known as the principle of equivalence.

Since the smooth specimens are tested under strain control, the LS approach uses the strain-life or ε-N curve. The LS approach is considered to be an estimation of life to crack initiation since it is assumed that once the equally stressed volume of material in the smooth specimen fails (Figure 2-1), the equally stressed volume in the notched specimen will fail. Therefore, cycles to failure (specimen rupture) of the smooth specimen is considered to be equal to cycles to crack initiation of the notched specimen.

2.4.2 LS Method

The LS approach estimates the fatigue crack initiation life for a notch located in a component subjected to variable amplitude loading. The LS method is composed of four steps:

1. Notch Stress and Strain Calculation
2. Cycle Counting
3. Mean Stress Correction
4. Damage Calculation

The method tracks the notch root stress-strain response to identify damaging events by use of a cycle counting procedure. For each damaging event, the effect of the mean stress is accounted for by an equivalent strain equation. The damage for each event is then calculated from the material strain-life curve. A description of the four steps follows.

Step 1 - Notch Stress-Strain Calculation:

The first step in the LS approach is to establish a relationship between the net section nominal stress range and the local stress-strain ranges at the notch root of a component. This could be accomplished numerically using finite element methods (FEM), or experimentally using strain gauge readings. Both of these approaches are usually dropped in favour of approximate relationships, such as those reviewed by Seeger *et al.* (1977). Due to its simplicity, the most widely used of these relationships is the one proposed by Neuber (1961). Known as Neuber's rule, it states that the geometric mean of the stress and strain concentration factors is equal to the theoretical stress concentration factor. Generally, this is expressed in terms of stress and strain ranges for the case when the stress range remote to the notch is linear elastic. Neuber's rule has the following form:

$$\Delta\sigma\,\Delta\varepsilon \cong \frac{(K_t\,\Delta S)^2}{E} \tag{2-3}$$

where $\Delta\sigma$ and $\Delta\varepsilon$ are the notch root stress and strain ranges respectively, K_t is the theoretical stress concentration factor, ΔS is the net-section nominal stress range, and E is the elastic modulus of the material. Equation 2-3 is solved using the material stress-strain curve to calculate the notch root strain from the applied stress. In fatigue loading, the cyclic stress-strain curve obtained from companion samples or the incremental step test is used to calculate stress and strain amplitudes, whereas the hysteresis curve is used to calculate stress and strain ranges. Massing (1926) proposed that the hysteresis curve is twice the cyclic curve if the tensile and compressive responses of the material are

identical. When the cyclic stress-strain curve from tests is not available, the following Ramberg-Osgood approximation may be used:

$$\Delta\varepsilon = \frac{\Delta\sigma}{E} + \left(\frac{\Delta\sigma}{K'}\right)^{\frac{1}{n'}} \tag{2-4}$$

where $\Delta\sigma$ and $\Delta\varepsilon$ are the notch root stress and strain ranges respectively, K' is the cyclic hardening coefficient, n' is the cyclic hardening exponent, and E is the elastic modulus.

Step 2 - Cycle Counting:

A damaging event is identified by use of a cycle counting procedure. Standard practices for cycle counting in fatigue analysis are detailed in ASTM Standard E 1049-85 (ASTM, 1995). Counting procedures such as the Rainflow method and its derivatives are considered to be superior since they are able to identify the overall largest cycle in the spectrum.

The notch root stress-strain calculation and the cycle counting steps are generally performed simultaneously. The combined procedure for cycle counting and notch stress-strain estimation is best explained using an example problem. The procedure uses Neuber's rule to calculate the notch root stress and strain from the applied load spectrum and the material stress-strain curve. The notch root response is tracked to identify closed hysteresis loops. A derivative of the Rainflow method called Closed Hysteresis Loop Counting will be used.

Combined method for notch root stress-strain calculation and cycle counting:

Figure 2-2 presents a typical spectrum and cyclic stress-strain curve for a component. The application of load A causes the notch root stress-strain response to reach point A in Figure 2-3[A]. The notch root stress and strain are calculated using the cyclic curve and Neuber's rule. The application of loads B and C follow the hysteresis curve until points B and C are reached in Figure 2-3[A]. The stress and strain ranges, AB and BC, are calculated using the hysteresis curve and Neuber's rule. Up to this point, a closed hysteresis loop has not been identified.

The application of load D causes an unloading from C (Figure 2-3[B]). The stress-strain path follows the hysteresis curve from C until B is reached. Point B corresponds to the previous largest valley load. The stress-strain path from B to D is calculated as an extension of the path from A to B. This phenomenon is known as "material memory", and restricts the stress-strain paths from crossing each other. Loop BC is closed, and a cycle of magnitude BC is counted.

The application of load E is shown in Figure 2-3[C]. The stress-strain path follows the hysteresis curve from D until A is reached. Point A corresponds to the previous largest peak load. The stress-strain path from A to E is calculated as an extension of the path from the origin to A. The cyclic curve is used to characterize this portion of the notch stress-strain response. Again, material memory restricts the stress-strain paths from crossing each other. Loop DA is closed, and a cycle of magnitude DA is counted.

Application of load F is computed in the same manner as for load B, and is shown in Figure 2-3[D].

Step 3 - Mean Stress Correction:

The combined procedure described above is used to identify closed hysteresis loops. For each closed hysteresis loop the effect of mean stress is accounted for by adjusting the strain amplitude of the loop so that it represents some "equivalent" strain amplitude at a stress ratio of R_σ=-1. This is accomplished using equivalent strain equations, such as those listed by Forness *et al.* (1989):

- SWT:
$$\left(\frac{\Delta\varepsilon}{2}\right)_{eq} = \sqrt{\frac{\sigma_{max}}{E}\frac{\Delta\varepsilon}{2}} \tag{2-5}$$

- Goodman:
$$\left(\frac{\Delta\varepsilon}{2}\right)_{eq} = \frac{\frac{\Delta\varepsilon}{2}}{\left(1-\frac{\sigma_o}{\sigma_{ul}}\right)} \tag{2-6}$$

- Gerber:
$$\left(\frac{\Delta\varepsilon}{2}\right)_{eq} = \frac{\frac{\Delta\varepsilon}{2}}{\left(1-\left(\frac{\sigma_o}{\sigma_{ul}}\right)^2\right)} \tag{2-7}$$

- Soderberg:
$$\left(\frac{\Delta\varepsilon}{2}\right)_{eq} = \frac{\frac{\Delta\varepsilon}{2}}{\left(1-\frac{\sigma_o}{\sigma_Y}\right)} \tag{2-8}$$

where $\Delta\varepsilon/2$ is the strain amplitude, σ_{max} is the maximum notch root stress, σ_o is the mean stress, σ_Y is the material yield stress, σ_U is the material ultimate stress, and the subscript "eq" denotes the equivalent strain amplitude.

The Smith-Watson-Topper (SWT) equation is commonly used in the LS approach. The formulation of the SWT equation requires that the strain-life curve be modified to represent a curve compatible with the SWT equation (Smith *et al.*, 1970). Instead of plotting strain amplitude versus life, the parameter $\sqrt{\frac{\sigma\,\Delta\varepsilon}{E\;2}}$, is plotted versus life. The original strain-life curve and the SWT compatible curve are identical in the region where the strain amplitude is in the elastic range of the material.

Step 4 - Damage Calculation:

Finally, the number of cycles to failure of the smooth specimen is calculated for each closed hysteresis loop from an experimentally obtained strain-life curve (at R_σ=-1). If the SWT equation is used to correct for mean stress, the SWT compatible strain-life curve is used. When the strain-life curve is not available from experiment, the following Manson-Coffin relation may be used:

$$\frac{\Delta\varepsilon}{2} = \frac{\sigma'_f}{E}\left(2N_f\right)^b + \varepsilon'_f\left(2N_f\right)^c \tag{2-9}$$

where $\Delta\varepsilon/2$ is the strain amplitude, σ_f' is the fatigue strength coefficient, N_f is the number of cycles to failure of the smooth specimen, ε_f' is the fatigue ductility coefficient, b is the fatigue strength exponent, and c is the fatigue ductility exponent.

The damage from each loop (D_i) is calculated as the inverse of the cycles to failure of the smooth specimen ($N_{f,i}$):

$$D_i = \frac{1}{N_{f,i}} \tag{2-10}$$

The total damage (D) for the component is then computed using Miner's linear damage rule:

$$D = \sum_{i=1}^{n} D_i \tag{2-11}$$

Once the entire spectrum is analyzed, the crack initiation life (CIL) of the notched component is calculated as the inverse of the total damage of the component:

$$CIL = \frac{1}{D} \tag{2-12}$$

Heuler and Schütz (1986) identified two areas of concern for the LS method: the damage accumulation and the principle of equivalence. These will be discussed in Sections 2.5 and 2.6, respectively.

2.5 Damage Accumulation

The first area of concern, damage accumulation, arises from predicting the fatigue behaviour in spectrum loading by linear damage accumulation calculated from smooth specimen constant amplitude strain-life data (at R_σ=-1). Some attempts to overcome the damage accumulation problem have involved introducing a modified baseline damage parameter curve. In this approach, the parameter, strain range, is replaced by quantities which are assumed to describe the fatigue damage properties of the material under constant as well as under variable amplitude loading. One such damage parameter, Z_d, is derived from short crack behaviour described on the basis of the cyclic J-integral approach (Heitmann *et al.*, 1983). The damage parameter has the following form:

$$Z_d = 2.9 \cdot \frac{\Delta\sigma_{eff}^{\,2}}{E} + \frac{2.5}{1+n'} \cdot \Delta\sigma \Delta\varepsilon_{pl} \qquad (2\text{-}13)$$

where $\Delta\sigma_{eff}$ is the effective stress range calculated as the difference between the applied stress and the stress required to open the crack, E is the elastic modulus, n' is the strain hardening exponent, $\Delta\sigma$ is the notch root stress range, and $\Delta\varepsilon_{pl}$ is the notch root plastic strain range. This damage parameter includes the effect of mean stress which is modelled on the basis of a crack closure argument.

Another approach to overcoming the damage accumulation problem in spectrum loading has involved the use of prestrained strain-life data. Prestraining refers to initial overloads applied to the smooth specimens used to generate the strain-life curve. The rationale behind the use of prestrained data in spectrum loading is to take into account the influence of large cycles on the following smaller ones (Bergmann *et al.*, 1979). Conle and Topper (1980) demonstrated that the use of non-prestrained data led to non-conservative life predictions in a variable amplitude loading study.

In variable amplitude loading, the peak load in the spectrum is applied once per block, but strain-life data is generated through constant amplitude tests, or in some cases, with initial prestrain. It has been suggested that a periodic overload must be applied to the smooth specimen when generating the strain-life data to reduce the non-conservatism of predictions made using non-prestrain data. Conle and Topper (1980) report that predictions made using periodically overstrained constant amplitude data closely approximate the test results, but are still non-conservative. More recently, DuQuesnay *et al.* (1995) report that the fatigue limit of smooth specimens made from aluminum 2024-T351 is significantly reduced when an overload of yield magnitude is applied periodically.

Finally, nonlinear damage accumulation rules have been proposed for use in place of Miner's rule. Some of the nonlinear damage accumulation rules require new material constants which must be determined from tests. This is a disadvantage when comparing

these models to Miner's rule. Schütz (1979) expressed the opinion that nonlinear damage rules had not reliably shown convincing improvements in prediction accuracy when compared to Miner's rule. However, Bleuzen *et al.* (1994) have recently identified the ONERA LS model with nonlinear damage accumulation to be appropriate for predicting fatigue life under complex loading sequences.

2.6 Principle of Equivalence

2.6.1 Concerns

The second area of concern in the LS approach is the assumed equivalence between the smooth specimen and the notched member. Concerns with the principle of equivalence include:

- Determination of stress and strain at the notch of a component: The stress and strain at the notch must be known in order to calculate the fatigue damage of a notched component from smooth specimen test data. This presents a problem since only the elastic solution is known exactly, and approximate relationships such as Neuber's rule must be used in the plastic regime.

- Effect of notch severity on fatigue life: Experimental observations have shown that stress concentrations in notched members have less effect in fatigue than is predicted by the stress concentration factor K_t. This effect is dependent on material and the geometry of the notch.

Differences between test results and predictions can be as large as an order of magnitude due to limitations in the principle of equivalence. The two concerns with the principle of equivalence will be discussed in Sections 2.6.2 and 2.6.3.

2.6.2 Notch Stress-Strain Estimation

The comparison of the fatigue damage at the notch of a component and in the smooth specimen used to generate the test data requires an estimation of the stress and strain at the notch. If the loading is fully elastic, then the exact solution can be found using Hooke's law and the stress concentration factor K_t. When there is yielding at the notch, the exact solution is not known, and approximate relationships such as Neuber's rule, and more recently, Glinka's Equivalent Strain Energy Density (ESED) method are used. Approximate relationships contain assumptions which may not be valid in certain situations. For instance, Neuber's rule does not model the multiaxial stress state present at the notch root of many engineering components. For this reason, many authors feel that a detailed elastic-plastic finite element (FE) analysis is the best way to obtain an accurate estimation of the notch stress and strain. The next sections will describe Neuber's rule, Glinka's ESED method, and FE analyses in more detail as they apply to local strain fatigue predictions.

2.6.2.1 Neuber's Rule and its Variations

Neuber showed that for a shear-strained prismatic body with an arbitrary non-linear stress-strain law, the geometric mean of the stress and strain concentration factors (K_σ

and K_ε) is equal to the theoretical stress concentration factor, K_t. This is expressed as follows:

$$K_t^2 = K_\sigma K_\varepsilon \tag{2-14}$$

The stress concentration factor, K_σ, is the ratio of the notch root stress and the net-section nominal stress:

$$K_\sigma = \frac{\sigma}{S} \tag{2-15}$$

The strain concentration factor, K_ε, is the ratio of the notch root strain and the net-section nominal strain, e:

$$K_\varepsilon = \frac{\varepsilon}{e} \tag{2-16}$$

Combining equations 2-14 through 2-16, Neuber's rule is re-written as:

$$\sigma \varepsilon = K_t^2 S e \tag{2-17}$$

Generally, this is re-written in terms of stress and strain ranges for the case when the stress range remote to the notch is linear elastic:

$$\Delta\sigma\,\Delta\varepsilon \equiv \frac{(K_t\,\Delta S)^2}{E} \tag{2-18}$$

The form presented in Equation 2-18 is widely used in fatigue life calculations using the LS approach. It shows that the product of the notch stress and strain ranges can be estimated by knowing the theoretical stress concentration factor, the applied stress range, and the elastic modulus of the material.

Although Neuber's rule was derived for a monotonic loading case, it was applied to fatigue loading by Manson and Hirschberg (1966). They suggested using the cyclic stress-strain curve instead of the monotonic curve for fatigue loading. Topper *et al.* (1969) were the first to refer to Neuber's work as "Neuber's rule". They showed that smooth specimen fatigue data could be used to adequately predict fatigue lives of notched members made from 2024 and 7075 aluminum alloys under fully reversed loading.

Many authors have questioned the unconditional use of Neuber's rule in fatigue life predictions, for example, Tipton (1991) and Glinka *et al.* (1988). The grounds for this challenge are the following:

- Neuber's rule was derived for a specific notch geometry and loading condition, but is used without question in many cases where the loading and notch geometry deviate substantially from Neuber's original work.

- It has been found in many cases to predict larger notch root strains when compared to finite element studies or direct measurement, resulting in overly conservative predictions.

Neuber derived his original work for a hyperbolic notch profile loaded under two-dimensional monotonic shear. The shear stress and strain at the notch root were the only non-zero stress and strain components, far from being a general solution to the notch stress-strain problem. Neuber recognized this limitation in his original work, and gave suggestions as to how the formulation may be generalized for arbitrary stress states by means of one of the well known theories of failure.

Tipton (1991) suggested that the conservative nature of Neuber's rule was due to the multiaxial stress state at the notch root which is not accounted for in the approximation. When a notched engineering component is loaded in tension, the material at the notch root tries to contract perpendicular to the axis of loading. The lesser stressed bulk material on either side of the notch prevents this from occurring, and a transverse stress at the notch root is created.

Hoffmann and Seeger (1985) developed a generalized method for estimating the multiaxial elastic-plastic notch stresses and strains using a modularized approach. Their method closely follows the recommendations set by Neuber in his original work and consists of two steps:

1. Relating the applied stress (S) to the equivalent notch stress and strain (σ_q and ε_q).
2. Relating the equivalent stress and strain to the principal stress and strain (σ_1 and ε_1).

The first step is accomplished by using Neuber's rule, but replacing the uniaxial quantities with an equivalent quantity calculated under the von Mises or Tresca yield criterion.

The theory of plasticity offers two possibilities to correlate the equivalent stress and strain to the principal stress and strain. The stress tensor [σ] is often divided into a hydrostatic stress tensor [$p\mathbf{I}$] and a deviatoric stress tensor [σ']. The flow rule of Prandtl-Reuss relates the principal plastic strain increments $d\varepsilon_i^p$ to the deviatoric stresses σ_i', the equivalent plastic strain increment $d\varepsilon_q^p$, and the equivalent stress σ_q. The Prandtl-Reuss flow rule has the following form:

$$d\varepsilon_i^p = \frac{3}{2}\frac{d\varepsilon_q^p}{\sigma_q}\sigma_i' \qquad (i = 1, 2, 3) \tag{2-19}$$

These equations represent the exact solution for isotropic hardening under the assumption of von Mises yield criterion. If the ratio between the deviatoric stress components

remains constant during loading, the Prandtl-Reuss law reduces to Hencky's rule which assumes the principal plastic strains ε_i^p to be a function of the deviatoric stresses:

$$\varepsilon_i^p = \frac{3}{2}\frac{\varepsilon_q^p}{\sigma_q}\sigma_i' \qquad (i = 1, 2, 3) \tag{2-20}$$

Hoffmann and Seeger (1985) assume that the ratio between deviatoric stress components does not change substantially in the vicinity of the notch. Thus, Hencky's rule will deliver results with sufficient accuracy. Hoffmann and Seeger have demonstrated the success of their method for thick bars and thick pressure vessels.

2.6.2.2 Equivalent Strain Energy Density (ESED)

Alternate approximate relationships have been proposed for use in place of Neuber's rule. One such relationship is the Equivalent Strain Energy Density (ESED) method proposed by Molski and Glinka (1981). In this approach, it is assumed that the strain energy density at the notch root does not change significantly if the localized plasticity is surrounded by predominantly elastic material. In other words, the computation of the strain energy density at the notch root will yield identical results for either the elastic or the elastic-plastic material law. The ESED relation has the following form:

$$\frac{1}{2}\frac{(K_t S)^2}{E} = \int_0^{\varepsilon} \sigma_{(\varepsilon)}\, d\varepsilon \tag{2-21}$$

where K_t is the theoretical stress concentration factor, S is the net-section nominal stress, E is the elastic modulus, $\sigma_{(\varepsilon)}$ is the notch root stress as a function of ε, the notch root strain.

According to Glinka *et al.* (1988), the ESED model is superior to Neuber's rule when predicting elastic-plastic notch stresses and strains. Sharpe *et al.* (1992) make the assertion that Neuber's rule is the single best model for cases which are plane stress. It was demonstrated in some cases that the measured or FE results for local strain lie between the predictions from the Glinka ESED model and Neuber's rule, with Neuber's rule giving the larger estimate for a given value of K_tS, e.g. (Molski and Glinka, 1981), (Sharpe *et al.*, 1992). In these instances, it was difficult to determine which model best fit the experimental data. It has been suggested that estimations made from Glinka's ESED model and Neuber's rule will give lower and upper bounds on the local strain, which can be used to tag an uncertainty with the life prediction (Sharpe *et al.*, 1992).

2.6.2.3 Finite Element (FE) Analysis

Many authors feel that a detailed elastic-plastic finite element analysis is the best way to obtain an accurate stress-strain estimation at the notch root of an engineering component. However, elastic-plastic FE analyses are far from being ready to use in everyday design applications, especially in cases of complex geometry, irregular loading and realistic transient material plasticity behaviour (Tipton, 1991). Even though this is the case, FE analyses are attractive since the level of detail used in the model can be tailored to a particular research program. For instance, some authors have opted to model a multiaxial

stress state at the notch root (Tregoning, 1992), while others have included the effects of creep (Umeda *et al.*, 1987).

The loading used in an FE analysis is generally monotonic (using cyclic material data), which is analogous to Neuber's rule which was formulated for monotonic loading, but extended to fatigue loading. FE analyses which use a representative load history are not common since they are time consuming, and are not possible in many FE packages.

Some researchers have used FE packages which have an integrated fatigue life program, such as the PC-based NISA/ENDURE (Kähönen, 1991) and the MSC/FATIGUE (Doerfler, 1997) programs. With these integrated packages, airframe components can be subjected to representative load histories to identify fatigue critical areas.

Doerfler's study showed that MSC/FATIGUE could benefit the preliminary design of airframe structures since it has the ability to locate areas in a structure which may be susceptible to crack initiation. This global ability does come at a high price when one considers the number of load cases that are studied in a typical aircraft development program.

Combined with the results from coupon and component test programs, packages such as NISA/ENDURE and MSC/FATIGUE could become valuable tools in an engineering design office.

2.6.3 Notch Severity

As mentioned previously, experimental observations suggest that stress concentrations in notched members have less effect in fatigue than is predicted by the stress concentration factor K_t. A so-called fatigue concentration factor, K_f is often used in place of K_t to represent this phenomenon. The fatigue concentration factor is defined as the ratio of the fatigue strengths of smooth and notched specimens, $S_e^{(smooth)}$ and $S_e^{(notched)}$, respectively. The fatigue concentration factor is expressed as:

$$K_f = \frac{S_e^{(smooth)}}{S_e^{(notched)}} \tag{2-22}$$

In order to calculate K_f from Equation 2-22, it is necessary to have the fatigue strengths of both smooth and notched specimens available from experiment. Usually, K_f is calculated at $N=10^7$ cycles for a stress ratio of $R_\sigma=-1$ (Nie *et al.*, 1994). Since experimental results are time consuming and expensive to obtain, empirical formulae such as those listed by Weixing *et al.* (1995) are used to calculate K_f. The formula proposed by Peterson (1959) is popular and has the following form:

$$K_f = 1+\frac{K_t-1}{\left(1+\frac{a}{r}\right)} \tag{2-23}$$

where "a" is a material constant, and r is the notch radius. The accepted rationale behind using K_f instead of K_t is to account for size effects at notches. The size effect is dependent

on material and stress gradient at the notch. A sharp notch has a steeper stress gradient and a smaller volume of highly stressed material when compared to a blunt notch (Figure 2-4). When a crack has grown outside the highly stressed material in the sharp notch case, the crack growth slows down since the effect of the stress concentration diminishes. In addition, as the volume of highly stressed material increases, the probability of fatigue failure increases since the likelihood of a flaw existing within the larger volume is greater than for a smaller volume (Dowling, 1979).

It is apparent that K_f calculated from Equation 2-23 is constant. However, Nie *et al.* (1994) propose a "Variable K_f" of the following form:

$$K_f = \frac{K_t}{3} \cdot \left(\sqrt{E/E_\sigma} + 2\sqrt{E_\sigma/E} \right) \tag{2-24}$$

where E and E_σ are the elastic and secant moduli. Their study showed that predictions based on the variable K_f, the Manson-Coffin relationship and Miner's rule were in agreement with test results for a critical location of a wing spar made from AISI-4340 steel and subjected to spectrum loading.

Walker (1977) noticed that the application of Neuber's rule with the fatigue concentration factor disregarded the multiaxial stress state at the notch root. He demonstrated that the success of this approach was not accidental, and that there was an equivalence between the following two methods:

1. Use of Neuber's rule with the fatigue concentration factor K_f.
2. Use of Neuber's rule with K_t and consideration of the multiaxial stress state.

Hence, Walker's approach suggests that the use of K_f may be an empirical method of accounting for notch root multiaxiality. However, this approach disregards the notion put forth by many that K_f accounts for size effects.

Bannantine *et al.* (1990) noted that there appears to be a limiting value of K_f based on observed behaviour. The limiting value is dependent on material, but has been shown to be approximately 5 or 6, even though K_t could be as large as 15. Bannantine *et al.* propose to use K_f to account for the smaller initiation life in sharp notches, where a significant crack propagation stage may exist. Thus, for sharp notches, local strain predictions made using K_f would be in better agreement with total life test results when compared to local strain predictions made using K_t. This suggests that the use of K_f may be an empirical method to account for crack propagation in sharp notches.

2.7 Fracture Mechanics

A new area of fatigue research involves the use of fracture mechanics approaches to characterize crack initiation. Linear Elastic Fracture Mechanics (LEFM) can only be used when the stress state at the crack tip can be described by an elastic stress field. This limits the applicability of LEFM to low stress levels and relatively long initial defects on the order of 1 mm (Miller, 1987). LEFM is unable to characterize the behaviour of short

cracks since the stress field at the tips of small defects in highly stressed materials cannot be described by an elastic stress field. Elastic-Plastic Fracture Mechanics (EPFM) approaches are being researched to simulate the growth of short cracks from the level of microstructure up to sizes compatible with LEFM.

Short crack behaviour is important when studying notches since a crack emanating from a notch will be growing in a stress field which is usually above the LEFM limit. In addition, as the crack grows out of the highly stressed material at the notch root, crack growth rate slows down, possibly to the point where the crack becomes non-propagating.

2.8 Summary

The local strain approach was developed to overcome some of the problems identified with the nominal stress approach, namely its empirical nature, and the disregard for the actual stress-strain response of the material.

The basis for the LS approach is that smooth specimens tested under strain-control can simulate the fatigue damage at the notch root of an engineering component. Equivalent fatigue damage is assumed to occur at the notch root and in the smooth specimen when both are subjected to identical stress-strain histories. The local strain approach is considered to be superior to the NS approach since it considers the stress and strain state at the notch root of a component. However, the local strain method contains assumptions that are not necessarily valid. Two particular areas of concern are the damage accumulation and the principle of equivalence.

Attempts to overcome the damage accumulation problem have resulted in nonlinear damage theories, use of prestrained and periodically overloaded material data, and the use of modified baseline damage parameters.

Limitations in the principle of equivalence can lead to order of magnitude differences between measured and predicted life. Neuber's rule was derived for a state of plane stress but is generally used unconditionally in situations which deviate from plane stress. An alternate approach, Glinka's ESED method, has been proposed which considers the strain energy density at the notch root. Approximate relationships such as Neuber's rule and Glinka's ESED method are useful to make first estimates of the notch root stress and strain, but a more accurate prediction would require further computational and/or experimental study of the case at hand.

The observed behaviour of the fatigue strengths of notched and smooth specimens has led to the use of a fatigue concentration factor (K_f) in LS predictions. The use of K_f may be an empirical method of considering the crack propagation stage in sharply notched members.

Current research focus in the area of fatigue crack initiation lies in using fracture mechanics to describe the growth of a microstructural flaw to a crack of sufficient size, compatible with LEFM.

Chapter 3 - Project Definition

In Chapter 2, it was established that there are areas of concern in the LS approach. One concern is the use of Neuber's rule (Neuber, 1961) to describe the notch root behaviour of an engineering component. As was seen, Neuber's rule provides an easy method for estimating the notch root stress and strain of the component. Neuber's rule was derived for a specific geometry and loading, but is generally used without question in many cases which deviate substantially from the specific case for which it was derived. It has been shown to be accurate in situations which are plane stress, but has been found to underestimate notch root strains in situations where a multiaxial stress state exists. In addition, Neuber's rule only represents the stress concentration of the notch through the use of the stress concentration factor, and does not take into account factors such as strain gradient and size effects. With these points in mind, it becomes apparent that Neuber's rule is limited in its application, and may be inappropriate to use in certain situations.

The objective of this thesis is to analyze the applicability of Neuber's rule in the local strain method. The predictive capability of Neuber's rule will be examined for two coupons, one having a low stress concentration, the other having a high stress concentration. The ability of the local strain method to predict the lives of the two coupons will be assessed.

To meet the objective, three tasks were carried out:

- Completion of a coupon test program to obtain total life test data for the two coupons subjected to spectrum loading (Chapter 4).
- Development of a local strain crack initiation prediction program similar to C_CI89 so that LS predictions could be made using different implementations of the notch root stress-strain estimation (Chapter 5).
- Development of elastic-plastic finite element models of the two coupons to observe the notch root stress and strain as a function of the net section nominal stress (Chapter 6).

The applicability of Neuber's rule in the LS approach was tested by completing a notch root stress-strain sensitivity study. This involved comparing the stress-strain estimation from Neuber's rule to the results of the FE analysis and other approximate relationships. The ability of the local strain method to predict the lives of the two coupons subjected to spectrum loading was tested by completing a crack initiation prediction sensitivity study. This involved comparing LS predictions with the coupon test results from Chapter 4. Local strain predictions were made for each of the methods used in the notch root stress-strain sensitivity study. The results of the two sensitivity studies are presented in Chapter 7.

Chapter 4 - Coupon Test Program

4.1 Introduction

A coupon test program was undertaken at SMPL-IAR to test two coupon geometries subjected to a CF-18 trailing edge flap hinge moment sequence. Two sequences were tested on each coupon geometry, one containing manoeuvring loads, and the other containing combined (manoeuvring and buffet) loads. The tests were performed as a part of a spectrum truncation sensitivity study at SMPL-IAR.

4.2 Coupons and Test Sequences

The coupons were manufactured from aluminum 7050-T7451. The first geometry, "Low K_t", contained a double edge semi-circular notch (Figure 4-1). The second geometry, "High K_t", contained a centrally located slot (Figure 4-2). The coupons will hereon be referred to as Low K_t and High K_t.

The coupons have the general designations of "P1L 548 YYY 030", and "P2L 540 YYY 030", respectively. The reference label, 'YYY', refers to a coordinate within the block of aluminum from which the coupons were machined. The reference label is unique for each coupon. Only the reference labels will hereon be quoted when referring to a particular coupon.

The sequences tested were representative of a trailing edge flap hinge moment sequence on the CF-18 aircraft. The sequences were developed by Bombardier Inc., Canadair Defense Systems Division (BI/CDSD). Each CF-18 is equipped with a Maintenance Signal Data Recording System (MSDRS) which records flight parameters, engine data, stores data, weapons data, and seven channels of strain data automatically at specified frequencies and on some specified events (Hewitt *et al.*, 1996). Since the trailing edge flap hinge moment is not directly measured by the MSDRS, it is predicted from a regression of measured flight loads against measured flight parameters through a Parametric Load Formulation (PLF). Buffet loads are also not measured by the MSDRS. The buffet loads were measured during a series of CF-18 flights and were added to the manoeuvre spectrum to obtain the combined (manoeuvre + buffet) spectrum. The test sequences represent 279 flights of combined Canadian Forces and Royal Australian Air Force usage.

The first sequence, designated tef_man05, contained manoeuvring loads only, and was truncated at 5% peak load range, resulting in 17534 turning points per block. The number of turning points corresponds to the number of load reversals in the spectrum. The second sequence, containing the combined (manoeuvring and buffet) loads and designated tef_sum05, was also truncated at 5% peak load range, resulting in 409380 turning points per block. In each instance, one block represents 279 unique flights with a total duration of 326 spectrum flight hours (sfh). Five coupons of each geometry were tested for each sequence, resulting in a total of 20 fatigue tests.

4.3 Test Procedure

A test procedure was developed using the MTS TestStar and TestWare SX software. The details of the test procedure can be found in Appendix A. Two load frames were used, each dedicated to a particular coupon geometry. A 55 kip (244 kN) load frame was used to test the Low K_t coupons, and a 22 kip (97.9 kN) load frame was used to test the High K_t coupons. The apparatus set-up and calibration information can also be found in Appendix A.

Initially, two coupons of each geometry were tested under the tef_man05 sequence so that the stress level for the test could be verified. The sequences and coupons were selected at random for the subsequent tests.

4.4 Detection of Crack Initiation

Prior work at SMPL-IAR on truncation sensitivity for the CF-18 centre fuselage spectrum, used acoustic emissions monitoring to estimate the crack initiation lives on some specimens. This study showed good correlation between initiation lives and total lives. Therefore, since crack initiation measurements are time consuming, and there was an urgency to complete the testing, SMPL-IAR decided not to measure initiation lives on the specimens tested with the trailing edge flap sequences.

In addition, SMPL-IAR was primarily interested in predicting the relative effects of spectrum truncation rather than absolute lives and thus the distinction between initiation and total life was initially not a concern for them.

4.5 Test Results

Test results for the Low K_t coupons are presented in Table 4-1. The tef_man05 sequence was tested using the peak load levels of 9.04/-4.85 kips (40.2/-21.6 kN). The load level was selected by SMPL-IAR so that the tested life was approximately 2.5 times the expected airframe lifetime. In the case of the tef_sum05 sequence, the peak load levels were 10.05/-4.85 kips (44.7/-21.6 kN). The load level for the tef_sum05 sequence was selected by SMPL-IAR so that the peak manoeuvring stress was the same as in the tef_man05 sequence.

Spectrum	YYY	Start	End	Turning Points	Missed/ ErrorTol	Blocks	Hours	Crack Start
tef_man05	083	14/01/98, 11:50	15/01/98	796735	0/90	45.44	14768	3, 5
	173	15/01/98, 10:10	16/01/98	814401	0/90	46.45	15095	3
17534	053	22/01/98, 10:10	23/01/98	854484	0/90	48.73	15838	4
pts. / block	089	23/01/98, 09:10	24/01/98	797865	0/90	45.50	14789	1
	197	26/01/98, 09:50	27/01/98	603401	0/90	34.41	11184	3
					Log Mean	**43.79**	**14232**	
tef_sum05	077	16/01/98, 09:32	18/01/98	4571310	0/90	11.17	3629	3
	131	18/01/98, 13:40	20/01/98	3759593	1/90	9.18	2985	1
409380	311	20/01/98, 10:45	22/01/98	4869689	0/90	11.90	3866	3
pts. / block	257	24/01/98, 13:28	26/01/98	3937343	0/90	9.62	3126	3
	239	27/01/98, 09:25	29/01/98	3996908	12/90	9.76	3173	2, 6
					Log Mean	**10.28**	**3339**	

Table 4-1: Test Results for Low K_t Coupons

Test results for the High K_t coupons are presented in Table 4-2. The tef_man05 sequence was tested using peak load levels of 7.27/-3.90 kips (32.3/-17.3 kN). In the case of the tef_sum05 sequence, the peak load levels were 8.08/-3.90 kips (35.9/-17.3 kN). These

load levels were selected to obtain equal lives with respect to the Low K_t coupons. A multiplier of 80.44% was used with respect to the Low K_t load level.

Spectrum	YYY	Start	End	Turning Points	Missed/ ErrorTol	Blocks	Hours	Crack Start
tef_man05	460	16/01/98, 12:38	17/01/98	1236213	194/100	70.50	22914	2,4
	454	17/01/98, 13:38	18/01/98	1321103	75/100	75.35	24487	2,5
17534	377	18/01/98, 13:35	19/01/98	1391490	88/100	79.36	25792	2,5
pts. / block	401	26/01/98, 10:15	27/01/98	1376495	1193/90	78.50	25514	2,5
	436	27/01/98, 09:50	28/01/98	1478906	30/90	84.35	27412	2,5
					Log Mean	**77.48**	**25180**	
tef_sum05	407	29/01/98, 15:00	01/02/98	6691799	12136/90	16.35	5313	1,5
	472	02/02/98, 14:25	05/02/98	5806495	13/90	14.18	4610	2,5
409380	442	05/02/98, 13:40	08/02/98	7034633	352/90	17.18	5585	2,5
pts. / block	395	09/02/98, 09:38	12/02/98	6862570	190/90	16.76	5448	2,5
	360	12/02/98, 14.05	15/02/98	7124228	424/90	17.40	5656	2,4
					Log Mean	**16.33**	**5308**	

Table 4-2: Test Results for High K_t Coupons

It should be noted that the first three High K_t coupons, 460, 454, 377, were tested before the LVDT and load cell were re-calibrated on 22 and 23 January 1998, respectively. The change in calibration was minimal, but required the MTS system to be re-tuned.

4.6 Accuracy of Applied Loads

The performance of the MTS system was tracked during the course of the testing to determine the accuracy with which the loads were applied to the coupons. Quantities of interest were missed end levels and the relative error between commanded and attained load. Missed end levels is a MTS specific term which refers to the number of turning points in the spectrum which were not applied to the coupon within a specified threshold. In most cases, the threshold value was 90 lbf (400 N).

For the Low K_t coupon, the loads were applied with a very high degree of accuracy. For the tef_man05 sequence, no end levels were missed, indicating that all of the loads in the spectrum were applied to the coupons within the threshold of 90 lbf (400 N). For the tef_sum05 sequence, only specimens 131 and 239 had missed end levels, corresponding to 1 end level and 12 end levels respectively. The missed end levels are insignificant in these cases since the spectrum size is 409380 turning points per block, and the resulting lives for the coupons are 9.18 and 9.76 blocks.

The accuracy of the application of the peak load was very high when compared to the commanded load for the Low K_t coupon. As an example, specimen 077, subjected to tef_sum05 had a peak load of 10050 lbf (44704 N) in tension and -4850 lbf (-21574 N) in compression. Six random measurements of the applied peak load resulted in an average of 10079 lbf (44834 N) in tension and -4855 lbf (21596 N) in compression. The relative error when compared to the command was 0.29% and 0.10% respectively.

For the High K_t coupon, the situation is different. For the tef_sum05 sequence, the largest number of missed end levels was 12136 for the first specimen tested, number 407. In this case, only 19 end levels were missed during application of the first block, while the MTS system was in "learning mode". The majority of the 12136 missed end levels occurred between blocks 14 and failure (16.35 blocks), after the specimen had cracked approximately one-third of the way across the net-section.

The tef_sum05 sequence is significantly different than the tef_man05 sequence in that it contains a large number of small amplitude cycles which are applied very quickly since the loading rate is constant. The large number of missed end levels for specimen 407 is likely due to the MTS system undershooting the small amplitude cycles by more than the tolerance of 90 lbf (400 N). This is due in part to the loading rate being constant as explained above, but also due to the fact that the coupon was cracked when the majority of end levels were missed. The MTS system "learns" how to apply the spectrum to the coupon in the first block when the coupon is not cracked. In this learning mode, the MTS system generates a computer file which is used after application of the first block. The computer file allows the MTS system to anticipate the next load demand. When cracking occurs, the computer file is no longer valid since the stiffness of the coupon is not the same as when it was not cracked. Thus, for specimen 407, the missed end levels are due to the MTS system undershooting the small amplitude cycles due to the loading rate being constant and the stiffness being reduced from the un-cracked case.

For the tef_man05 sequence, the largest number of missed end levels was 1193 for specimen 401. This coupon was the first to be tested after re-calibration of the LVDT and load cell. In addition, the error tolerance was lowered from 100 lbf (445 N) (used for specimens 460, 454, and 377) to 90 lbf (400 N). The re-calibration and the change in the error tolerance required the MTS system to be re-tuned. The majority of missed end levels occurred during the re-tuning effort, while the MTS system was in "learning mode".

The accuracy of the application of the peak load was very high when compared to the commanded load for the High K_t coupon. As an example, specimen 395, subjected to tef_sum05 had a peak load of 8084 lbf (35959 N) in tension and -3901 lbf (17353 N) in compression. Seven random measurements of the applied peak load resulted in an average of 8122 lbf (36128 N) in tension and -3903 lbf (17361 N) in compression. The relative error when compared to the command was 0.47% and 0.05% respectively.

As a whole, the loads were accurately applied to both the Low and High K_t coupons.

4.7 Crack Initiation Sites

Tables 4-1 and 4-2 list the crack initiation sites, by number, for each of the coupons tested. The numbers refer to the locations defined in Figure 4-3. The site from which the crack initiated was determined by a visual inspection of the fracture surface.

For the Low K_t coupon, the dominant failure mode was a single corner crack. In the case of specimens 083 and 239, there is evidence of cracks initiating from two corners of the net-section. For the High K_t coupon, the dominant failure mode was a double edge crack with initiation at the mid-thickness of the coupon.

4.8 Summary

A coupon test program was undertaken as part of a spectrum truncation sensitivity study at SMPL-IAR. The following results were obtained:

- Total life results are available for the Low and High K_t coupons subjected to the tef_man05 and tef_sum05 sequences. A sample size of five specimens per sequence was used for each coupon geometry.
- For the Low K_t coupon, the application of the tef_man05 sequence results in a life of 14232 sfh (logarithmic mean), while application of the tef_sum05 sequence results in a life of 3339 sfh (logarithmic mean).
- For the High K_t coupon, the application of the tef_man05 sequence results in a life of 25180 sfh (logarithmic mean), while application of the tef_sum05 sequence results in a life of 5308 sfh (logarithmic mean).

Chapter 5 - Local Strain Software

5.1 Introduction

As mentioned in Chapter 1, the local strain computer program, C_CI89, is used in IFOSTP. This chapter presents a description of the local strain method used in C_CI89. In addition, a description of the local strain program designed for this study will be presented. Finally, differences between C_CI89 and another local strain program, LOOPIN8, will be highlighted.

5.2 Description of C_CI89

The LS method used in C_CI89 is composed of four steps (Forness *et al.*, 1989):

1. Cycle Counting - Closed Hysteresis Loops
2. Notch Stress and Strain Calculation - Neuber's Rule
3. Mean Stress Correction - Equivalent Strain Equations
4. Damage Calculation - Miner's Rule

The LS approach used in C_CI89 is similar to the method outlined in Chapter 2. Data used in the C_CI89 LS approach are the following:

1. Applied stress sequence arranged in peak-valley pairs.
2. Material cyclic stress vs. stress*strain curve
3. Material strain amplitude vs. life curve at R_σ=-1
4. Material elastic modulus and proportional limit

5.3 McCracken Fatigue Life Prediction Program

To meet the project objective defined in Chapter 3, it is necessary to study different implementations of the notch root stress and strain estimation used in the local strain approach. The computer program C_CI89 is proprietary and is neither clearly written nor well documented. Making changes to C_CI89 to explore different implementations of the notch root stress and strain was therefore considered undesirable. A computer program similar to C_CI89 was developed for this research program with the following purposes:

1. To aid in the understanding of the local strain approach, and
2. To serve as a platform upon which capabilities not found in C_CI89 could be added.

The McCracken Fatigue Life Prediction Program (hereafter referred to as McCracken) was conceived of in response to these two points.

McCracken was implemented in Microsoft Visual C++ version 4.0, and is a Windows 95/NT 4.0 application. McCracken is executed by running McCracken.exe from Windows Explorer. The McCracken prediction environment is depicted in Figure 5-1.

Running a prediction using McCracken requires the completion of four steps:

1. Configure the material properties
2. Configure the load spectrum
3. Configure the prediction
4. Go

A menu option and associated button on the toolbar are provided to allow the user to complete these four steps.

5.3.1 Material Properties Dialog Box

The material properties dialog box is displayed in Figure 5-2. It allows the user to configure the material used in the prediction. The inputs in this dialog box are the cyclic stress vs. stress*strain curve filename, the strain-life curve filename, the modulus of elasticity, the proportional limit, and the ultimate tensile strength. The required format of the material data files is presented in Appendix B.

5.3.2 Spectrum Dialog Box

The spectrum dialog box is displayed in Figure 5-3. It allows the user to configure the load spectrum used in the prediction. The inputs in this dialog box are the load spectrum filename, the reference value, the number of turning points, the coupon design limit stress (DLS), the stress concentration factor, and the number of flight hours per block. The trailing edge flap spectra developed at SMPL-IAR are expressed in terms of a hinge

moment. The reference value provides a means of converting the load sequence to an equivalent stress sequence. The DLS refers to the peak stress in the load spectrum.

An option in McCracken is the ability to run the predictions for a number of different design limit stresses. This is accomplished by entering values for the maximum K_t*DLS, the K_t*DLS increment, and the number of K_t*DLS breakpoints to calculate. This information can be used to plot K_t*DLS vs. Life for the component. The required format of the load spectrum file is presented in Appendix B.

5.3.3 Prediction Methods Dialog Box

The prediction methods dialog box is presented in Figure 5-4. It allows the user to configure the way in which the prediction is to be made. The user has the option to configure five aspects of the local strain approach:

1. Nominal stress vs. notch root stress-strain relationship
2. Cycle ordering
3. Cycle counting
4. Equivalent strain relationship
5. Material properties

For aspects 1 and 4, multiple options are listed to enable the user to configure the manner in which the prediction is made.

The standard adopted for IFOSTP is to use the following options when making a prediction using C_CI89 (Foster, 1993):

- Use of prestrained material data
- Move peak load to the front of the spectrum
- Use of "Closed Hysteresis Loop Counting"
- Smith-Watson-Topper (SWT) equivalent strain equation

This standard was used in this thesis, except where noted.

5.3.4 Executing the Prediction

After the material, load spectrum and prediction methods are configured, the program is ready to be executed. The toolbar button labeled "Go" executes the local strain algorithms. The results are displayed to the screen once the calculations are complete.

5.3.5 Documenting Results

The results can be saved to disk after the prediction is made using the menu option "Results-Save". The user can specify a filename for the results file. All results files are given the ".res" extension. The format of the results file is given in Appendix B.

5.4 Validation of McCracken

5.4.1 Overview of Validation

The McCracken software was validated by comparing predictions to those made by C_CI89 for the trailing edge flap hinge moment sequences described in Chapter 4.

5.4.2 Material Data

The materials database in C_CI89 contains data for aluminum 7050-T74. This data was used in both the C_CI89 and McCracken predictions. The cyclic stress vs. stress*strain and strain-life curves are shown in Figures 5-5 and 5-6, respectively. The prestrain and non-prestrain data are plotted on Figure 5-6, as well as the SWT compatible strain-life curve which is generated by the program.

5.4.3 Comparison of C_CI89 and McCracken Predictions

Crack initiation predictions for the tef_man05 sequence are presented in Table 5-1.

Kt*DLS [ksi]	C_CI89 Prediction [sfh]	McCracken Prediction [sfh]	Relative Error [%]
97.60	4442	4445	0.08
89.80	6024	6029	0.08
82	8282	8288	0.08
74.2	10942	10921	-0.19
66.4	15438	15407	-0.20
58.6	23489	23432	-0.24
50.8	42398	42257	-0.33
43	80642	80295	-0.43
35.2	186529	185122	-0.75

Table 5-1: Comparison of C_CI89 and McCracken Predictions for tef_man05

The McCracken predictions are in excellent agreement with the C_CI89 predictions. The maximum error (relative to C_CI89) over the K_t*DLS range in question is 0.75%.

The C_CI89 predictions were made at SMPL-IAR and used the maximum manoeuvre range as the reference value. This was done since SMPL-IAR was interested in the

effects of truncation which is typically quoted as a function of the largest cycle in the spectrum. The predictions made for this study use the maximum value in the spectrum as the reference. Therefore, a conversion had to be made to express the C_CI89 predictions in a format suitable for comparison with McCracken predictions. The error between C_CI89 and McCracken predictions is due to interpolation error when converting the C_CI89 prediction to one in terms of the maximum spectrum value.

5.5 Comparison of Local Strain Prediction Programs

5.5.1 C_CI89 vs. LOOPIN8

The Northrop local strain program, LOOPIN8 (Porter, 1983), was initially reviewed for use in IFOSTP. LOOPIN8 is similar to C_CI89 in its local strain algorithm. However, it uses a custom equivalent strain equation which is not included in C_CI89. In addition, LOOPIN8 does not allow the use of other equivalent strain equations.

It was noted by Foster (1993) that predictions made using LOOPIN8 were significantly lower than those from C_CI89 even though the material data used showed good agreement with the data used in C_CI89. A study was performed to verify the discrepancy between the use of the SWT and LOOPIN8 equivalent strain equations. The LOOPIN8 equivalent strain equation has the following form:

$$\left(\frac{\Delta\varepsilon}{2}\right)_{eq} = \frac{\Delta\varepsilon}{2} + 0.000655\left(1+R_{\varepsilon}\right) + 0.197\left(1-R_{\sigma}\right)\left(\frac{\sigma_a}{E}\right) \qquad (5\text{-}1)$$

where R_ε and R_σ are the strain and stress ratios, and σ_o is the mean stress. From Figure 5-7, it can be seen that the LOOPIN8 equivalent strain equation predicts a lower life for the tef_man05 sequence than the SWT equation. The difference is significant and is consistent with the results of Foster (1993).

5.5.2 C_CI89 vs. McCracken

Some of the numerical techniques used in the C_CI89 program were improved upon in McCracken. An audit of the C_CI89 source code revealed that the solution of Neuber's rule was not strictly correct. C_CI89 calculates the product of the notch root stress and strain using Neuber's rule, and then interpolates through a stress vs. stress*strain data file to solve for the notch root stress. The method used in McCracken is consistent with the method presented by Bergengren *et al.* (1993). In this method, the stress vs. strain curve is used instead of the stress vs. stress*strain curve. The product of the notch root stress and strain is calculated using Neuber's rule. Next, iteration is used to find a point on the stress vs. strain curve so that the product of stress and strain for that point is equal to the value calculated using Neuber's rule.

The two solution techniques only display a difference in the interpolated regions of the stress-strain curve. The difference is most pronounced in the elastic region of the stress-strain curve. In this region the C_CI89 technique leads to erroneous results. C_CI89 uses the stress vs. stress*strain curve which is created by multiplying the abscissa of the stress vs. strain curve by the ordinate, and re-plotting this value as the new abscissa. In doing

so, any regions of the original stress vs. strain curve which were linear (i.e. elastic region) are now non-linear in the new stress vs. stress*strain curve. Even though this is the case, C_CI89 plots the elastic region of the stress vs. stress*strain curve as linear. Figure 5-8 plots the C_CI89 representation of the stress vs. stress*strain curve next to what one would expect. Use of C_CI89 data and the C_CI89 solution to Neuber's rule in the elastic region results in erroneous predictions of notch root stress and strain. For this reason, C_CI89 uses Hooke's Law to calculate the notch root stress and strain when in the elastic region of the material.

Outside the elastic region, the difference between the C_CI89 and McCracken solutions to Neuber's rule is small. The small difference in stress-strain estimation may not justify the extra computational effort required by the McCracken solution. However, the McCracken solution of Neuber's rule is valid in all regions of the stress-strain curve, including the elastic region. In addition, the McCracken solution uses the more familiar stress vs. strain curve instead of the unconventional stress vs. stress*strain curve.

When calculating the cycles to failure for a closed hysteresis loop, C_CI89 does not allow the life to go beyond 10^{20} cycles. This can be a problem in a spectrum with a large number of small amplitude cycles, where the long life region of the strain-life curve is extrapolated to get the cycles to failure. McCracken does not force the life to a maximum of 10^{20} cycles in cases where an extrapolation has to be made.

5.6 Summary

A computer program to predict crack initiation life using the local strain approach was developed and validated. The relative error between the McCracken and C_CI89 predictions is small (maximum error on the order of 0.75%) for the material and spectrum tested. The difference is due to the conversion of the C_CI89 predictions to express them in terms of the maximum spectrum value. The McCracken program presents a suitable platform for implementation of new notch root stress-strain estimation methods since it was specifically designed to allow such modification.

Chapter 6 - Finite Element Analysis

6.1 Introduction

An elastic-plastic finite element analysis (FEA) was performed for both the Low and High K_t coupons. The objective of the FE analysis was to observe the notch root stress and strain as a function of the net section nominal stress for each coupon.

The FEA for each coupon was divided into two components:

1. Initial elastic FEA, and
2. Elastic-plastic FEA

The initial elastic FEA was performed to verify the stress concentration factor.

The FE analysis was performed using the ABAQUS finite element program (HKS Inc. 1997), and run on a Silicon Graphics 'Indy' computer.

6.2 Constitutive Models

The material considered in the analysis was aluminum 7050-T74. The material data presented in the C_CI89 materials database (Klohr, 1990) formed the basis for the

constitutive models. The cyclic stress vs. strain curve for aluminum 7050-T74 is presented in Figure 6-1.

The ABAQUS FE program requires that the material be described in the elastic region by Young's modulus, and in the plastic region by stress vs. plastic strain data. Figure 6-1 shows the stress vs. plastic strain data plotted next to the stress vs. strain curve.

The "Classical Metal Plasticity" model in ABAQUS was used with the von Mises failure criterion. The plasticity model uses an associated plastic flow rule to determine the inelastic deformation rate. The flow rule specifies the inelastic deformation rate to be in the direction normal to the yield surface as the material yields. According to HKS Inc. (1997), this assumption is acceptable for most calculations with metals.

6.3 Loading

When the coupons are tested in fatigue, they are placed in the hydraulic grips of the MTS load frame such that the longitudinal axis of the coupon is aligned with the hydraulic actuator. The picture of the Low K_t apparatus set-up in Appendix A demonstrates this. The coupons are subjected to axial loading which can be approximated by a uniformly distributed load applied to the top and bottom surfaces.

6.4 FEA of Low K_t Coupon

6.4.1 Geometry of Low K_t FE Model

The Low K_t coupon is depicted in Figure 4-1. It consists of a rectangular strip with two semi-circular edge cutouts. The design stress concentration factor is 1.4. Three planes of symmetry at x = 0", y = 0", and z = 0" allowed one-eighth of the coupon to be considered. Symmetric boundary conditions were used on the one-eighth FE model. Nodal displacements were not allowed for nodes lying on the following planes:

Plane	Definition
1	x = 0"
2 - "net section"	y = 0"
3	z = 0"

A three dimensional FE model was constructed using 20 node 3-D elements. A mesh convergence study was performed using models which contained 432, 1008, 1800, and 3600 elements. Each of the models were loaded with a 5 ksi (34.47 MPa) distributed load applied to the top surface of the coupon. The von Mises stress along the edge defined by y = 0", z = 0", was plotted for the 432 and 3600 element meshes to determine convergence. Figure 6-2 shows that the results from the 432 element mesh are not as refined as the results from the 3600 element mesh. The results from the 1008 and 1800 element meshes were found to agree with the results from the 3600 element mesh.

The mesh selected for the analysis, shown in Figure 6-3, has 1800 elements and 8913 nodes. Bergengren *et al.* (1993) used a similar mesh in an elastic-plastic FE analysis of double edge notch coupon made from steel DP400.

6.4.2 Elastic FEA of Low K_t Coupon - Verification

The Low K_t FE model was loaded elastically to verify the design stress concentration factor, K_t, and to verify the stress distribution at the net section. The stress concentration factor found in the analysis was 1.41, whereas the design was for 1.4. Other sources were used to verify the design K_t with the following results:

Source	K_t
FE model	1.41
SMPL-IAR Design K_t (Weiss, 1997)	1.40
(Young, 1989)	1.40
(Pilkey, 1994)	1.41

The stress concentration factor obtained in the analysis agrees with what is presented in literature for this geometry. It should be noted that life predictions which are made for this coupon at SMPL-IAR use a stress concentration factor of 1.39, which was obtained from a 2-D plane stress FE analysis.

The following approximate relationship, presented by Glinka and Newport (1987), was used to verify the elastic stress vs. distance response at the net section:

$$\sigma = K_t \cdot S\left[1 - 2.33\left(\frac{x}{r}\right) + 2.59\left(\frac{x}{r}\right)^{1.5} - 0.907\left(\frac{x}{r}\right)^{2} + 0.037\left(\frac{x}{r}\right)^{3}\right] \qquad (6\text{-}1)$$

where x is the distance from the notch root, r is the notch radius, S is the net-section nominal stress, and K_t is the stress concentration factor.

Figure 6-4 presents a comparison of the FE results with those predicted by Equation 6-1. Glinka and Newport's relationship was not in agreement with the FE results at the net section of the Low K_t coupon. Glinka and Newport (1987) assert that the relation is valid for a symmetrical semi-circular edge notch in the region $x < 3r$. However, Equation 6-1 was verified by Glinka and Newport (1987) for a coupon which was very wide when compared to the notch root radius. For the Low K_t coupon, the notch root radius is large when compared to the overall width of the coupon. With this in mind, the approximate relationship may not be suitable to predict the elastic response of this geometry.

6.4.3 Elastic-Plastic FEA of Low K_t Coupon

The Low K_t FE model was loaded incrementally as described by HKS Inc. (1997) up to the maximum applied stress. The criterion for force convergence was based upon minimizing the residual force. The residual force is defined as the difference between external loads and internal forces. The force convergence of the model is summarized in Table 6-1.

Parameter	Value	Units
Maximum Stress (gross section)	28	[ksi]
Number of Load Increments	14	[-]
Largest Residual Force	0.0004586	[%]
Run Time	15.5	[hours]

Table 6-1: Force Convergence for Low K_t Coupon

The criterion for the residual force was 0.5%. As can be seen, the largest residual force for the model was negligible, on the order of 0.0004%. This indicates that force convergence was well within the required tolerance, and that the number of load increments is sufficient to model the coupon up to the maximum applied stress.

6.5 FEA of High K_t Coupon

6.5.1 Geometry of High K_t FE Model

The High K_t coupon is depicted in Figure 4-2. It consists of a rectangular strip with a centrally located slot. Three planes of symmetry at x = 0", y = 0", and z = 0" allowed one-eighth of the coupon to be considered. Symmetric boundary conditions were used on the one-eighth FE model. Nodal displacements were not allowed for nodes lying on the following planes:

Plane	Definition
1	x = 0"
2 - "net section"	y = 0"
3	z = 0"

A three dimensional FE model was constructed using 20 node 3-D elements. A mesh convergence study was performed using models which contained 600, 1314, 2280, and 4500 elements. Each of the models were loaded with a 2 ksi (13.79 MPa) distributed load applied to the top surface of the coupon. The von Mises stress along the edge defined by y = 0", z = 0", was plotted for the 600 and 4500 element meshes to determine convergence. Figure 6-5 shows that the 600 element mesh provides a crude approximation of the stress gradient near the notch. The results from the 1314 and 2280 element meshes were found to agree with the results from the 4500 element mesh.

The mesh selected for the analysis, shown in Figure 6-6, has 2280 elements and 11153 nodes.

6.5.2 Elastic FEA of High K_t Coupon - Verification

The High K_t FE model was loaded elastically to verify the stress concentration factor, K_t. The stress concentration factor found in the analysis was 3.18. The value used at SMPL-IAR for life predictions is 2.88, which was obtained from a 2-D plane stress FE analysis. Other sources were used to verify the design K_t with the following results:

Source	K_t
FE model	3.18
(Young, 1989)	3.12
(Pilkey, 1994)	3.13
(ESDU, 1983)	3.23

The stress concentration factor obtained in the analysis agrees with what is presented in literature for this geometry.

6.5.3 Elastic-Plastic FEA of High K_t Coupon

The High K_t FE model was loaded incrementally as described by HKS Inc. (1997) up to the maximum applied stress. The criterion for force convergence was based upon minimizing the residual force. The force convergence of the model is summarized Table 6-2.

Parameter	Value	Units
Maximum Stress (@ gross section)	45	[ksi]
Number of Load Increments	16	[-]
Largest Residual Force	0.0003158	[%]
Run Time	22.3	[hours]

Table 6-2: Force Convergence for High K_t Coupon

The criterion for the residual force was 0.5%. As can be seen, the largest residual force for the model was negligible, on the order of 0.0003%. This indicates that force convergence was well within the required tolerance, and that the number of load increments is sufficient to model the coupon up to the maximum applied stress.

6.6 Results of Elastic-Plastic FEA

The following plots were generated for each of the FE analyses:

- Maximum principal stress (SP3) vs. distance from notch root

- Maximum principal strain (EP3) vs. distance from notch root
- von Mises stress vs. distance from notch root

The ABAQUS naming convention for principal stresses and strains is used, where SP3>SP2>SP1, and EP3>EP2>EP1.

The plots were generated for two locations at the net-section, the mid-thickness (y = 0", z = 0"), and the surface of the coupon (y = 0", z = 0.125"). The results are presented for various levels of net section nominal stress.

6.6.1 Low K_t Coupon

Figures 6-7 and 6-8 present SP3 vs. distance from the notch root for the mid-thickness and surface of the Low K_t coupon, respectively. Although the mid-thickness results are larger than the surface results for a given value of net-section nominal stress, the difference between the two is small.

Figures 6-9 and 6-10 present EP3 vs. distance from the notch root for the mid-thickness and surface of the coupon. The largest strain is at the notch root, with the mid-thickness strains larger than the surface strains for a given value of net section nominal stress.

Figures 6-11 and 6-12 present the von Mises stress vs. distance from the notch root for the mid-thickness and surface of the coupon. Although the von Mises stress was not of

primary interest in this study, it was observed since it was used as the failure criterion in the FE program.

6.6.2 High K_t Coupon

Figures 6-13 and 6-14 present SP3 vs. distance from the notch root for the mid-thickness and surface of the High K_t coupon, respectively. As expected, the stresses at the mid-thickness are larger than the stresses at the surface for a given value of net section nominal stress. The differences between the mid-thickness and surface results are more pronounced than in the Low K_t case.

Figures 6-15 and 6-16 present EP3 vs. distance from the notch root for the mid-thickness and surface of the coupon. The largest strain is at the notch root, with the mid-thickness strains larger than the surface strains for a given value of net section nominal stress.

Figures 6-17 and 6-18 present the von Mises stress vs. distance from the notch root for the mid-thickness and surface of the coupon.

6.7 Discussion of FE Results

The results of the elastic-plastic analysis (Figures 6-7 to 6-12 and 6-13 to 6-18) illustrate the progression of the stress state at the net section. As the value of the net-section nominal stress increases, the maximum value of SP3 moves inwards from the notch root. This is due to the influence of transverse stresses and is consistent with yielding at a notch as described by Broek (1989). The movement of the maximum value of SP3 is more pronounced in the High K_t coupon due to the strong triaxial stress state.

For the Low K_t coupon, the notch root stress and strain are plotted against the net section nominal stress in Figures 6-19 and 6-20 respectively. The results for the mid-thickness and the surface of the coupon are nearly identical, indicating that there is not a large degree of constraint associated with this geometry. Sharpe *et al.* (1992) suggest that the ratio of principal strains, α, can be used as a measure of the constraint at the notch root. When α is very close to the negative of Poisson's ratio for the material, the constraint is low, and the stress state approaches that of plane stress. For the Low K_t coupon, α was found to be -0.3, which is close to the negative of Poisson's ratio for aluminum 7050-T7451.

The situation for the High K_t coupon is different. Figures 6-21 and 6-22 plot the notch root stress and strain against the net section nominal stress. A large difference exists between the surface and mid-thickness results, indicating a large degree of constraint associated with this geometry. In this case, α was found to be -0.22. Sharpe *et al.* (1992) suggest that as α approaches zero, the notch root constraint increases and the stress state approaches that of plane strain.

Although the stress concentration factors found in the analyses agree with the "handbook" values, the value of K_t for the High K_t coupon was found to be in serious disagreement with the value used at SMPL-IAR. The value found in this analysis was 3.18 which agrees with the values given in (ESDU, 1983), (Young, 1989), and (Pilkey, 1994). The value used at SMPL-IAR is 2.88 which was obtained from a 2-D plane stress FE analysis.

The High K_t coupon is constrained at the notch root as explained previously. Thus, the assumption of 2-D plane stress is not valid.

6.8 Summary

The following summarizes the FE analyses performed on the Low and High K_t coupons:

- The elastic FE analyses verified the stress concentration factor with "handbook" values.
- The progression of the stress state at the net section has shown that the maximum value of the largest principal stress moves inwards from the notch root as yielding progresses. This is consistent with known theory.
- The stress states at the notch root of the Low and High K_t coupons are different. The Low K_t coupon is close to plane stress, whereas the High K_t coupon experiences a triaxial stress state at the notch root with a significant amount of constraint.
- Notch root stress and strain vs. net-section nominal stress data have been derived in a form suitable for comparison to Neuber's rule and other approximate relationships.

Chapter 7 - Sensitivity Study

7.1 Objective

As mentioned in Chapter 2, the local strain approach to fatigue life prediction requires a relationship between the net section nominal stress and the notch root stress and strain. This chapter presents a sensitivity study performed on the stress and strain estimation used in the local strain approach. The sensitivity study was performed for the Low and High K_t coupons by varying the method used to calculate the notch root stress and strain. The study was divided into two components:

1. Sensitivity of notch root stress and strain estimation.
2. Sensitivity of crack initiation predictions for the trailing edge flap hinge moment sequences described in Chapter 4.

The objective of the study was to identify the best stress-strain estimation technique when compared to the FE analysis, and to assess the ability of the local strain method to predict the lives of the coupons when compared to the test results in Chapter 4. The McCracken Fatigue Life Prediction Program described in Chapter 5 was used to perform the analysis.

7.2 Description of the Stress and Strain Estimation Methods

The methods analyzed in this study are:

- Neuber's rule (Neuber, 1961)
- Glinka's Equivalent Strain Energy Density Method (Molski and Glinka, 1981)
- Hoffmann and Seeger Generalized Method (Hoffmann and Seeger, 1985)
- Elastic-Plastic FE analysis (Chapter 6)

A brief description of the solution technique for Neuber's rule, Glinka's ESED method, and Hoffmann and Seeger's method will be presented, followed by the results of the stress-strain estimation study and the crack initiation prediction study.

7.2.1 Solution Technique for Neuber's Rule

The derivation of Neuber's rule was presented in Chapter 2. The two forms analyzed in this study are:

$$\sigma \varepsilon = K_t^2 Se \tag{2-17}$$

$$\sigma \varepsilon \cong \frac{(K_t S)^2}{E} \tag{2-18}$$

Equation 2-17 will be referred to as Neuber (Nonlinear), while Equation 2-18 will be referred to as Neuber rule. Equations 2-17 and 2-18 are solved using the following method:

1. Calculate the right sides of the equations. In the case of Equation 2-17, the net-section nominal strain is calculated as the strain value on the cyclic stress-strain curve whose stress value is equal to the net-section nominal stress.
2. Use iteration to find a point on the cyclic stress-strain curve whose product of stress and strain is equal to the value calculated in Step 1.

7.2.2 Solution Technique for Glinka's ESED Method

Glinka's equivalent strain energy density (ESED) method (Molski and Glinka, 1981) is expressed as:

$$\frac{1}{2}\frac{(K_t S)^2}{E} = \int_0^{\varepsilon} \sigma(\varepsilon)\, d\varepsilon \tag{2-21}$$

Equation 2-21 is solved using the following method:

1. Calculate the left side of the equation.
2. Use iteration to find a point on the cyclic stress strain curve such that the integral calculated in Equation 2-21 is equal to the value calculated in Step 1.

7.2.3 Solution Technique for Hoffmann and Seeger's Generalized Method

The method to estimate multiaxial elastic-plastic notch stresses and strains proposed by Hoffmann and Seeger (1985) was described in Chapter 2. The method is comprised of two steps:

1. Relating the applied stress to the equivalent notch stress and strain. The principal elastic stresses at the notch root σ_{e1}, σ_{e2}, σ_{e3}, obtained from an elastic FE analysis are used to calculate the equivalent stress concentration factor K_{tq}. The equivalent notch stress and strain (σ_q and ε_q) are calculated from Neuber's rule.

$$a_e = \frac{\sigma_{e2}}{\sigma_{e1}} \tag{7-1}$$

$$b_e = \frac{\sigma_{e3}}{\sigma_{e1}} \tag{7-2}$$

$$K_{tq} = K_t \sqrt{\frac{1}{2}\left[(1-a_e)^2 + (1-b_e)^2 + (a_e - b_e)^2\right]} \tag{7-3}$$

$$\sigma_q \varepsilon_q = \frac{(K_{tq} S)^2}{E} \tag{7-4}$$

2. Relating the equivalent notch stresses and strains to the principal notch stresses and strains. This is accomplished by using the finite law of Hencky (Equation 2-20). In order to solve the set of equations, it is necessary to make an assumption regarding one of the principal strains. Hoffmann and Seeger (1985) make the assumption that the ratio of principal strains (α) is the same in the elastic and elastic-plastic cases. The solution of Hencky's equations, expressed in terms of the principal strains (ε_1, ε_2), the principal stresses (σ_1, σ_2, σ_3), Poisson's ratio (ν), and the equivalent quantities from step 1 (σ_q, ε_q) is then:

$$\alpha = \frac{\varepsilon_2}{\varepsilon_1} \qquad \textit{(constant)} \tag{7-5}$$

$$\sigma_3 = 0 \qquad \textit{(traction free surface)} \tag{7-6}$$

$$\upsilon' = \frac{1}{2} - \left(\frac{1}{2} - \upsilon\right)\frac{\sigma_q}{E\varepsilon_q} \tag{7-7}$$

$$a = \frac{\sigma_2}{\sigma_1} = \frac{(\varepsilon_2/\varepsilon_1) + \upsilon'}{1 + \upsilon'(\varepsilon_2/\varepsilon_1)} \tag{7-8}$$

$$\sigma_1 = \frac{1}{\sqrt{1 - a + a^2}}\sigma_q \tag{7-9}$$

$$\varepsilon_1 = \frac{1 - \upsilon' a}{\sqrt{1 - a + a^2}}\varepsilon_q \tag{7-10}$$

Equations 7-9 and 7-10 are the notch root stress and strain respectively. In Chapter 6, it was found that the High K_t coupon has a large degree of constraint at the notch root. The Low K_t coupon was found to be in a state of nearly plane stress. As such, the Hoffmann and Seeger method will only be used for the High K_t coupon.

7.3 Sensitivity of Notch Root Stress and Strain

The independent variable in each of the estimation methods presented above, including the FE analysis, is the net section nominal stress. Therefore, the notch root stress and strain are presented as functions of the net section nominal stress for each method.

7.3.1 Low K_t Coupon

The notch root stress and strain results are presented in Figures 7-1 and 7-2, respectively for the Low K_t coupon. Figure 7-1 shows that Neuber's rule provides an adequate

estimation of the notch root stress when compared to the FE results. From the strain results of Figure 7-2, it can be seen that a similar statement can also be made.

When compared to Neuber's rule, Glinka's ESED method predicts a smaller notch root stress and strain for a given value of the net section nominal stress. It would appear that Glinka's ESED method provides a lower bound on the notch root strain. This is consistent with the results of Sharpe *et al.* (1992).

7.3.2 High K_t Coupon

The notch root stress and strain results are presented in Figures 7-3 and 7-4, respectively for the High K_t coupon.

The results of the sensitivity study are quite interesting. In Chapter 2, it was established that Neuber's rule overestimates the notch root strain in a situation where a multiaxial stress state exists. This is certainly evident in this analysis. In addition, Figure 7-3 illustrates that Neuber's rule provides a lower estimate of the notch root stress when compared to the FE results. The Hoffmann and Seeger modification to Neuber's rule (Equation 2-18) provides a reasonable approximation of the multiaxial effect. As was the case with the Low K_t coupon, Glinka's ESED method provides a lower estimate of the notch root stress and strain state when compared to Neuber's rule and the FE results.

7.4 Sensitivity of Crack Initiation Predictions

Local strain crack initiation predictions were made for the trailing edge flap hinge moment sequences. The predictions were made using the IFOSTP standard options, outlined in Chapter 5, and with the McCracken inputs listed in Table 7-1.

Coupon	Spectrum	Turning Points	Reference Value [in*kips]	K_t	DLS [ksi]
Low K_t	tef_man05	17534	200.16	1.41	48.21
	tef_sum05	409380	223.45	1.41	53.60
High K_t	tef_man05	17534	200.16	3.18	23.27
	tef_sum05	409380	223.45	3.18	25.87

Table 7-1: McCracken Inputs for Crack Initiation Sensitivity Study

7.4.1 Low K_t Coupon

Comparisons between the crack initiation predictions and the test results (total life) are presented in Figure 7-5. The results show that predictions made using Neuber's rule to estimate the stress and strain at the notch root are in good agreement with the test results (total life) for both the tef_man05 and tef_sum05 sequences. In addition, the predictions made using the FE results and Glinka's ESED method are nearly identical to those made using Neuber's rule.

7.4.2 High K_t Coupon

Comparisons between the crack initiation predictions and the test results (total life) are presented in Figure 7-6. Unlike the results for the Low K_t coupon, the results for the High K_t coupon show that the predictions made for the tef_man05 and tef_sum05 sequences are very conservative with respect to the test results (total life). In addition, the predictions made using the FE results are "more conservative" than those made using Neuber's rule. This is a surprising result since it was established in Section 7.3.2 that Neuber's rule overestimates the notch root strain for the High K_t coupon when compared to the FE results. Since the number of cycles to failure for each closed hysteresis loop is calculated from the strain-life curve (Figure 5-6), it was expected that predictions made using Neuber's rule would be conservative with respect to predictions made using the FE results.

This result is explained by noting the multiaxial stress state at the notch root of the High K_t coupon, and the use of the Smith-Watson-Topper equivalent strain equation. In Section 7.3.2, it was established that the FE results demonstrate a smaller notch root strain and a larger notch root stress when compared to Neuber's rule. Moreover, the SWT equation modifies the strain amplitude according to Equation 2-5 which is listed here for reference:

$$\left(\frac{\Delta\varepsilon}{2}\right)_{eq} = \sqrt{\frac{\sigma_{max}}{E}\frac{\Delta\varepsilon}{2}} \qquad (2\text{-}5)$$

The net effect of the lower strain and the higher stress for the multiaxial case leads to a larger value of equivalent strain when compared to using Neuber's rule. Hence, predictions made using the FE results for the High K_t coupon will be conservative with respect to predictions made using Neuber's rule.

7.5 Summary

The following summarizes the results of the sensitivity study:

- Neuber's rule provides a reasonable estimation of the notch root stress and strain for the Low K_t coupon.
- The Hoffmann and Seeger modification to Neuber's rule provides adequate estimates of the multiaxial effect for the High K_t coupon.
- For both the Low and High K_t coupons, Glinka's ESED method predicts a lower notch root stress and strain than Neuber's rule and the FE results.
- Crack initiation predictions made using Neuber's rule are in agreement with the test results (total life) for the Low K_t coupon.
- Predictions made for the High K_t coupon are conservative when compared to the test results. Due to notch root multiaxiality and the use of the SWT equation, crack initiation predictions made using the FE results are conservative when compared to those made using Neuber's rule.

- The local strain method displays a considerable difference in predictive capability between the Low and High K_t coupons. A discussion of this point will be made in Chapter 8.

Chapter 8 - Discussion of Results

8.1 Introduction

As stated in the project definition (Chapter 3), the objective of this thesis is to examine the applicability of Neuber's rule in the local strain approach and to assess the ability of the local strain method to predict the lives of the Low and High K_t coupons. With this in mind, it becomes clear that this thesis must answer two questions:

1. Is Neuber' rule applicable for the two coupons presented ?
2. Does the local strain method adequately predict the lives of the two coupons subjected to spectrum loading ?

The discussion of these two questions will be made in the following sections, using results from the studies presented earlier. In addition, a discussion will be made for two other sources of error in the LS approach: material data and equivalent strain equations.

8.2 Applicability of Neuber's Rule

Neuber's rule was derived for a two dimensional state of stress, and has been shown to provide accurate estimations of notch root stress and strain in plane stress situations. Sharpe *et al.* (1992) make the assertion that Neuber's rule is the single best model for

plane stress situations, which was supported by the results for the Low K_t coupon. In the case of the High K_t coupon, a multiaxial stress state exists, hence Neuber's rule is inadequate to describe the notch root response. This result suggests that Neuber's rule should not be used unconditionally, but should be verified by an elastic-plastic finite element analysis when possible. The Hoffmann and Seeger modification to Neuber's rule appears to be a promising way of accounting for the multiaxial stress state at the notch root.

The form of Neuber's rule which does not assume Hooke's Law, Neuber (Nonlinear), is not commonly used in the literature even though it accounts for non-linearity in the net section nominal stress-nominal strain response. In this study, it was found that predictions made with the traditional form of Neuber's rule were closer to the FE results than those made using Neuber (Nonlinear). It is not known if other researchers have observed similar performance of the Neuber (Nonlinear) method.

In this analysis, Glinka's ESED method provided a lower bound on both the notch root stress and notch root strain for the Low and High K_t coupons. The basis for the ESED method is the assumed equivalence between the strain energy density calculated from the elastic and elastic-plastic material laws. This assumption is valid when the local plastic zone is small in comparison with the elastic portion of the material surrounding the notch. Figures 6-7 and 6-13 show that yielding occurs across a significant portion of the net-section as the nominal stress increases. This indicates that the Glinka ESED method may

not be appropriate to use once the net-section nominal stress is greater than the yield stress.

The results of this study suggest that Neuber's rule is adequate for the Low K_t coupon, and Neuber's rule with the Hoffmann and Seeger modification is adequate to estimate the notch root stress and strain of the High K_t coupon. In this study, the method used to estimate the notch root stress and strain has a relatively small effect on the predictions of crack initiation life as demonstrated in Figures 7-5 and 7-6. However, the effect of the notch root stress-strain estimation method in the LS approach is dependent on material, spectra and notch geometry. Variations in these three parameters will yield different results than those presented in this thesis. Therefore, in situations different from those considered in this thesis, it cannot be concluded with certainty that the notch root stress-strain estimation will also have a relatively small effect on the predictions of life to crack initiation. Further study involving different coupon geometries, spectra and material would provide insight into the effect of notch root stress-strain estimation on the prediction of crack initiation life.

8.3 Agreement between LS Predictions and Test Results

8.3.1 Introduction

The results of the sensitivity study presented in Chapter 7 display a large difference in the capability of the local strain method to predict the lives of the Low K_t and High K_t coupons subjected to the trailing edge flap hinge moment sequences. In short, crack initiation predictions made for the Low K_t coupon are in agreement with the test results (total life), while the predictions made for the High K_t coupon are extremely conservative

with respect to the test results. This raises the question of why the local strain method is able to predict the lives of the Low K_t coupons and not able to predict as well for the High K_t coupons. This point will be discussed in terms of the observed behaviour of the coupons with respect to crack initiation life versus total life, and in terms of the fatigue concentration factor. In addition, a method to calculate total life will be presented which includes a definition of the size of a crack at initiation.

8.3.2 Crack Initiation vs. Total Life

The coupon tests described in Chapter 4 were part of a program at SMPL-IAR to study the relative effects of truncation on life and were not directly aimed at correlating test lives with predictions. For the purpose of this thesis, the assumption was made initially that the crack initiation phase comprised a very large portion of the total life. During the course of the testing, attempts were made to "catch" the crack initiation of the coupons by visual observation.

For the Low K_t coupon, the attempt to "catch" the crack initiation was in part unsuccessful, as a crack was never observed during testing. However, notes were made at intervals during testing of when these inspections were made which allows the time to initiation to be estimated. The last recording of this information for the coupons listed in Table 8-1 indicates that the crack propagation phase is small, and could be smaller than 9% of the total life in the case of specimen 077, and smaller than 26% in the case of specimen 311. At the time this information was recorded, no visible cracks were present in the coupons, indicating that the crack "initiated" after these recordings were taken.

Specimen	Last record of turning points applied	Turning points at failure	Life remaining after last record
077	4153094	4571310	9%
311	3582825	4869689	26%
239	3186407	3996903	20%

Table 8-1: Indication of Crack Propagation Phase for Low K_t Coupons

In the case of the High K_t coupon, visible cracks were detected after they had grown across the net section of the coupon. Table 8-2 lists the approximate crack length, number of turning points applied to the coupons at first detection of the crack, and percent life remaining (based on the number of turning points at failure). The High K_t case is very different from the Low K_t situation in that cracks were visibly seen and propagated for a significant portion of the total lives of the coupons. The total amount of time spent propagating the cracks is not known since the number of cycles to initiation was not isolated.

Specimen	Number of turning points applied	Crack length [in] (from notch root)	Life Remaining [%]
377	1244914	0.3125	10.5
436	1255994	0.3125	15.1
407	5857764	0.208	12.5
472	5217399	0.208	10.1
395	5898705	0.156	14.0

Table 8-2: Crack Length at First Detection for High K_t Coupons

Experimental observations suggest that the crack propagation phase of the Low K_t coupon accounts for a very small portion of the total life. In the case of the High K_t coupon, observations suggest that the crack propagation phase accounts for a significant portion of the total life. These observations are supported by a limited fracture mechanics study of the coupons using the FRANC2D/L crack propagation simulator (James and Swenson, 1997). The FRANC2D/L program is a two-dimensional finite element program which uses a regenerative meshing algorithm to propagate a crack using linear elastic fracture mechanics (LEFM). A crack with length 0.01" (0.254 mm) was placed at the notch root of both coupons. Using the simulator, the stress intensity factor at the crack tip was plotted versus crack length as measured from the notch root for both the Low and High K_t coupons. The results of this study, presented in Figure 8-1, show that the Low K_t coupon has a much larger stress intensity at the crack tip than the High K_t coupon for a

given crack length. As a result, the Low K_t coupon would experience a shorter crack propagation stage than the High K_t coupon, consistent with observed behaviour.

8.3.3 Fatigue Concentration Factor

In Chapter 2, the fatigue concentration factor was discussed as a method of improving local strain predictions by accounting for size effects in sharp notches. The most direct and reliable way to determine K_f is by experiment (Weixing *et al.*, 1995). However, an attempt of such magnitude was not feasible during the course of this research program due to time and economic constraints. The problem with using empirical formulae to calculate K_f is that they require material constants which can only be calculated from data for smooth and notched specimens available from previous tests. In addition, data may not be available for the specific material in question. An estimate of the material constant for the Peterson formula was given as 0.025" (0.635 mm) for aluminum alloys (Peterson, 1959).

The values of K_f calculated from Equation 2-23 for the Low and High K_t coupons are listed in Table 8-3.

Coupon	K_t	K_f (Peterson)
Low K_t	1.41	1.39
High K_t	3.18	2.82

Table 8-3: Fatigue Concentration Factors for Low and High K_t Coupons

The K_f value for the Low K_t coupon is very close to the K_t value, resulting in little difference in predicted life. The use of K_f instead of K_t in the local strain predictions for the High K_t coupons result in larger predictions of life when plotted on the K*DLS curve of Figure 7-6. The predictions are more in line with the test results for total life. This result is consistent with the observations of Topper *et al.* (1969), who showed that measured notched fatigue lives (initiation + propagation) and lives predicted from smooth specimens agree within a factor of 2 when K_f is used in place of K_t in Neuber's rule.

The apparent success of this method is questionable since there is no way of knowing how applicable the material constant "a" is for the material used in this analysis. The value of 0.025" (0.635 mm) is supposedly constant for all aluminum alloys according to Peterson (1959). Topper *et al.* (1969) use a value of 0.028" (0.711 mm) for both 2024 and 7075 aluminum alloys. Efforts to obtain other values for aluminum were unsuccessful. The majority of data available for the calculation of K_f are for steels and are given in references such as the SAE Fatigue Design Handbook (1988).

Another concern with the use of K_f is that the stress and strain estimation at the notch root is altered. Using K_f instead of K_t in both Neuber's rule and Glinka's ESED method results in smaller predictions of the notch root stress and strain. The FE analyses presented in Chapter 6 cannot be modified to represent the stress concentration by K_f instead of K_t, leading to an important consequence of this method: the stress and strain

experienced by the notch root of the coupons in testing will be larger in magnitude than the stress and strain predicted by Neuber's rule with K_f for local strain predictions.

Furthermore, the notion put forth by Bannantine *et al.* (1990) that the use of K_f is an empirical method to account for crack propagation in sharp notches cannot be dispelled. The basis for the use of K_f in place of K_t is the observed difference in the fatigue strengths of smooth and notched specimens. The fatigue strength of the notched specimen is taken as the stress level to cause failure at 10^7 cycles. In the case of the notched specimen, the crack propagation stage may comprise a significant portion of the total life. Hence, K_f inherently includes a first order consideration of the crack propagation in the specimens used to generate the "notched specimen" S-N data.

The use of K_f in the LS approach is questionable when considering the above discussion. In the case of the High K_t coupon, crack propagation was observed to be a significant portion of the total life. Therefore, crack propagation must be taken into account to obtain an accurate estimate of total life for the High K_t coupon. A method to predict total life, consisting of initiation and propagation is discussed in the next section along with a definition of the size of the crack at "initiation".

8.3.4 Estimating Total Life

Several authors have supported the notion that crack propagation analyses must be performed to obtain an accurate estimate of total life as the severity of a notch increases. Nelson and Socie (1982) indicate that in some cases crack growth analyses are required to

properly assess the component fatigue life, while in other cases such as blunt notches, crack initiation analyses alone are sufficient.

Dowling (1979) noted that the differing strain gradients between smooth and notched specimens will cause error in local strain predictions if a significant portion of life considered as initiation is actually spent in crack growth. Dowling proposed that a definition of initiation as a crack of sufficiently small size overcomes this problem. Crack initiation analyses are valid until a crack reaches the initiation size, and propagation analyses are performed from the initiation size to failure. The proposed initiation size is derived from fracture mechanics and has the following form:

$$l' = \frac{c}{(1.12 \cdot K_t / F)^2 - 1} \tag{8-1}$$

where F is a dimensionless function of geometry and c is the notch depth. The value of F can be found from handbooks listing stress intensity factors such as the one by Tada *et al.* (1978). For moderate to sharp notches, the value of l' falls in the range of r/4 to r/20. For the Low K_t coupon, the value of l' is approximately 0.05" (1.27 mm), whereas for the High K_t coupon, the value is approximately 0.01" (0.254 mm).

Dowling demonstrated that combined initiation/propagation predictions were in excellent agreement with test results for the initiation and total life of blunt and sharply notched coupons made from AISI 4340 steel.

Dowling's approach shows promise since the notch size effect is considered in a more rigorous manner than in the method which considers K_f instead of K_t, namely, the crack propagation out of the highly stressed volume of material at the notch root. When used in conjunction with crack initiation and growth measurements, this method would prove useful in predicting total life in fatigue test programs such as the spectrum truncation sensitivity studies at SMPL-IAR.

8.4 Material Properties

One source of error common to all fatigue predictions methods is the applicability of the material data used. In this study, it is not known how well the C_CI89 materials database models the behaviour of the materials and forms used at SMPL-IAR. ASTM Standard E 606-92 (ASTM, 1995) describes the standard practice for strain-controlled fatigue testing, and lists recommended requirements when reporting data. The requirements include: material and specimen description; description of equipment, testing environment, testing conditions and procedures; and finally, the test results for the cyclic stress-strain and strain-life properties. A similar reporting scheme was used by Endo and Morrow (1969) in their study on cyclic stress-strain and fatigue behaviour of representative aircraft metals. By contrast, the C_CI89 materials database only includes the cyclic stress-strain and strain-life curves for the materials.

Even though this is the case, no logical reason exists to use data from other sources (Straznicky, 1996). The values of the material fatigue properties are only one factor

contributing to the inaccuracy of the local strain predictions. Therefore it cannot be decided without support from a detailed study that the use of one particular data set will provide the best agreement with experimental results.

The C_CI89 materials database contains strain-life data for aluminum 7050-T74 in prestrain and non-prestrain conditions. The difference between the prestrain and non-prestrain data for aluminum 7050-T74 is shown in Figure 5-6. The effect of the prestraining reduces the cycles to failure for a given strain amplitude. Figure 8-2 shows predictions made for the Low K_t coupon subjected to the tef_man05 sequence using the prestrain and non-prestrain material data. The prestrain predictions are closer to the test results, while the non-prestrain predictions are non-conservative with respect to the test results. This limited study suggests that the prestrain data should be used to account for the influence of large cycles on the following smaller ones in variable amplitude loading. The use of strain-life data generated with periodic overloads seems to be a promising approach when considering the damage accumulation problem described in Chapter 2. However strain-life data generated with periodic overloads is not available in the literature for the material considered in this thesis. In general, such data is only available for specific research studies.

8.5 Equivalent Strain Equations

In Chapter 7, it was demonstrated that the LS predictions made using the FE results for the High K_t coupon were conservative with respect to the predictions made using Neuber's rule. This was explained in terms of the multiaxial stress state at the notch root

of the High K_t coupon and the use of the SWT equivalent strain equation. Even though the SWT equation is commonly used in the literature, for example by Bergmann *et al.* (1979), the inclusion of the SWT equation in the LS predictions for this study must be justified. Figure 8-3 presents LS predictions for the High K_t coupon subjected to the tef_man05 sequence. The predictions were made using the FE results and for the following equivalent strain equations: SWT, LOOPIN8, Modified Goodman, Gerber, and Soderberg. The prediction made using Neuber's rule with the SWT equation is plotted for reference on Figure 8-3. The results show a large difference between the use of the SWT equation and the LOOPIN8 and Gerber equations. According to Bannantine *et al.* (1990), the Soderberg equation is seldom used since it is considered to be conservative, while test results generally fall between the Goodman and Gerber curves. Forness *et al.* (1989) recommend the use of the SWT equation due to its independence from empirically derived constants as in the case of the LOOPIN8 equation. In addition, the SWT equation becomes undefined when $\sigma_{max}<0$, indicating that the SWT equation predicts zero damage for a closed hysteresis loop that is fully compressive. For the other equations presented, this condition must be imposed, while for the SWT equation, the condition is "built-in". For this study, the SWT equation has shown good agreement with test results for the Low and High K_t coupons, and should continue to be used in IFOSTP.

Chapter 9 - Conclusions

9.1 Conclusions

This thesis analyzed the applicability of Neuber's rule in local strain crack initiation predictions. In addition, the ability of the local strain method to predict the lives of the two coupons used in this study was assessed. Based on the research performed for this thesis, the following conclusions are drawn:

1. Local strain crack initiation predictions contain a number of assumptions which can lead to considerable error. Two particular areas of concern identified in this study are the damage accumulation problem and the principle of equivalence. The damage accumulation problem arises from predicting the fatigue behaviour in spectrum loading by linear damage accumulation calculated from smooth specimen constant amplitude strain-life data (at R_σ=-1). Concerns with the principle of equivalence include determination of stress and strain at the notch of an engineering component, and the effect of notch severity on fatigue life.

2. The notch root of the Low K_t coupon is very close to a state of plane stress. The notch root of the High K_t coupon is constrained, leading to a multiaxial stress state.

3. Neuber's rule is adequate to predict the notch root stress and strain of the Low K_t coupon. In the case of the High K_t coupon, the Hoffmann and Seeger modification to Neuber's rule provides adequate estimates of the notch root stress and strain. If possible, elastic-plastic FE analyses should be performed to verify the applicability of Neuber's rule in fatigue test programs.

4. Experimental observations and a limited fracture mechanics study suggest that the crack propagation phase in the Low K_t coupon is small, whereas in the High K_t coupon, it could account for a significant portion of the total life.

5. Local strain predictions for the trailing edge flap hinge moment sequences demonstrate a large difference in predictive capability between the Low and High K_t coupons. This is due to the differing crack propagation phases in these coupons.

6. Although the fatigue concentration factor provides local strain predictions which are closer to the test results (total life) for the High K_t coupon, its use is questioned for three reasons: the availability and applicability of material data; the modification of the stress-strain estimation which results from the use of K_f; and the empirical manner in which this method accounts for the crack propagation phase in sharply notched coupons.

7. A method to predict total life (initiation and propagation) has been identified which accounts for the notch size effect in a more rigorous manner than in the method which uses the local strain approach with the fatigue concentration factor.

9.2 Recommendations for Future Research

The following is proposed for future research in the area of the prediction of fatigue crack initiation:

1. Isolate crack initiation and monitor crack growth in future coupon test programs at SMPL-IAR with the intent of estimating total life using the combined initiation/propagation approach identified in this study.

2. Develop an in-house materials database for the materials appropriate to the specific CF-18 locations under study. Although this is a large undertaking, any uncertainty in using C_CI89 material data at SMPL-IAR would be removed. This effort should ideally include the development of non-prestrain, prestrain and periodically overloaded strain-life data in addition to the development of cyclic stress-strain properties.

3. Study the problem of damage accumulation in the local strain approach. This would provide insight into the problem of predicting the fatigue behaviour in spectrum loading by linear damage accumulation calculated from constant amplitude strain-life data. The study should include damage parameters and non-linear damage rules, both of which may better represent the fatigue damage under spectrum loading.

4. Study the growth of microstructural flaws to characterize crack initiation at notches. The behaviour of such flaws requires the use of Elastic-Plastic Fracture Mechanics.

9.3 Summary of Contributions

This thesis has made the following contributions to the general knowledge in the field of the prediction of fatigue crack initiation:

1. The applicability of Neuber's rule to plane stress situations was verified by an elastic-plastic finite element analysis.

2. A method of estimating multiaxial elastic-plastic notch stresses and strains was verified to be an effective means of accounting for notch root multiaxiality.

References

American Society for Testing and Materials (ASTM). (1995). Standard E 606-92. Standard Practice for Strain-Controlled Fatigue Testing.

American Society for Testing and Materials (ASTM). (1995). Standard E 1049-85. Standard Practices for Cycle Counting in Fatigue Analysis

Bannantine, J.A., Comer, J.J., Handrock, J.L. (1990). Fundamentals of metal fatigue analysis. Englewood Cliffs, NJ, U.S.A.: Prentice-Hall Inc.

Baotong, L., Xiulin, Z. (1993). An approach for predicting fatigue crack initiation life of a low alloy steel below room temperature. Engineering Fracture Mechanics, 46 (2), 339-346.

Bergengren, Y., Gustavsson, A., Larsson, M., Melander, A., Bork, C.P., Golmann, M., Hünecke, J., McDowell, D.L. (1993). Fatigue properties under constant and variable amplitude loading of notched fatigue specimens of a high strength sheet steel (Report No. IM-3121). Stockholm, Sweden: Swedish Institute for Metals Research.

Bergmann, J., Seeger, T., Weisgerber, D., Sippel, K.O. (1979). The sensitivity of the local approach to the quality of input data in the fatigue service life prediction of aircraft components. Proceedings of the International Symposium on the Low-Cycle Fatigue Strength and Elasto-Plastic Behaviour of Metals, Stuttgart, 1979, 301-317.

Bleuzen, C., Chaudonneret, M., Farcy, L., Flavenot, J.F., Ranganathan, N. (1994). Fatigue testing and life prediction for notched specimens of 2024 and 7010 alloys subjected to aeronautical spectra. In C. Amzallag (Ed.), Automation in Fatigue and Fracture: Testing and Analysis, ASTM STP 1231 (pp. 508-530). Philadelphia, PA, U.S.A.

Broek, D. (1989). The practical use of fracture mechanics. Dordrecht, The Netherlands: Kluwer Academic Publishers.

Buch, A. (1980). Verification of fatigue crack initiation life prediction results (TAE No. 400). Haifa, Israel: Israel Institute of Technology.

Conle, A., Topper, T.H. (1980). Overstrain effects during variable amplitude service history testing. International Journal of Fatigue, 2 (3), 130-136.

Doerfler, M.T. (1997). An evaluation of service life analysis of metallic airframe structure with MSC/FATIGUE. MacNeal-Scwendler Corporation Website, Paper 3397. Website: http://www.macsch.com/aerospace/

Dowling, N.E. (1979). Notched member fatigue life predictions combining crack initiation and propagation. Fatigue of Engineering Materials and Structures, 2, 129-138.

DuQuesnay, D.L., MacDougall, C., Dabayeh, A., Topper, T.H. (1995). Notch fatigue behaviour as influenced by periodic overloads. International Journal of Fatigue, 17 (2), 91-99.

Endo, T., Morrow, J. (1969). Cyclic stress-strain and fatigue behaviour of representative aircraft metals. Journal of Materials, 4 (1), 159-175.

Engineering Sciences Data Unit (ESDU). (1983). Elastic stress concentration factors geometric discontinuities in flat bars or strips of isotropic materials, Item No. 69020.

Forness, S.D., McFarland, J.L., Meyer, E.S., O'Neill, J.W. (1989). Final Report: Structural methods standardization team number 8, Task: Crack initiation. McAir.

Foster, W.A. (1993). An investigation into the fatigue crack initiation program C_CI89 (Technical Note 45). Melbourne, Australia: Department of Defense, Defense Science and Technology Organisation, Aeronautical Research Laboratory.

Glinka G., Newport, A. (1987). Universal features of elastic notch tip stress fields. International Journal of Fatigue, 9 (3), 143-150.

Glinka G., Ott W., Nowack H. (1988). Elasto-plastic plane strain analysis of stresses and strains at the notch root. Journal of Engineering Materials and Technology, 110 (3), 195-204.

Heitmann, H., Neumann, P., Vehoff, H. (1983). Random load fatigue of steels: service life prediction based on the behaviour of micro-cracks. Proceedings of the International Conference on the Application of Fracture Mechanics to Materials and Structures, Freiburg, FRG, 1983.

Heuler, P., Schütz, W. (1986). Assessment of concepts for fatigue crack initiation and propagation life prediction. Journal of Materials Technology, 17 (11), 397-405; 17 (12), 449-456.

Hewitt, R.L., Hiscocks, R.J., Bernard, G. (1996). Load spectrum determination for an aircraft with a digital flight control system - CF-18 centre fuselage example. Canadian Aeronautics and Space Journal, 42 (1), 5-9.

Hibbit, Karlsson & Sorensen (HKS) Inc. (1997). ABAQUS/Standard User's Manual, Vol. I-III, Version 5.7.

Hoffmann M., Seeger T. (1985). A generalized method for estimating multiaxial elastic-plastic notch stresses and strains, Parts 1 and 2. Journal of Engineering Materials and Technology, Transactions of the ASME, 107, 250-260.

James, M., Swenson, D. (1997). FRANC2D/L: A crack propagation simulator for plane layered structures, Short user's guide version 1.4.

Kähönen A. (1991). FEM and fatigue life calculation using the PC-based NISA II/ENDURE software package (Report No. 735). Espoo, Finland: Technical Research Centre of Finland.

Klohr, J.D. (1990). Computer program documentation for C_CI89. McDonnell Aircraft Company.

Manson S., Hirschberg M. (1966). Crack initiation and propagation in notched fatigue specimens. Proceedings of the First International Conference on Fracture, Vol. 1, 1966.

Massing, G. (1926). Proceedings of the 2nd International Congress on Applied Mechanics, Zurich, 1926.

Miller, K.J. (1987). The behaviour of short fatigue cracks and their initiation, Part II - A general summary. Fatigue and Fracture of Engineering Materials and Structures, 10 (2), 93-113.

Molski K., Glinka G. (1981). A method of elastic-plastic stress and strain calculation at a notch root. Materials Science and Engineering, 50 (1), 93-100.

Nelson, D.V., Socie, D.F. (1982). Crack initiation and propagation approaches to fatigue analysis. In P.R. Abelkis & C.M. Hudson (Eds.), Design of Fatigue and Fracture Resistant Structures. ASTM STP 761 (pp. 110-132). Philadelphia, PA, U.S.A.

Neuber H. (1961). Theory of stress concentration for shear-strained prismatical bodies with arbitrary nonlinear stress-strain law. Journal of Applied Mechanics, Transactions of the ASME, 28 (4), 544-550.

Nie H., Wu F.M., Liu J.F. (1994). A variable K_f - Neuber's rule for predicting fatigue crack initiation life. Fatigue & Fracture of Engineering Materials & Structures, 17 (9), 1015-1023.

Peterson R.E. (1959). Notch-sensitivity. In Sines & Waisman (Eds.), Metal Fatigue (pp. 293-306). New York, U.S.A.: McGraw-Hill.

Pilkey, W. (1994). Formulas for stress, strain, and structural matrices. New York, U.S.A.: John Wiley & Sons Inc.

Porter, P.G. (1983). A rapid method to predict fatigue crack initiation Volume II - computer program user's instructions. Northrop Corporation - Aircraft Division.

Schütz, W. (1979). The prediction of fatigue life in the crack initiation and propagation stages - a state of the art survey. Engineering Fracture Mechanics, 11 (2), 405-421.

Seeger T., Beste A., Amstutz H. (1977). Elastic-plastic stress-strain behaviour of monotonic and cyclic loaded notched plates. Proceedings of the 4th International Conference on Fracture, Waterloo, ON., Canada, June 1977, 943-951.

Sharpe W.N., Yang C.H., Tregoning R.L. (1992). An evaluation of the Neuber and Glinka relations for monotonic loading. Journal of Applied Mechanics, Transactions of the ASME, 59 (2), S50-S56.

Simpson, D.L. (1997). Review of Canadian aeronautical fatigue work 1995-1997 (Report No. LTR-ST-2094). Ottawa, ON., Canada: National Research Council Canada, Institute for Aerospace Research.

Smith, K.N., Watson, P., Topper, T.H. (1970). A stress-strain function for the fatigue of metals. Journal of Materials, 5 (4), 767-778.

Society of Automotive Engineers (SAE), Inc. (1988). SAE Fatigue design handbook AE-10 (2nd ed.).

Straznicky, P. (1996). Effect of low amplitude cycles in spectrum loading (Report No. IAR-CR-31). Ottawa, ON., Canada: National Research Council Canada, Institute for Aerospace Research.

Tada, H., Paris, C., Irwin, G. (1978). The stress analysis of cracks handbook. St. Louis, U.S.A.: Del Research Corporation.

Tipton S. (1991). A review of the development and use of Neuber's rule for fatigue analysis. SAE Transactions, 100 (5), 143-148.

Topper T., Wetzel R., Morrow J. (1969). Neuber's rule applied to fatigue of notched specimens. Journal of Materials, 4 (1), 200-209.

Tregoning R.L. (1992). Elasto-plastic notch root strains: Measurements versus finite-element predictions. Experimental Techniques, 16 (6), 41-45.

Umeda H., Sakane M., Ohnami M. (1987). Comparison of local strain at the notch root between FEM analysis and experimental strain measurement under creep-fatigue conditions, JSME International Journal, 30 (268), 1543-1550.

Walker E.K. (1977). Multiaxial stress-strain approximations for notch fatigue behaviors. Journal of Testing and Evaluation, 5 (2), 106-113.

Weiss, J., Note to Tuegel, E., 22 April, 1997.

Weixing, Y., Kaiwuan, X., Yi, G. (1995). On the fatigue notch factor, K_f. International Journal of Fatigue, 17 (4), 245-251.

Young, W.C. (1989). Roark's formulas for stress & strain (6^{th} ed.). New York, U.S.A.: McGraw-Hill.

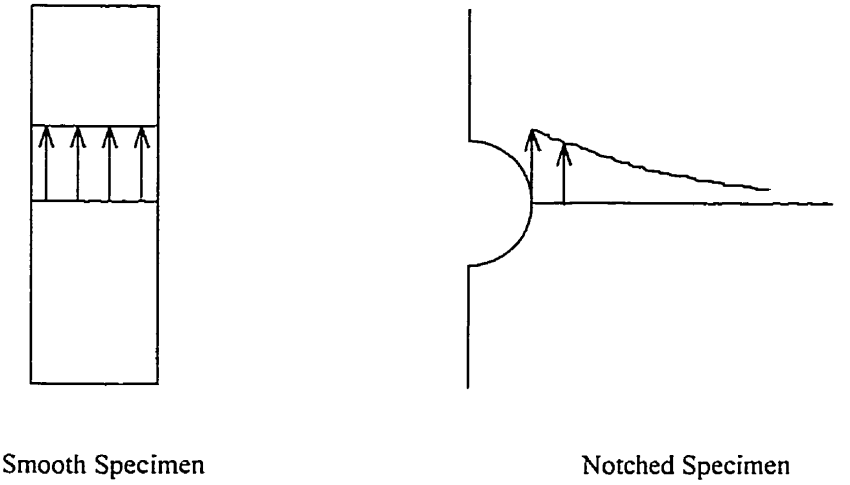

Figure 2-1: Equivalence between Smooth and Notched Specimens

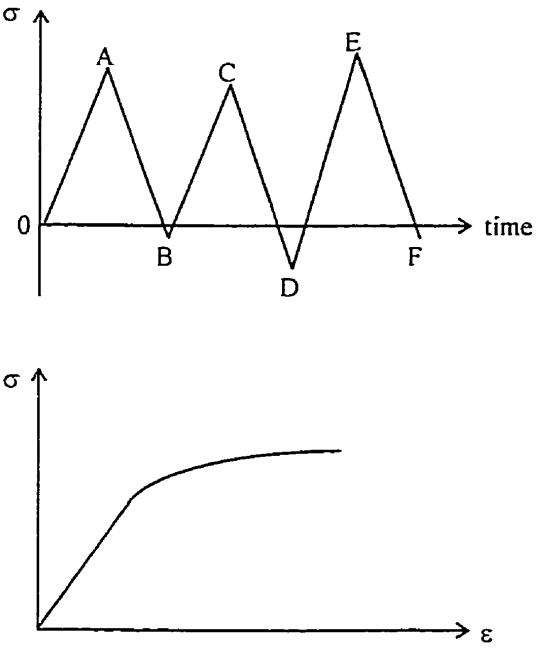

Figure 2-2: Local Strain Method - Load Spectrum and Cyclic Stress-Strain Curve

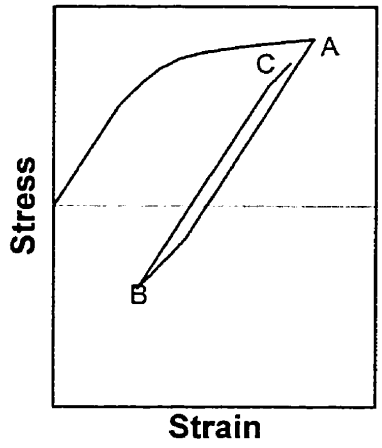

[A]

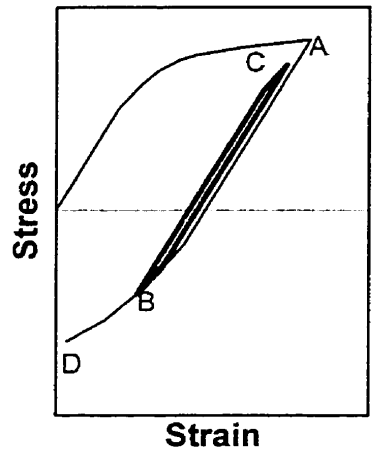

[B]

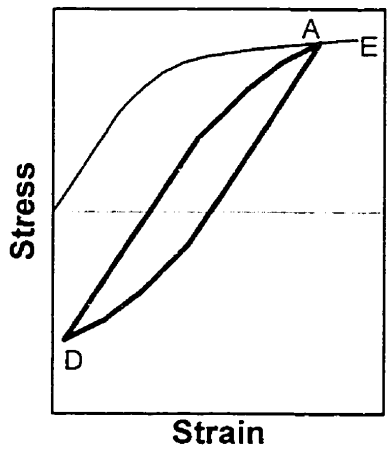

[C]

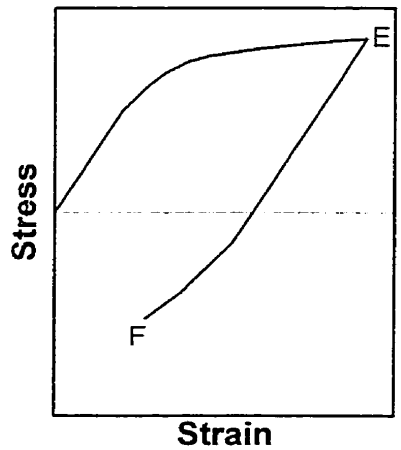

[D]

Figure 2-3: Local Strain Method - Hysteresis Loop Tracking

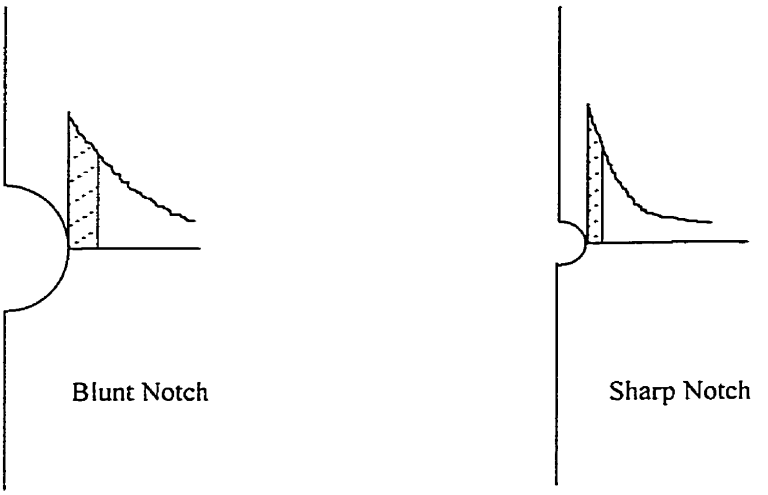

Figure 2-4: Volume of Critically Stressed Material at Blunt and Sharp Notches

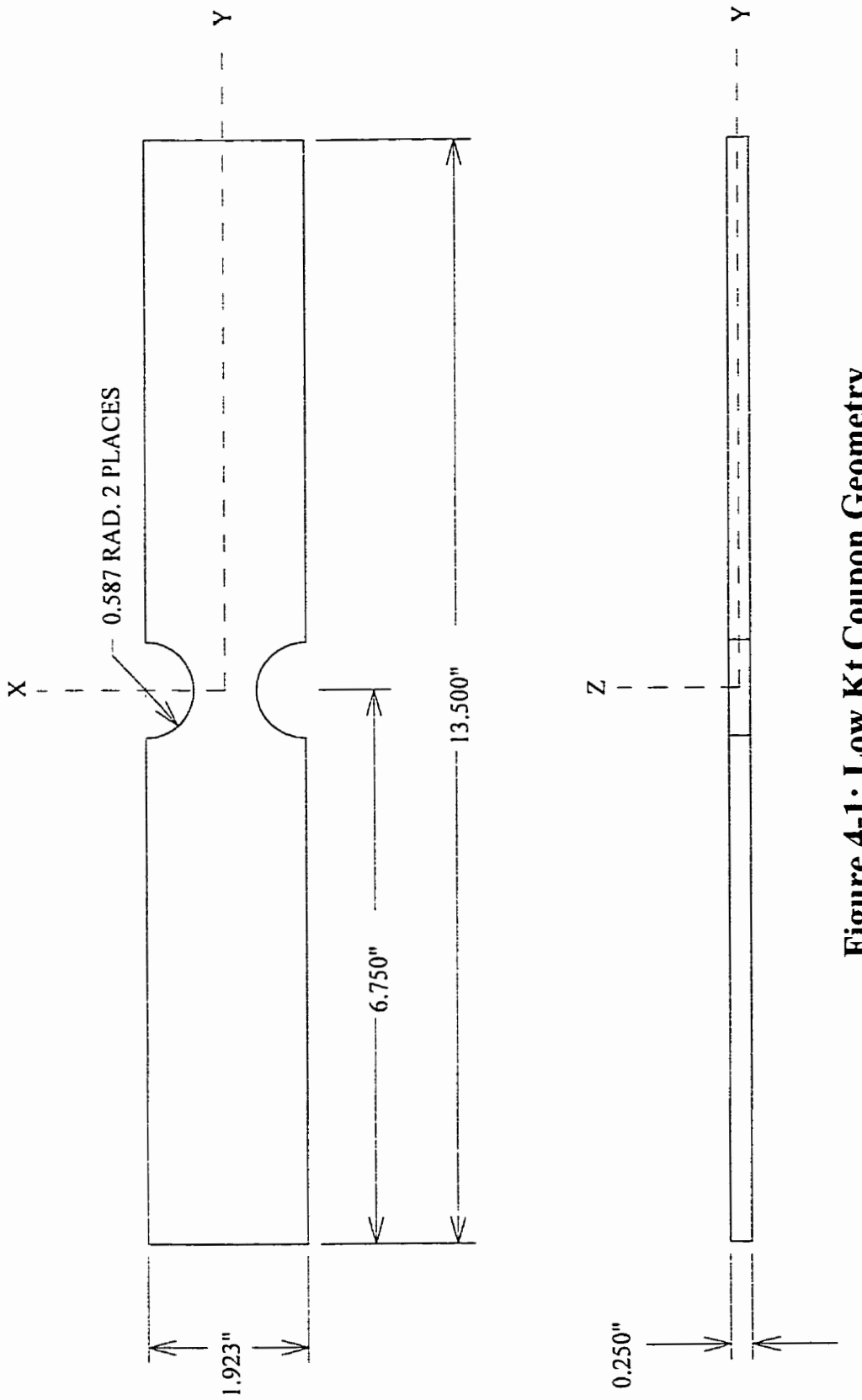

Figure 4-1: Low Kt Coupon Geometry

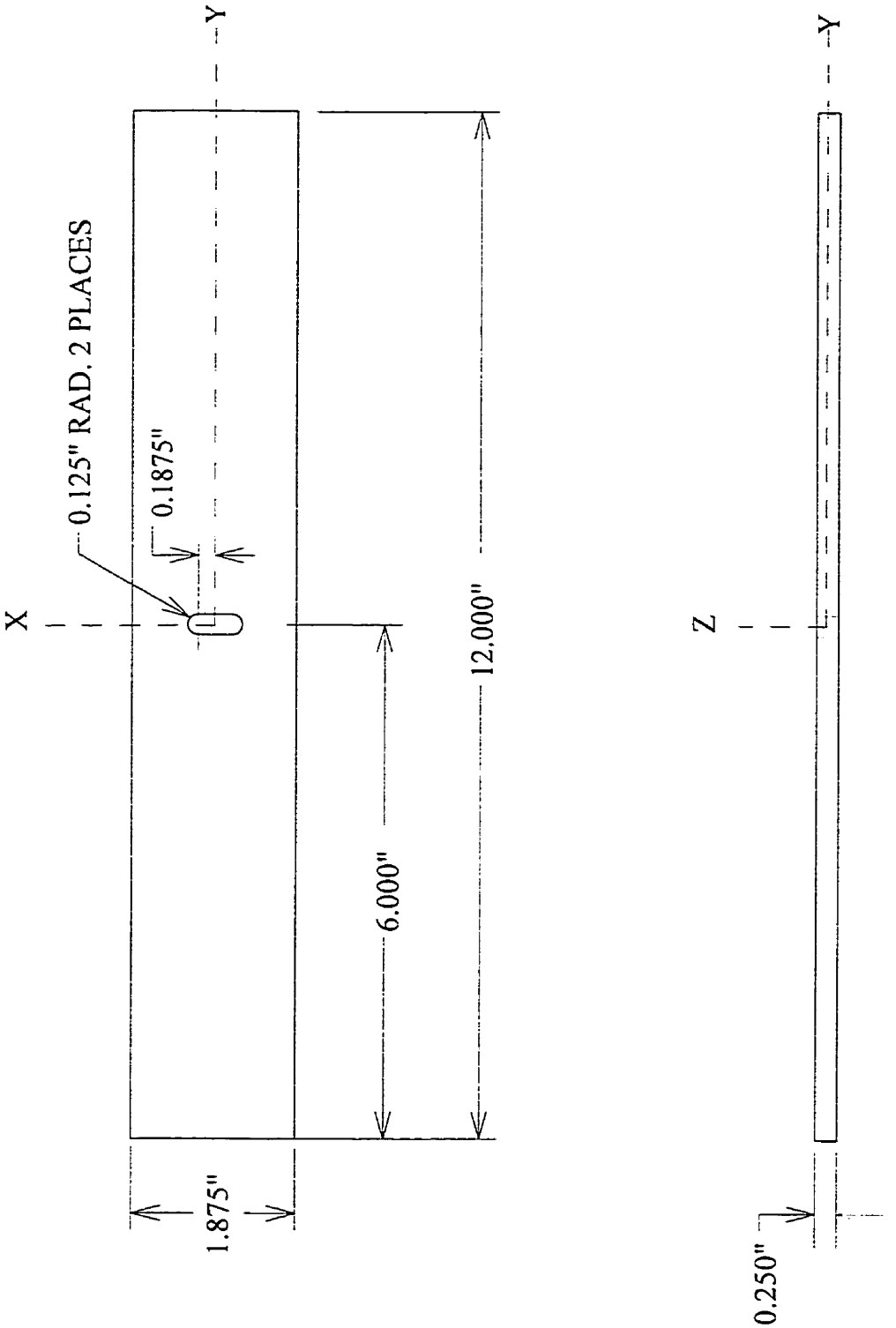

Figure 4-2: High Kt Coupon Geometry

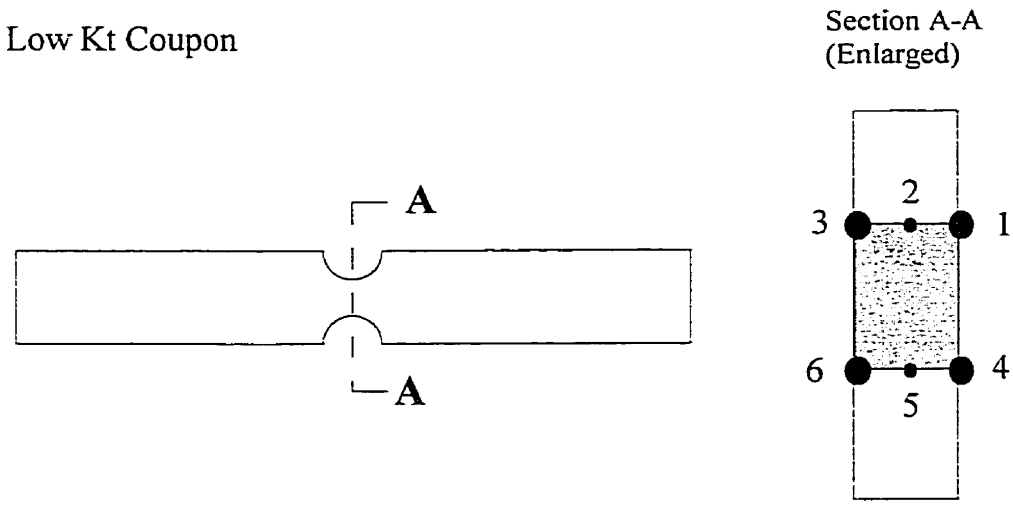

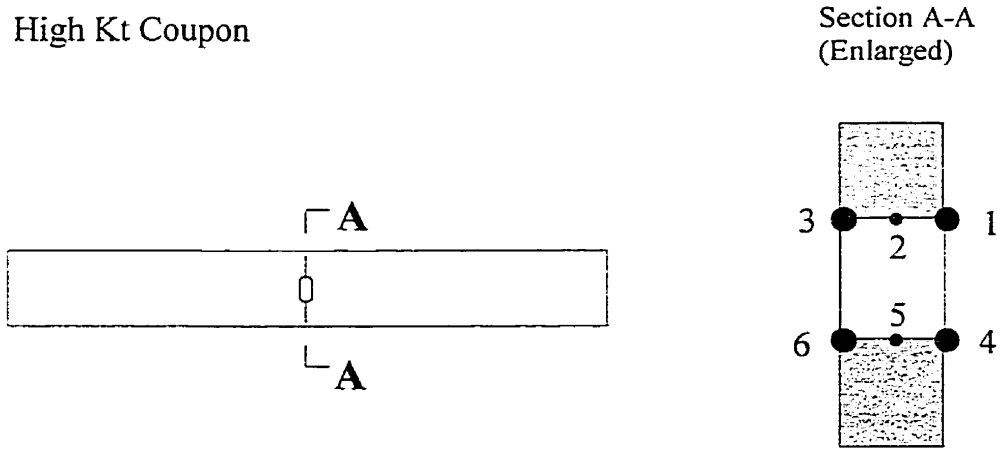

Figure 4-3: Possible Crack Initiation Sites

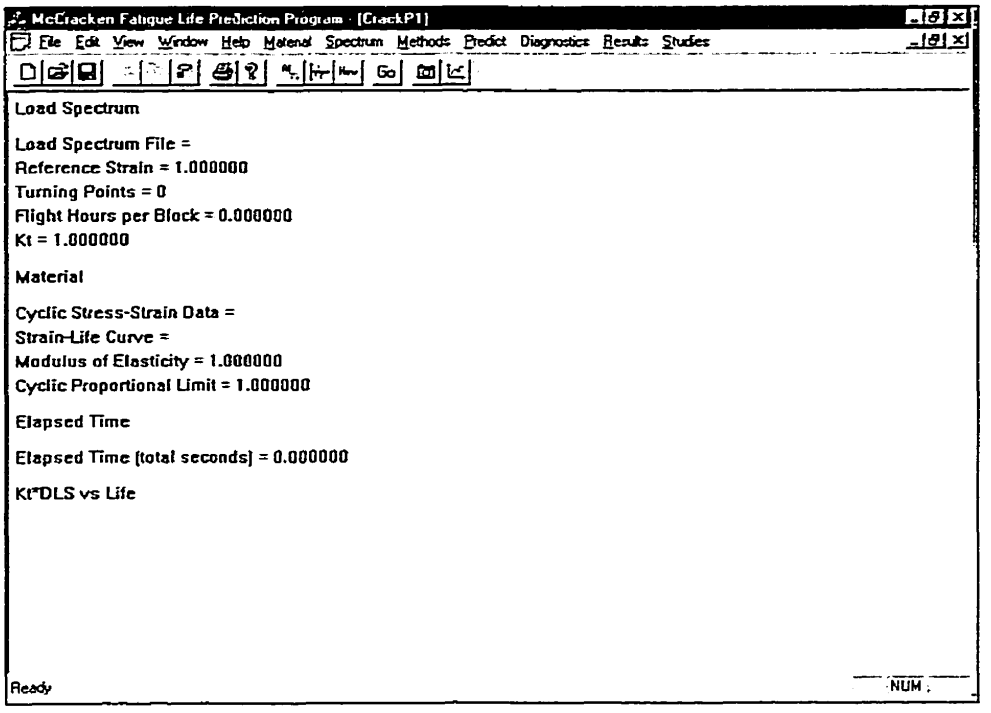

Figure 5-1: McCracken Prediction Environment

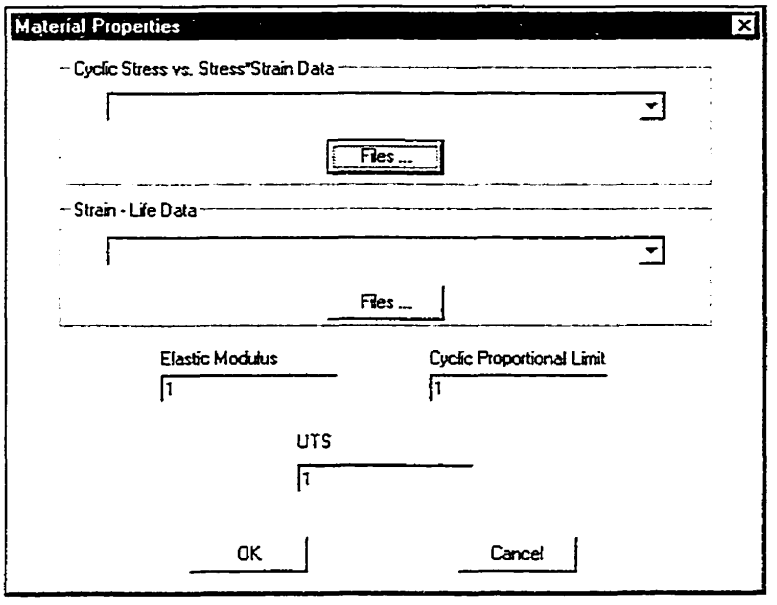

Figure 5-2: Material Properties Dialog Box

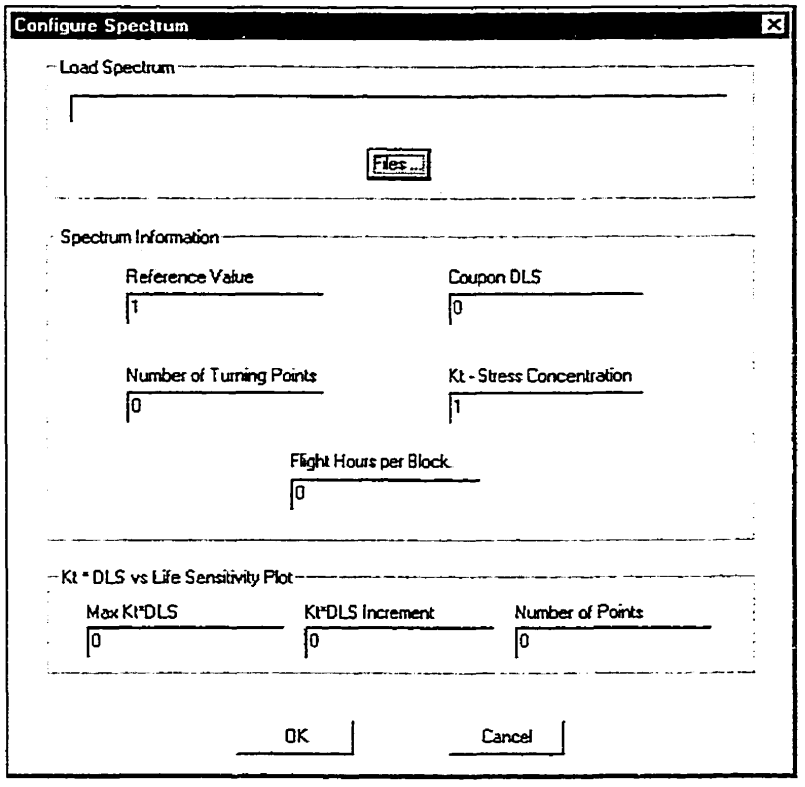

Figure 5-3: Spectrum Dialog Box

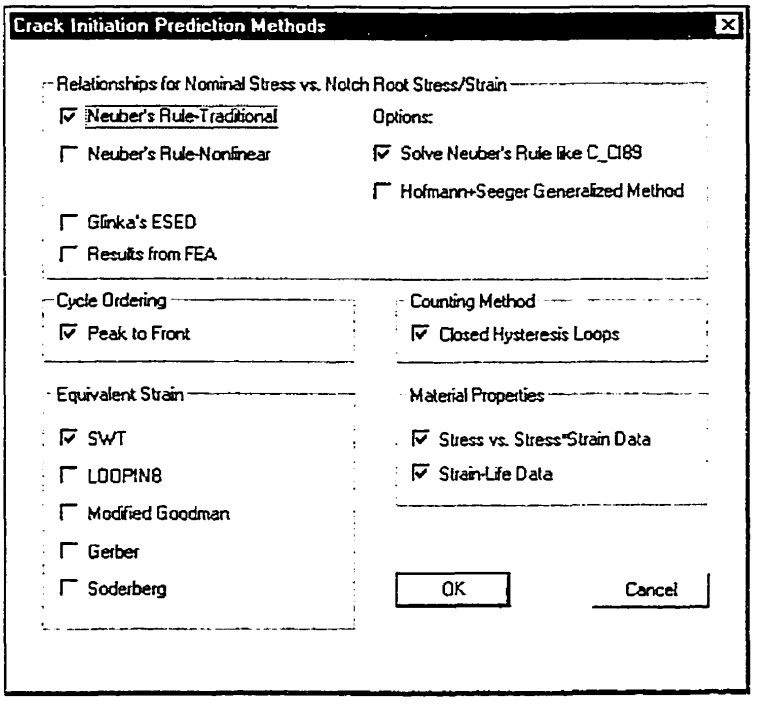

Figure 5-4: Prediction Methods Dialog Box

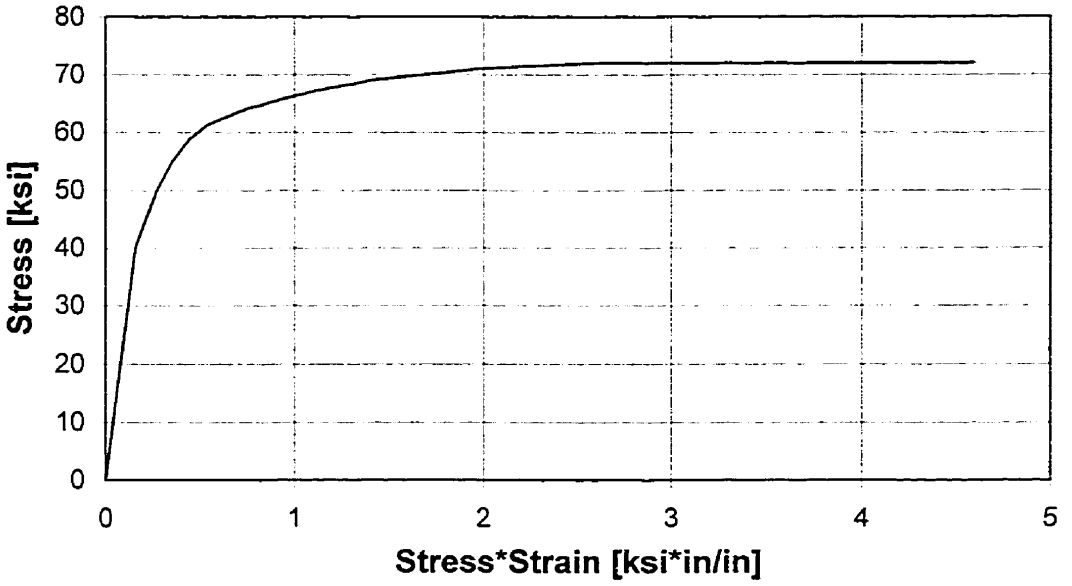

Figure 5-5: Cyclic Stress vs. Stress*Strain Curve - Al 7050-T74

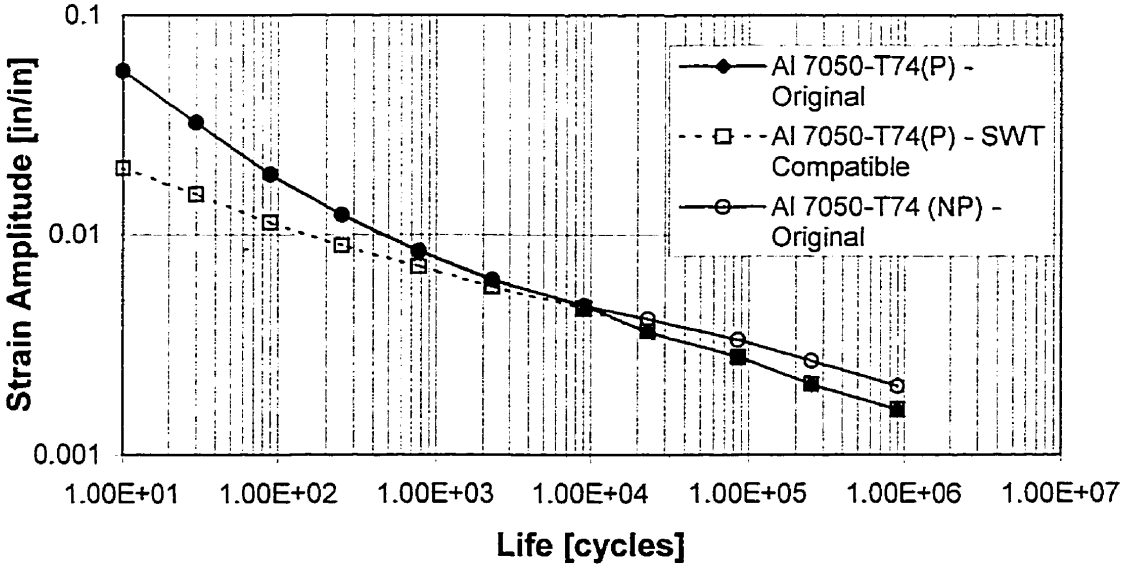

Figure 5-6: Strain-Life Curve - Al-7050-T74

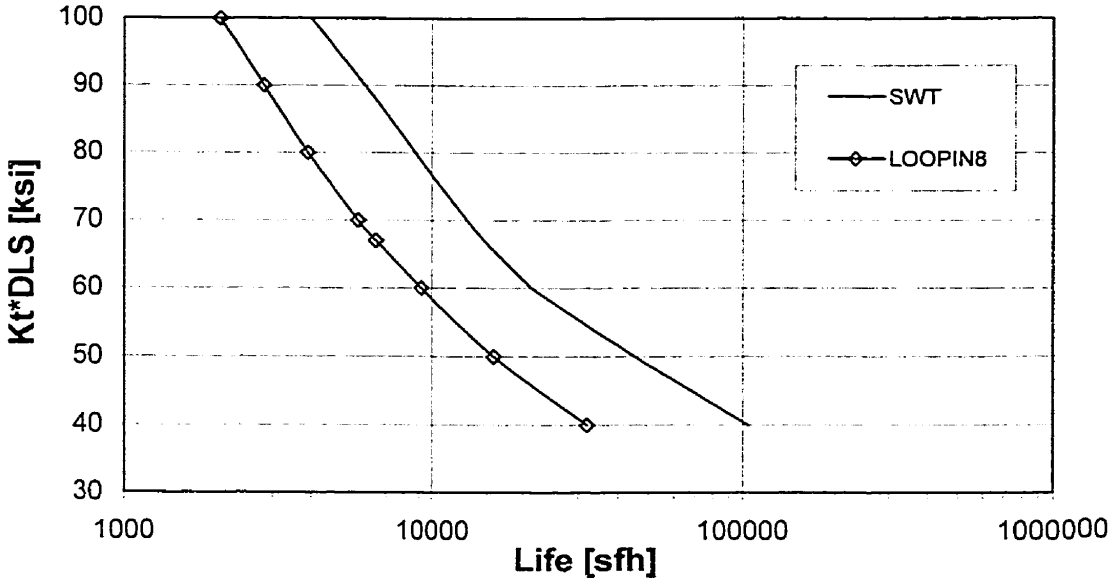

Figure 5-7: Comparison of SWT and LOOPIN8 Equivalent Strain Equations

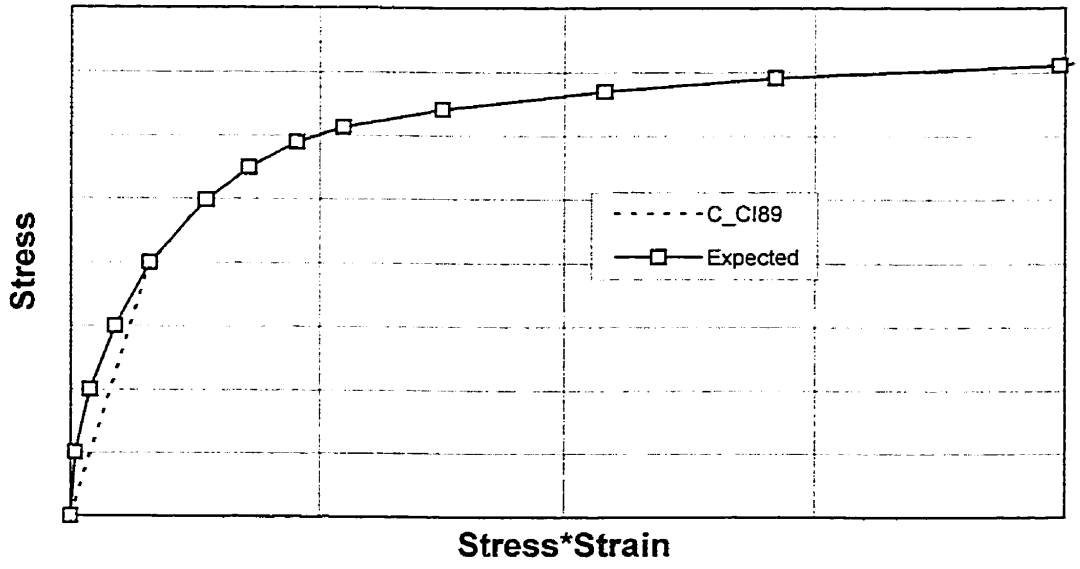

Figure 5-8: C_CI89 Representation of Stress vs. Stress*Strain Curve

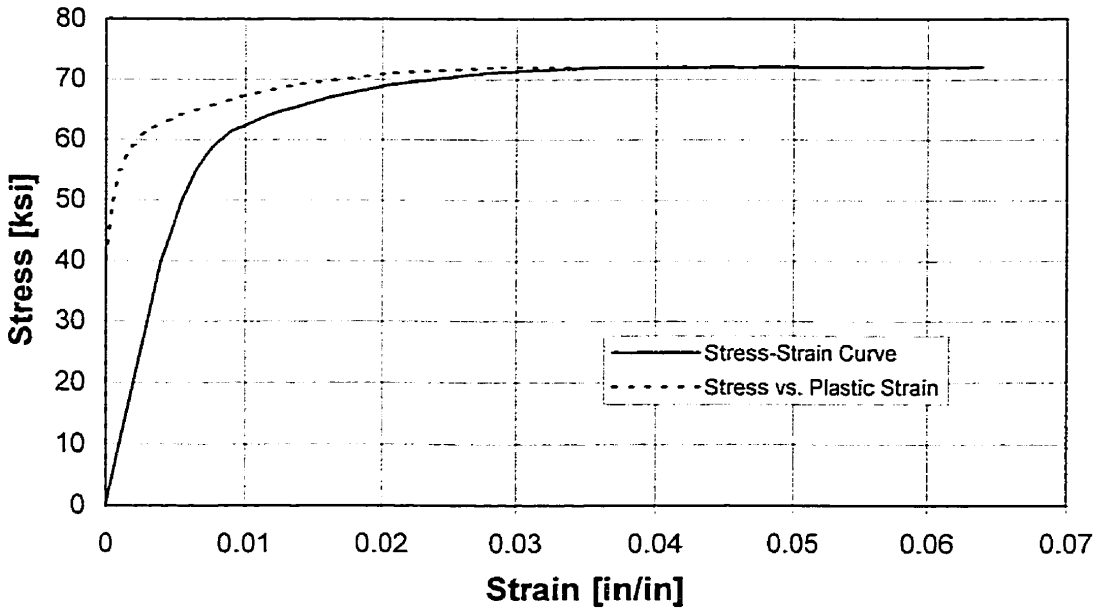

Figure 6-1: Aluminum 7050-T74 Stress-Strain Curve

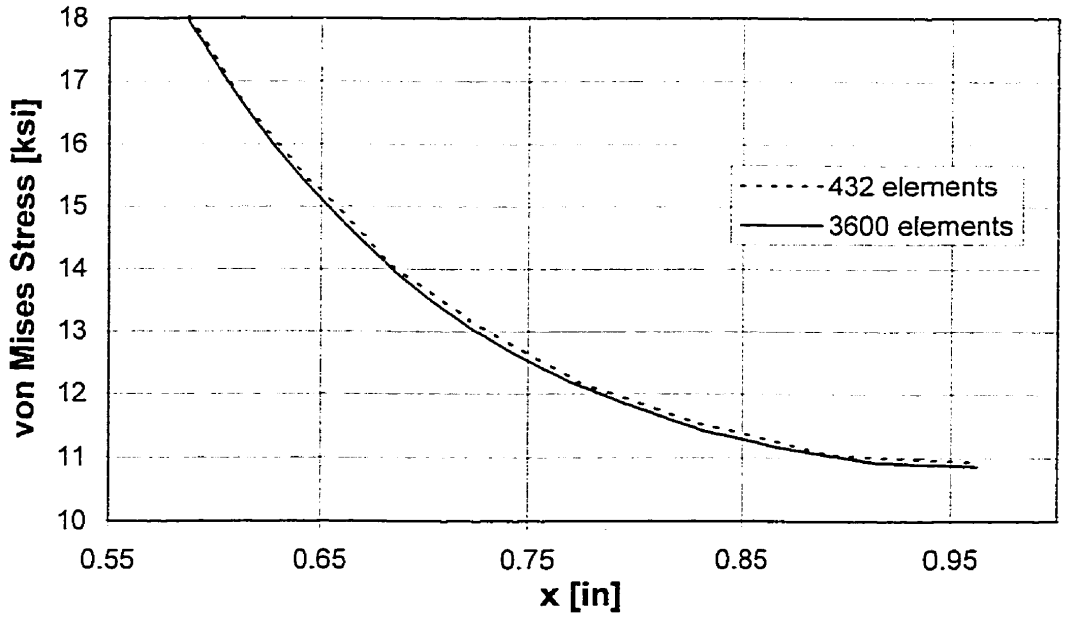

Figure 6-2: Low K_t Coupon Mesh Convergence Study

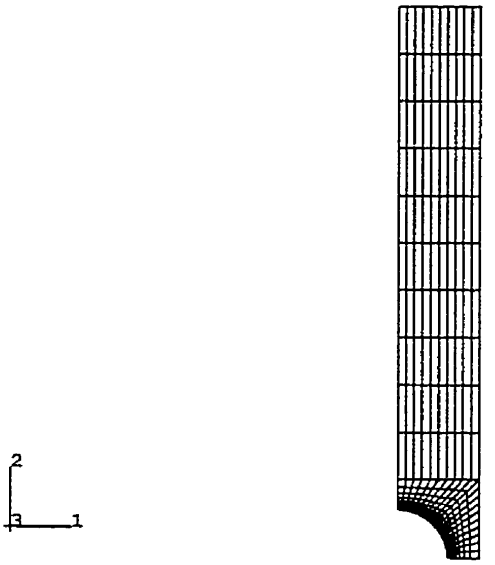

Figure 6-3: Finite Element Geometry of Low K_t Coupon

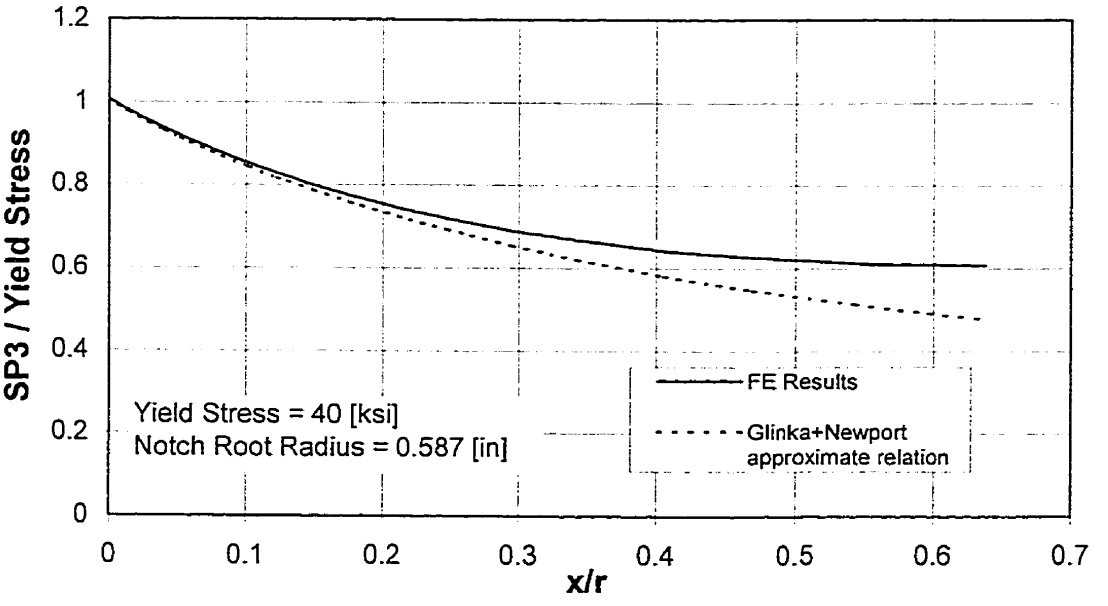

Figure 6-4: Comparison between FE results and approximate relationship for stress vs. distance

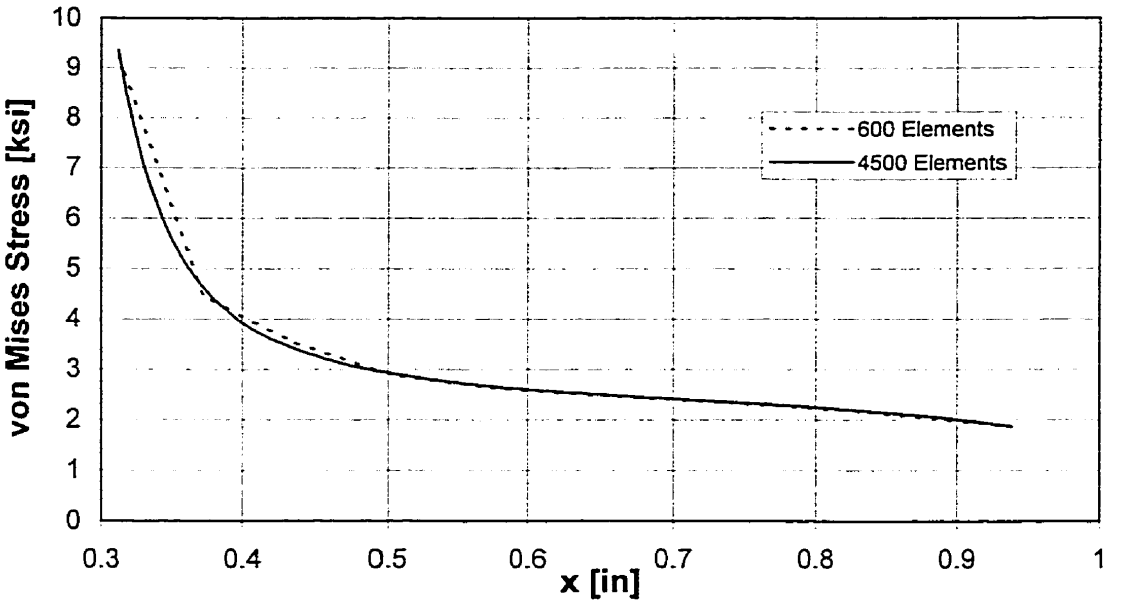

Figure 6-5: High K_t Coupon Mesh Convergence Study

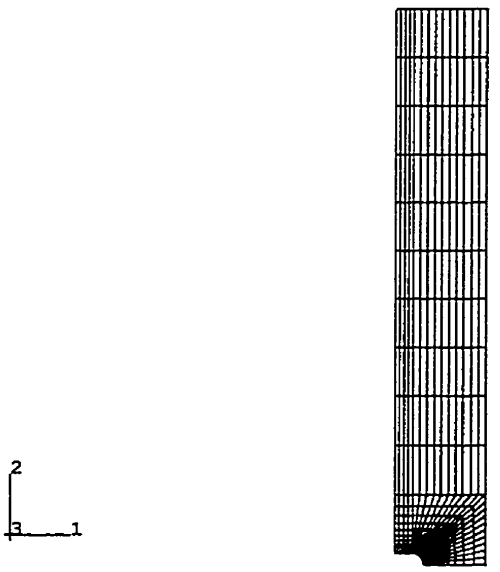

Figure 6-6: Finite Element Geometry of High K_t Coupon

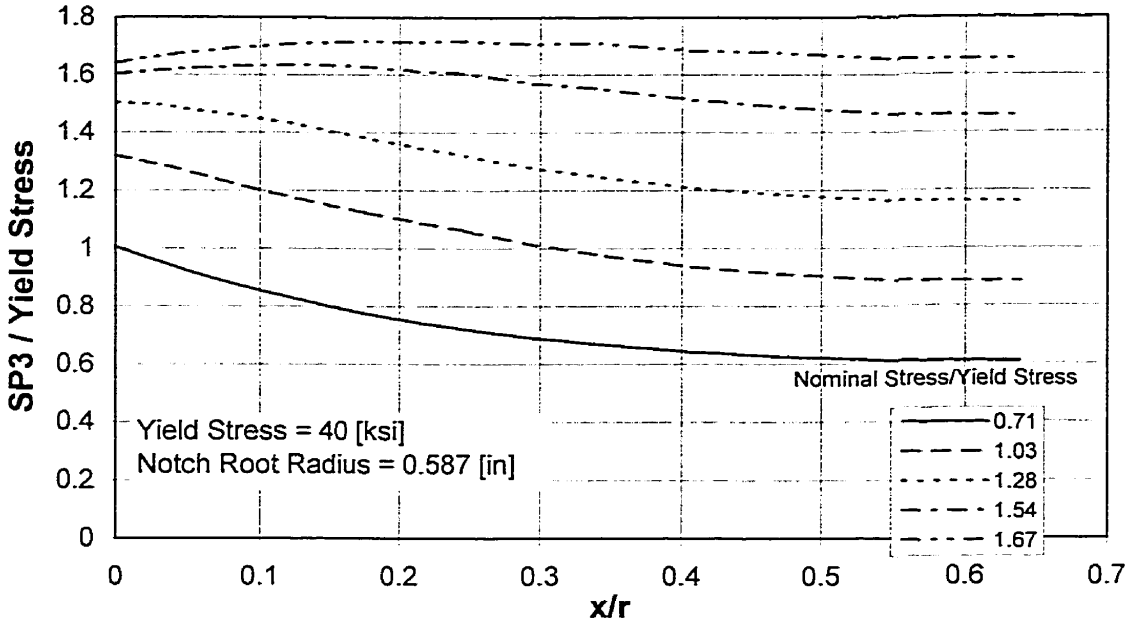

Figure 6-7: SP3 vs. Distance from Notch Root - Mid-Thickness of Low K_t Coupon

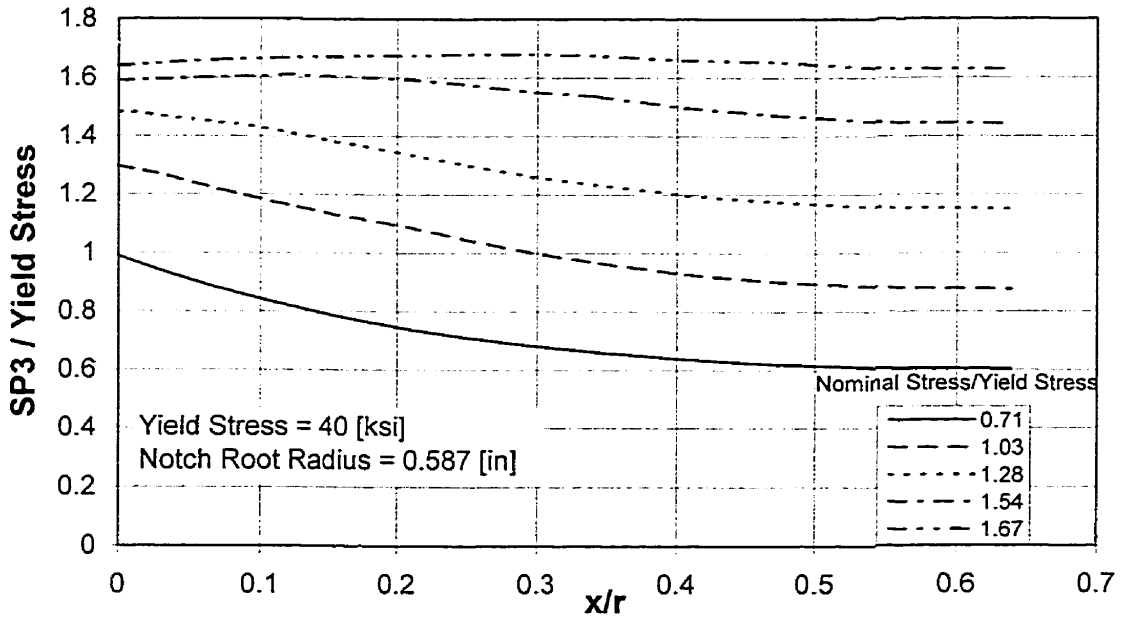

Figure 6-8: SP3 vs. Distance from Notch Root - Surface of Low K_t Coupon

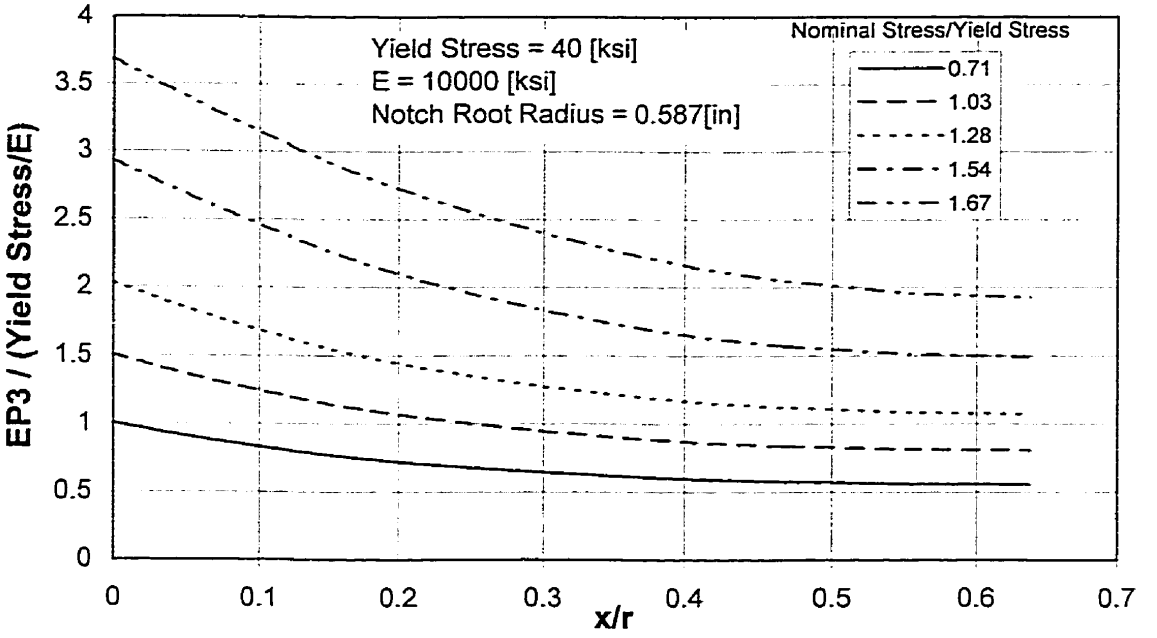

Figure 6-9: EP3 vs. Distance from Notch Root - Mid-Thickness of Low K_t Coupon

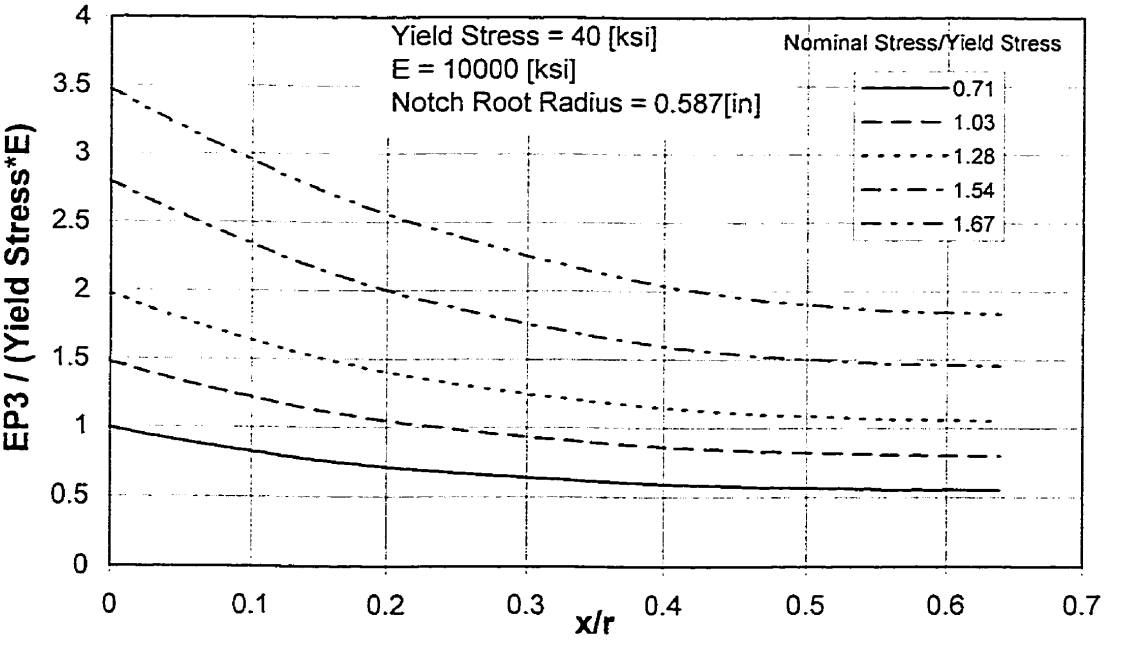

Figure 6-10: EP3 vs. Distance from Notch Root - Surface of Low K_t Coupon

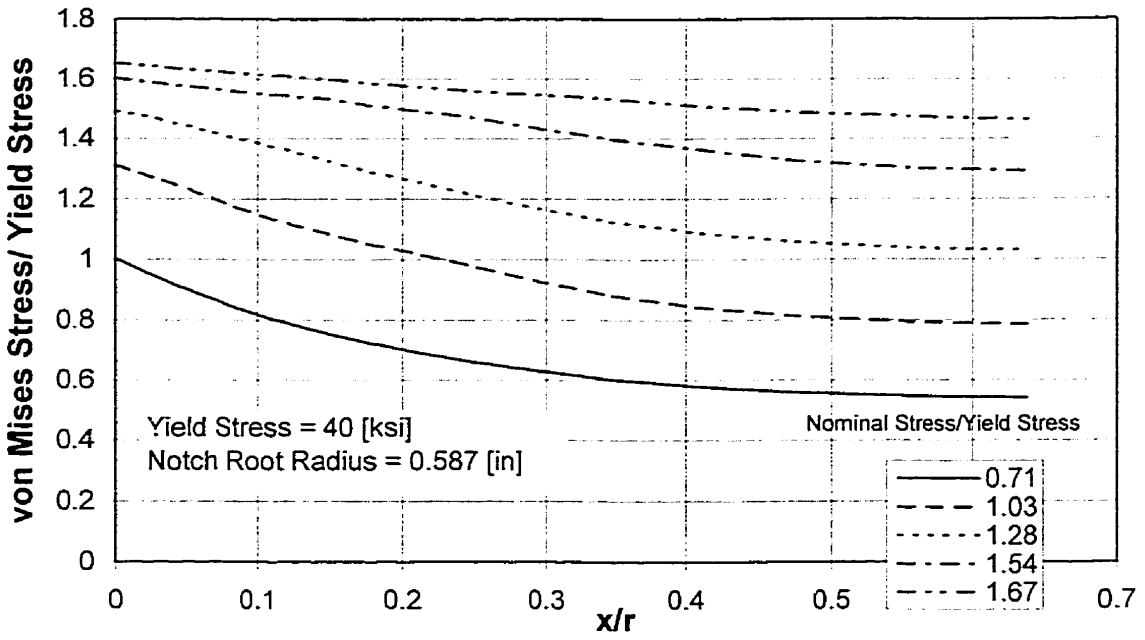

Figure 6-11: von Mises Stress vs. Distance from Notch Root - Mid-Thickness of Low K_t Coupon

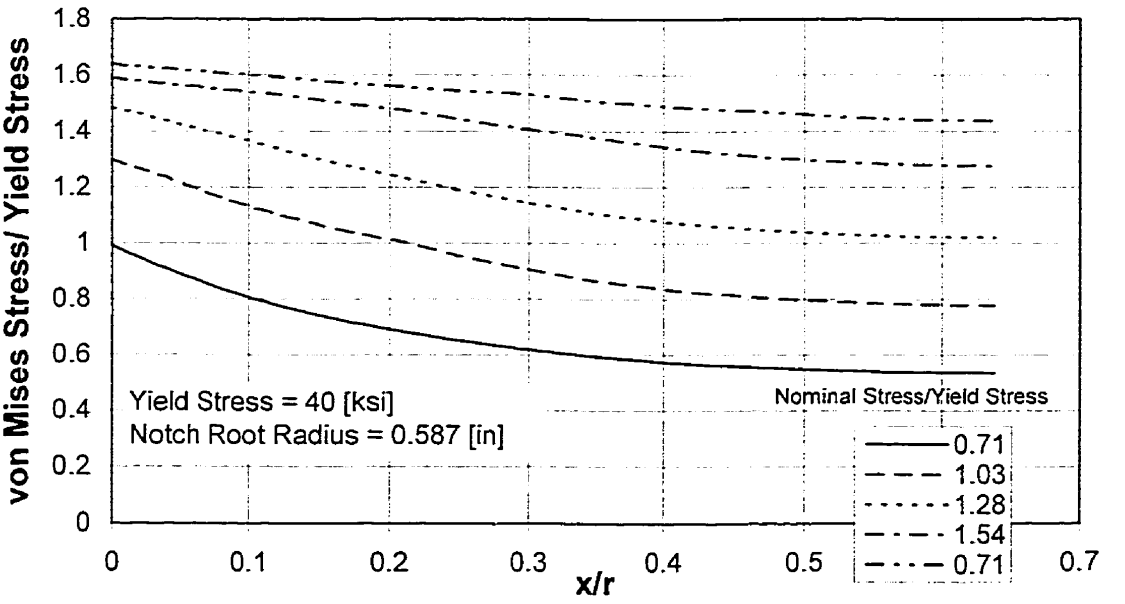

Figure 6-12: von Mises Stress vs. Distance from Notch Root - Surface of Low K_t Coupon

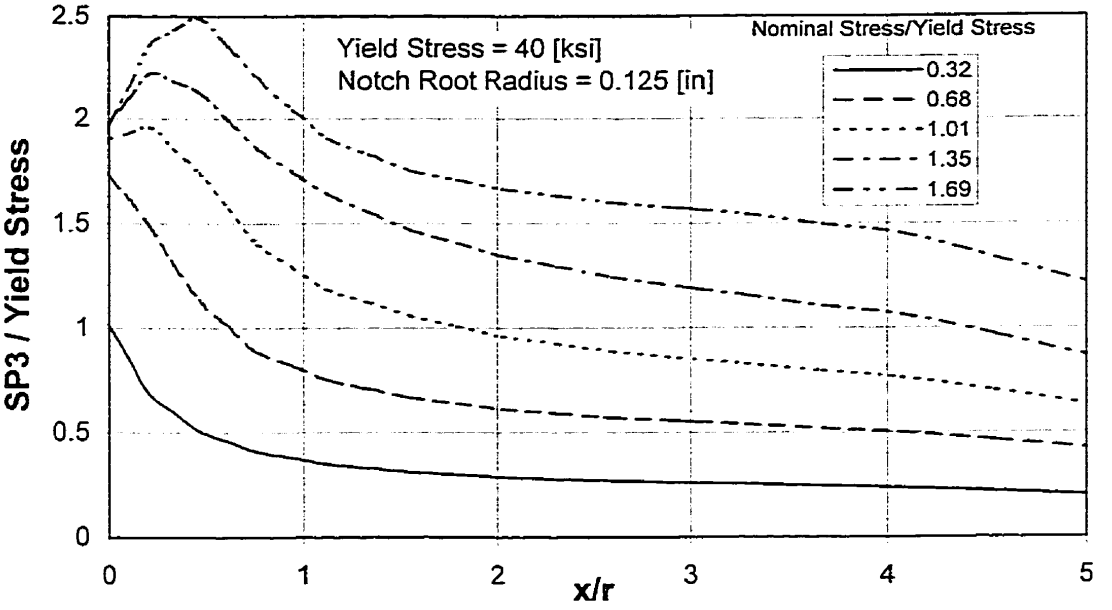

Figure 6-13: SP3 vs. Distance from Notch Root - Mid-Thickness of High K_t Coupon

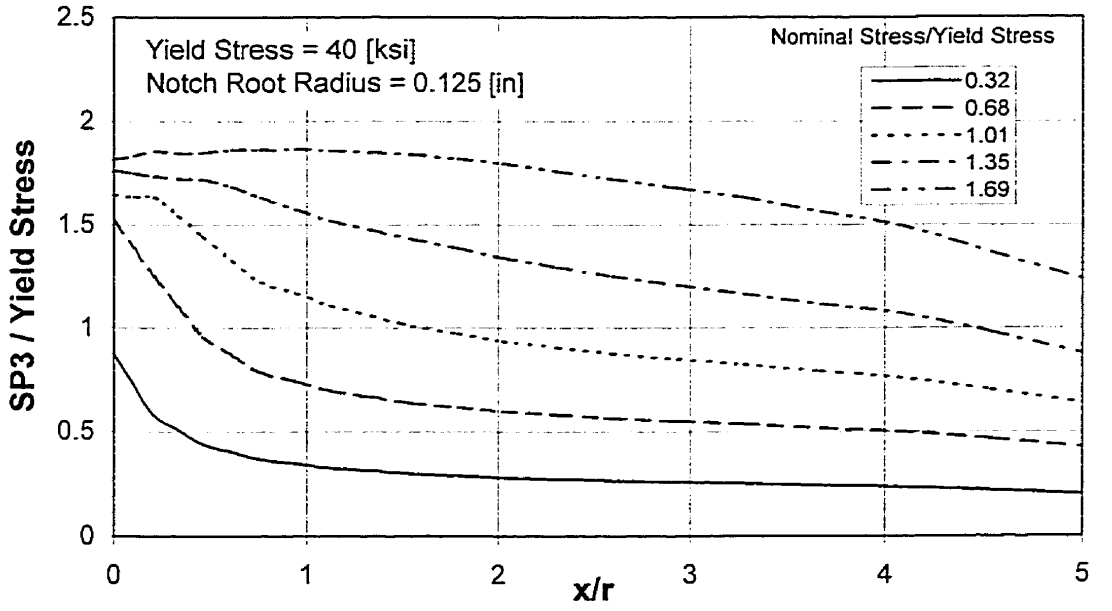

Figure 6-14: SP3 vs. Distance from Notch Root - Surface of High K_t Coupon

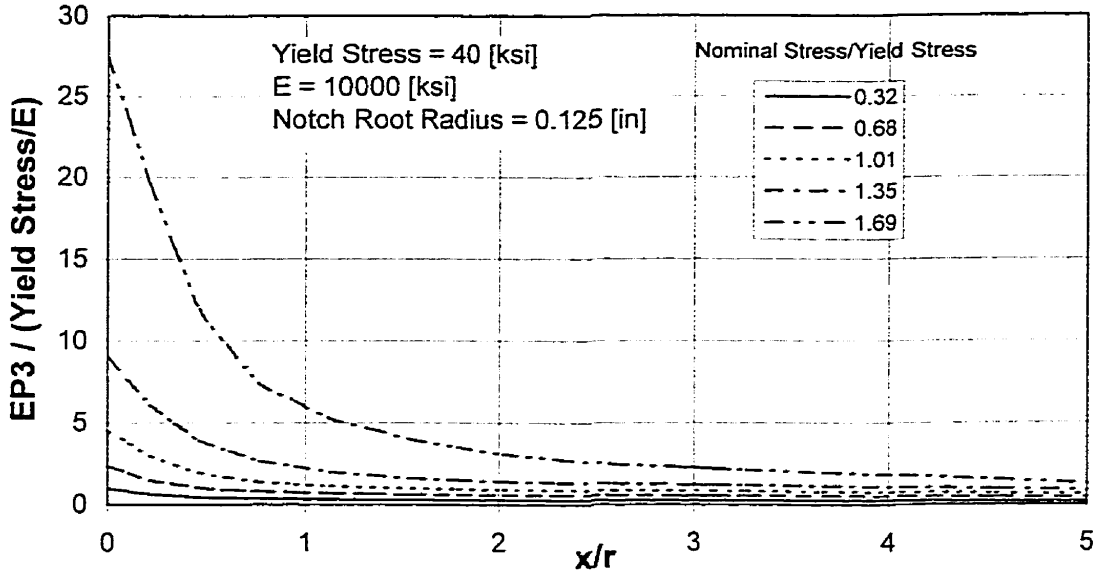

Figure 6-15: EP3 vs. Distance from Notch Root - Mid-Thickness of High K_t Coupon

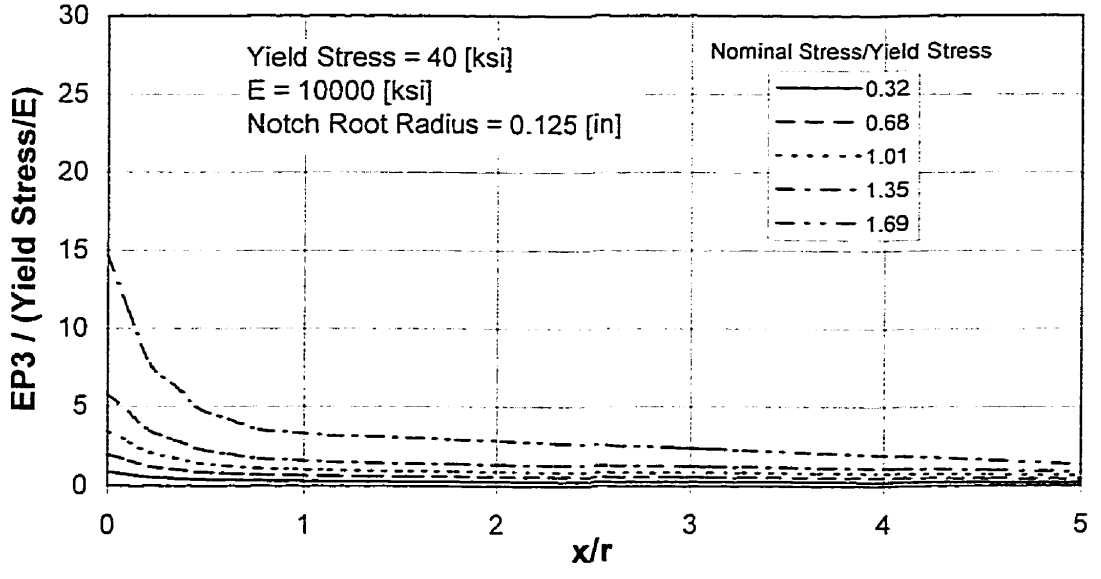

Figure 6-16: EP3 vs. Distance from Notch Root - Surface of High K_t Coupon

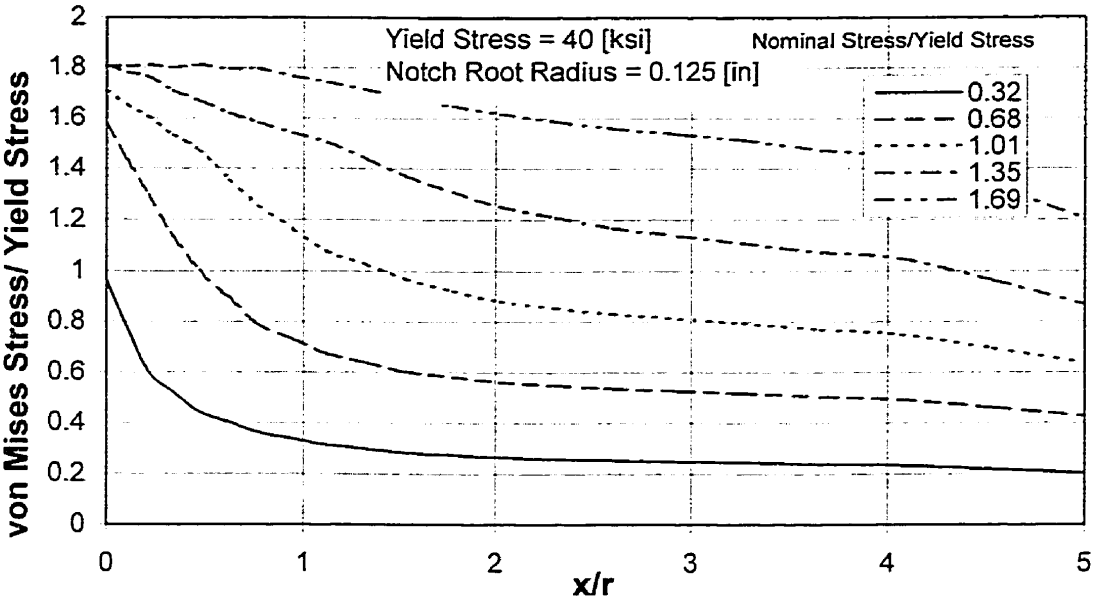

Figure 6-17: von Mises Stress vs. Distance from Notch Root - Mid-Thickness of High K_t Coupon

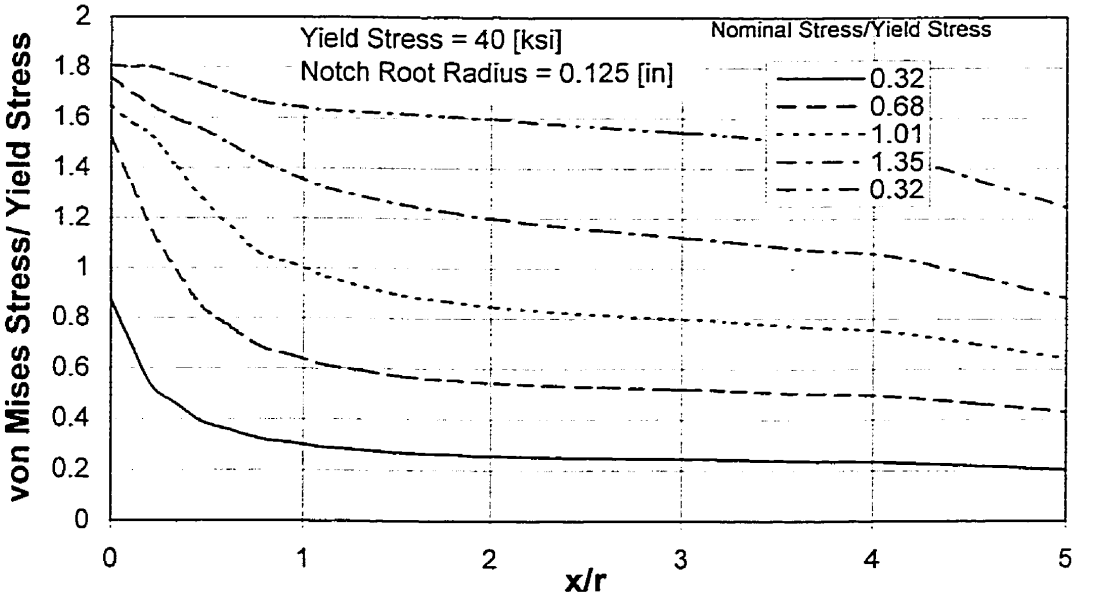

Figure 6-18: von Mises Stress vs. Distance from Notch Root - Surface of High K_t Coupon

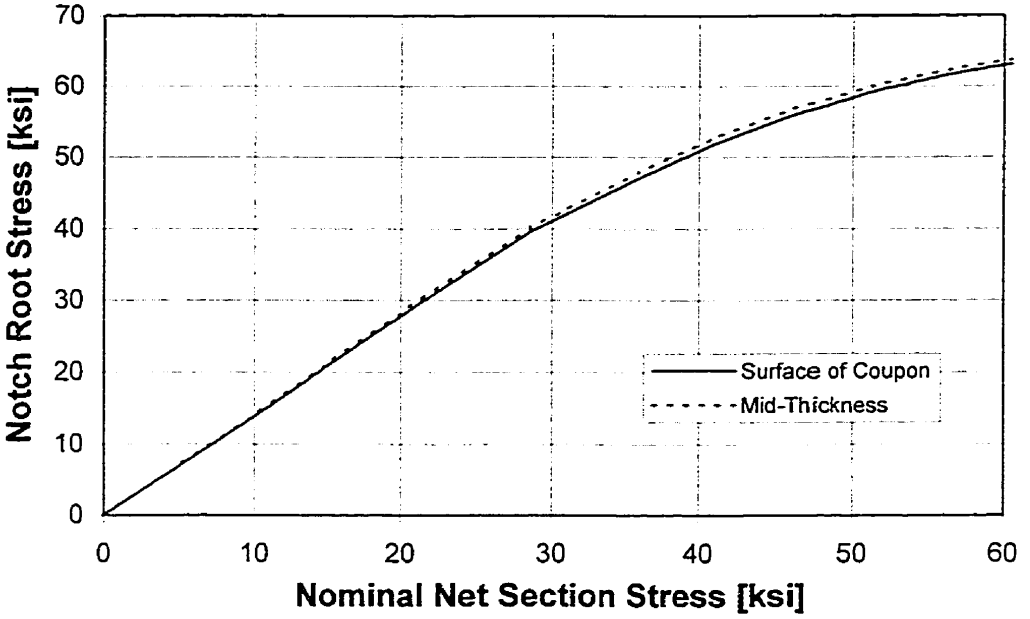

Figure 6-19: Notch Root Stress vs. Net Section Nominal Stress - Low K_t Coupon

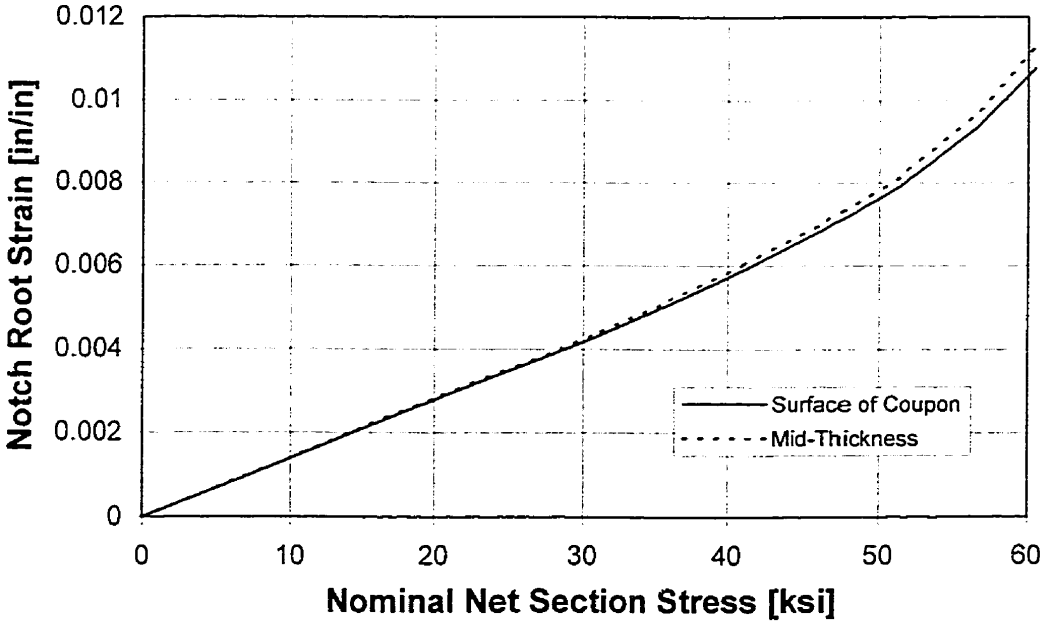

Figure 6-20: Notch Root Strain vs. Net Section Nominal Stress - Low K_t Coupon

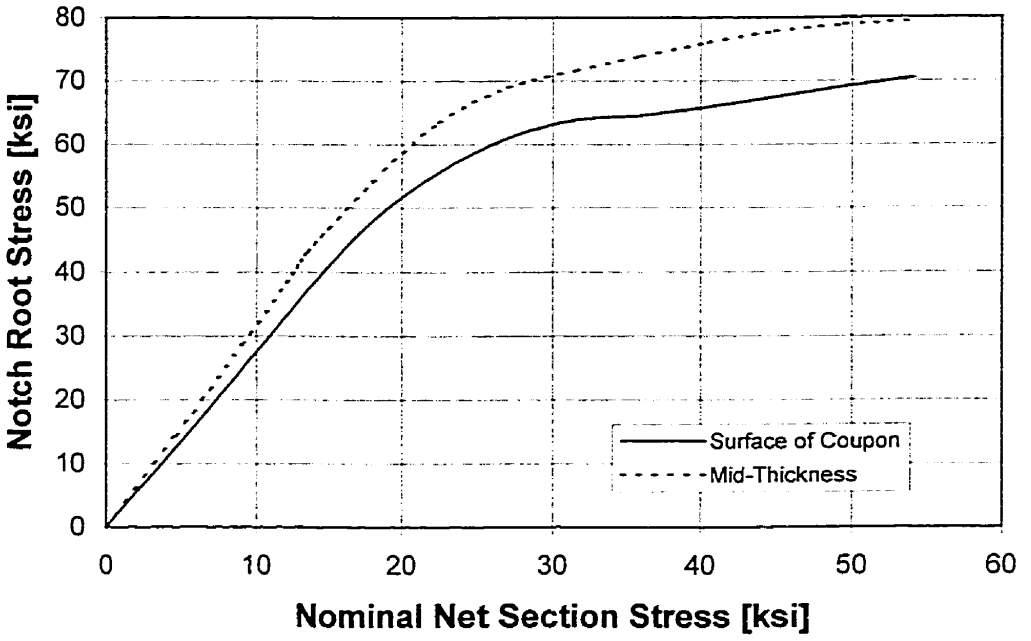

Figure 6-21: Notch Root Stress vs. Net Section Nominal Stress - High K_t Coupon

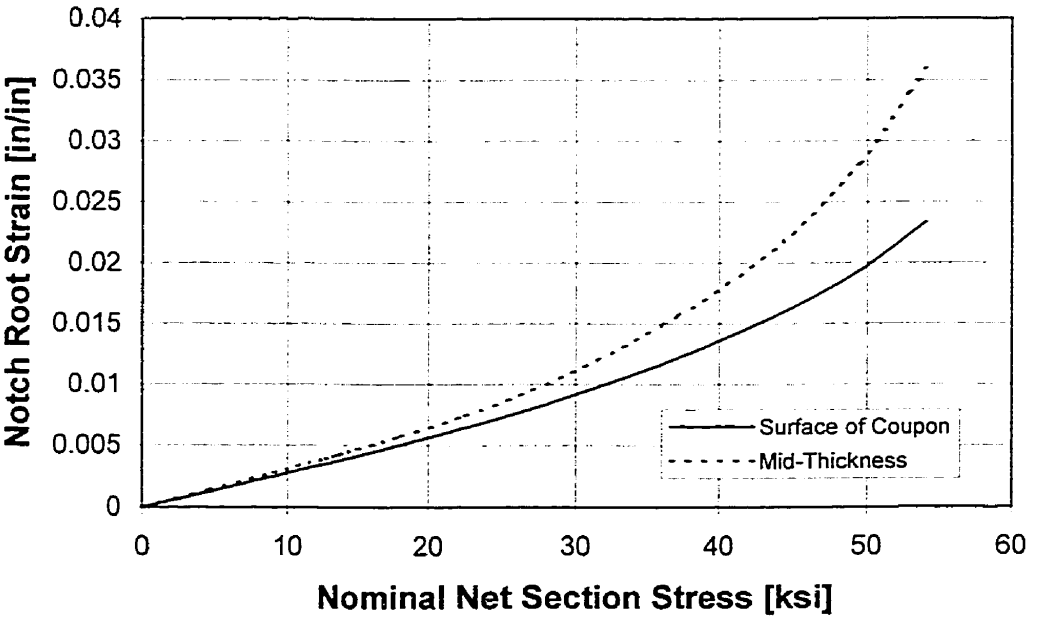

Figure 6-22: Notch Root Strain vs. Net Section Nominal Stress - High K_t Coupon

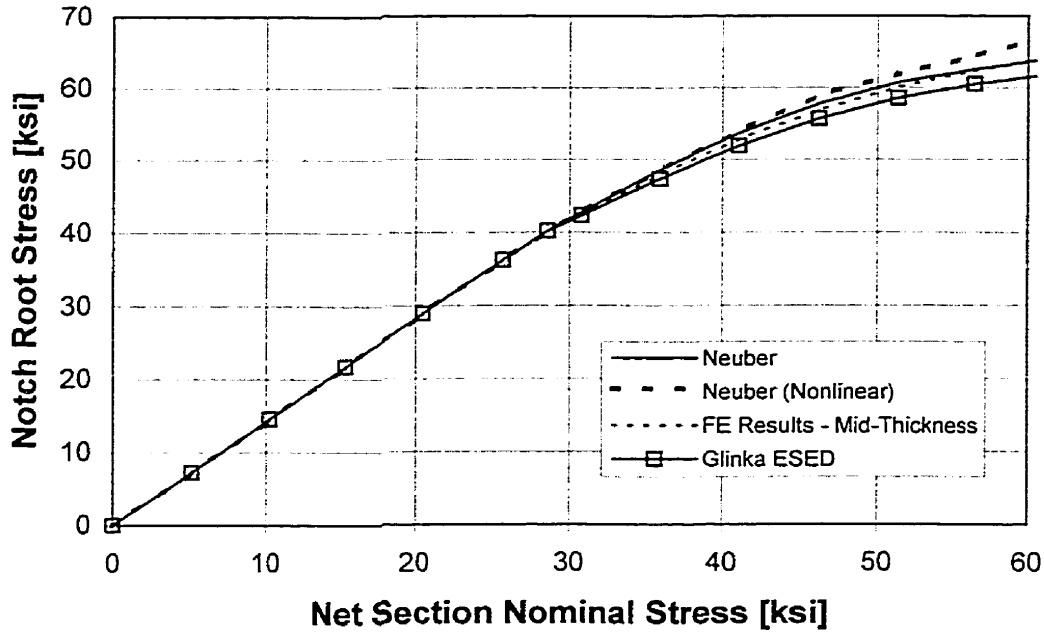

Figure 7-1: Low K_t Coupon - Stress Estimation

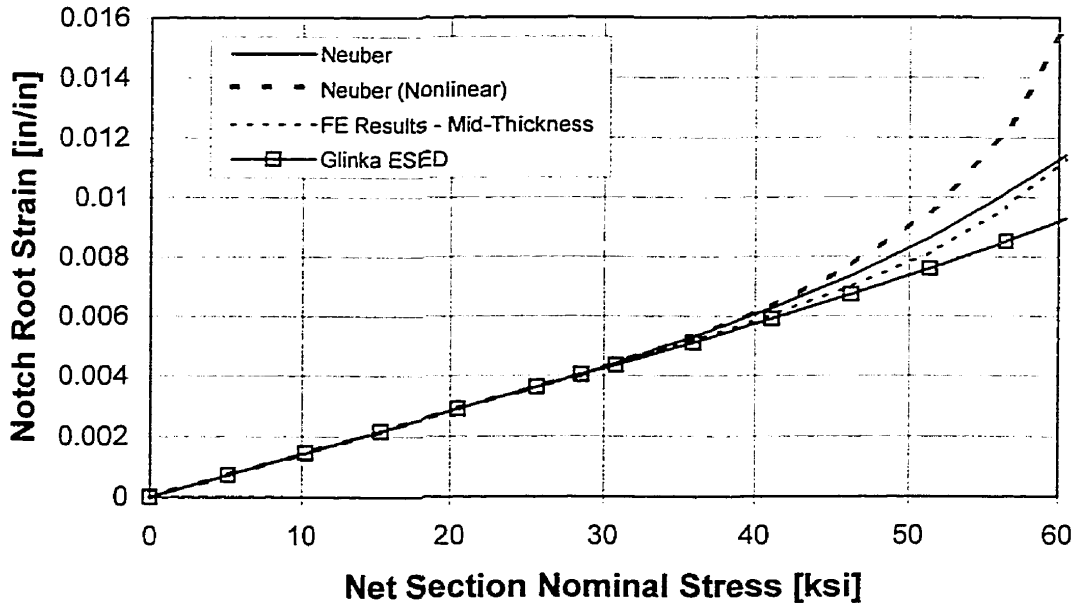

Figure 7-2: Low K_t Coupon - Strain Estimation

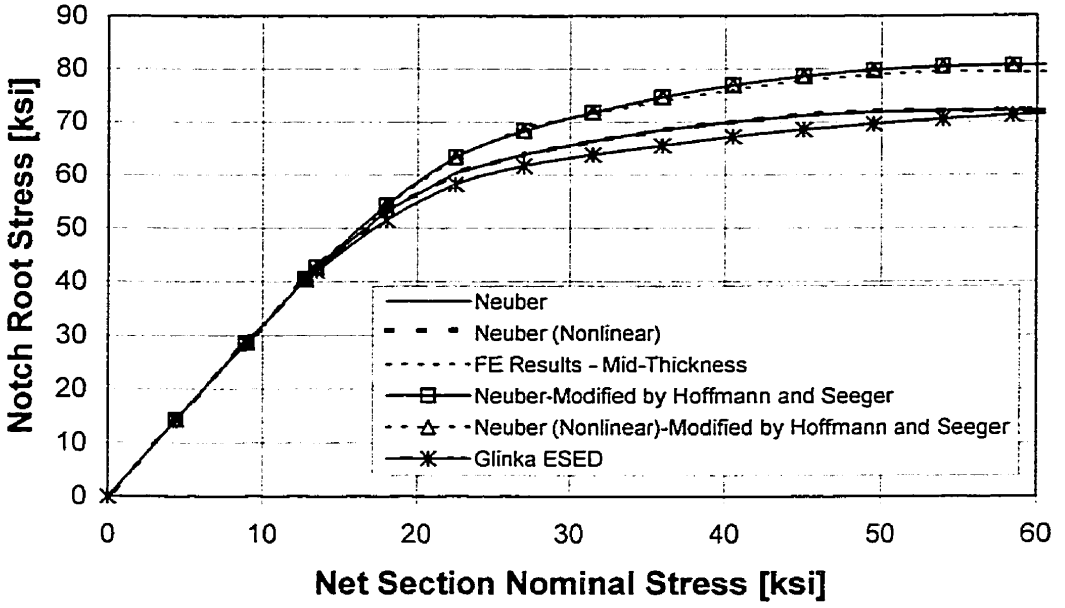

Figure 7-3: High K_t Coupon - Stress Estimation

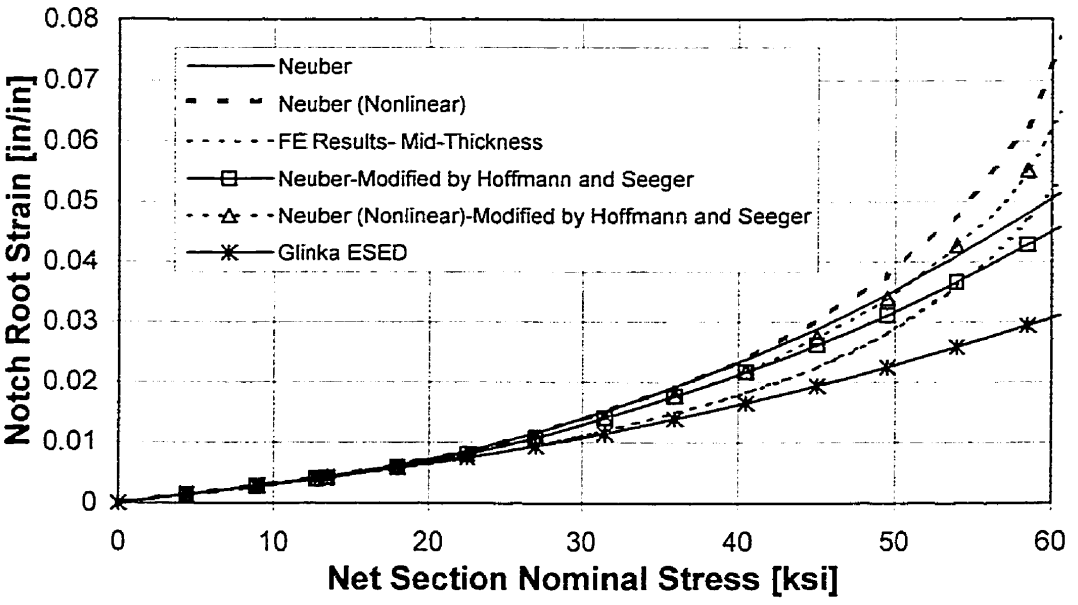

Figure 7-4: High K_t Coupon - Strain Estimation

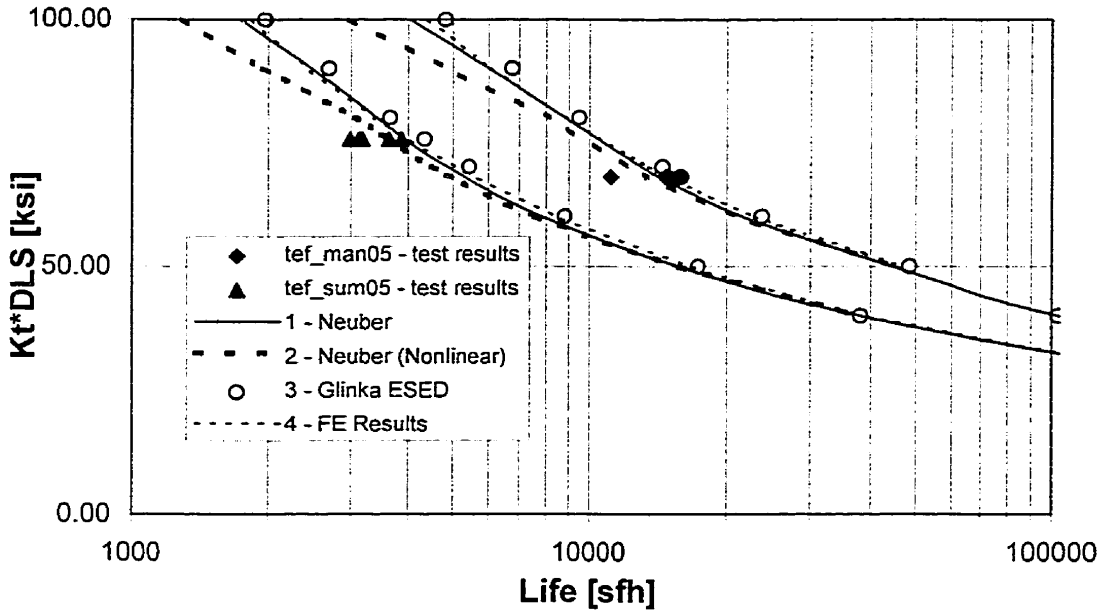

Figure 7-5: Low K_t Coupon - Crack Initiation Prediction Sensitivity Study

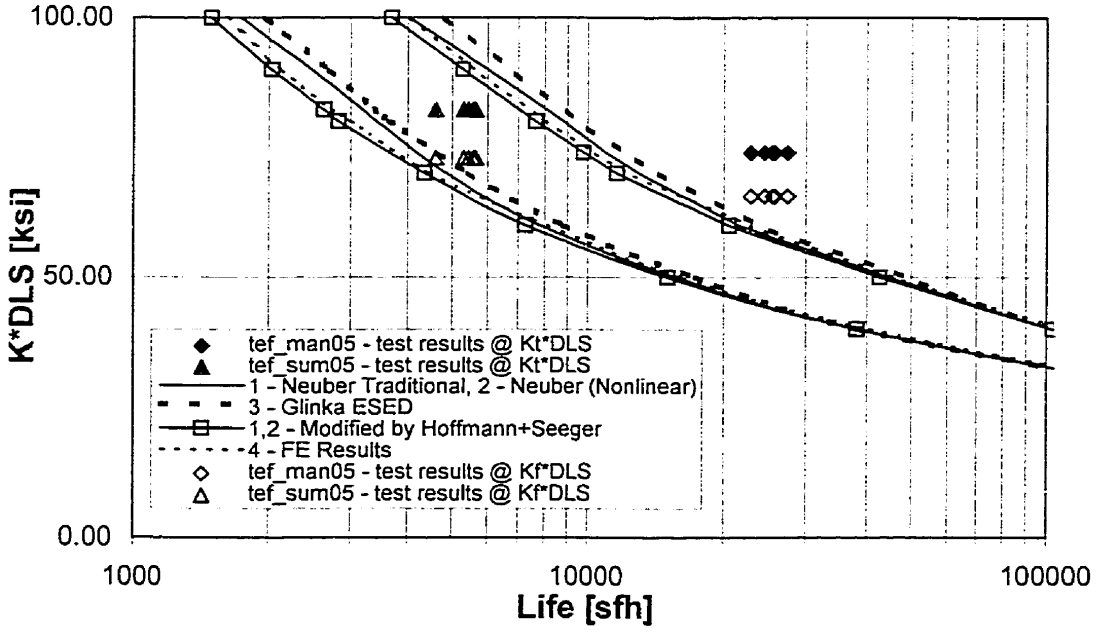

Figure 7-6: High K_t Coupon - Crack Initiation Prediction Sensitivity Study

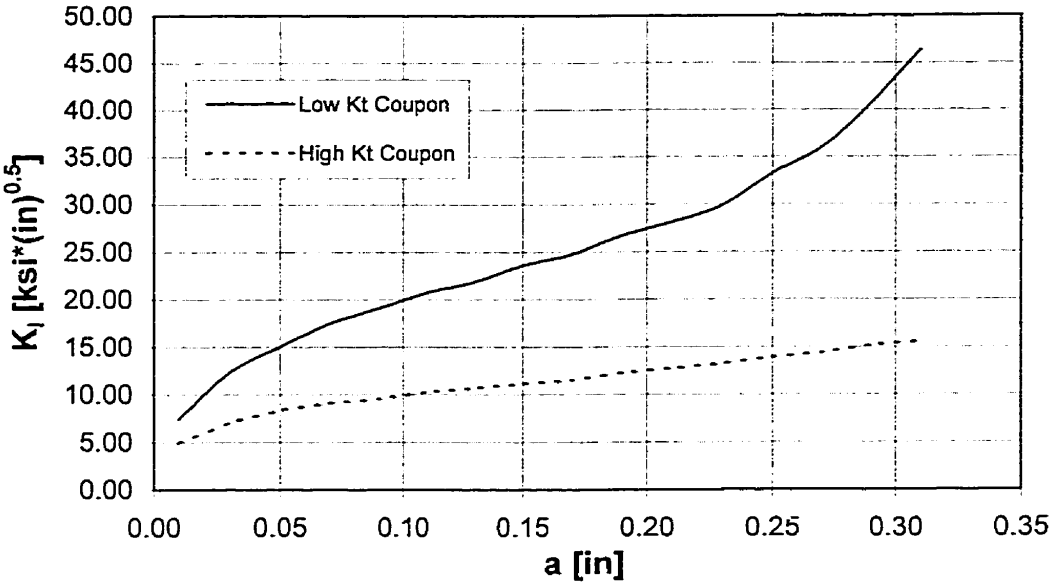

Figure 8-1: Stress Intensity Factor vs. Crack Length

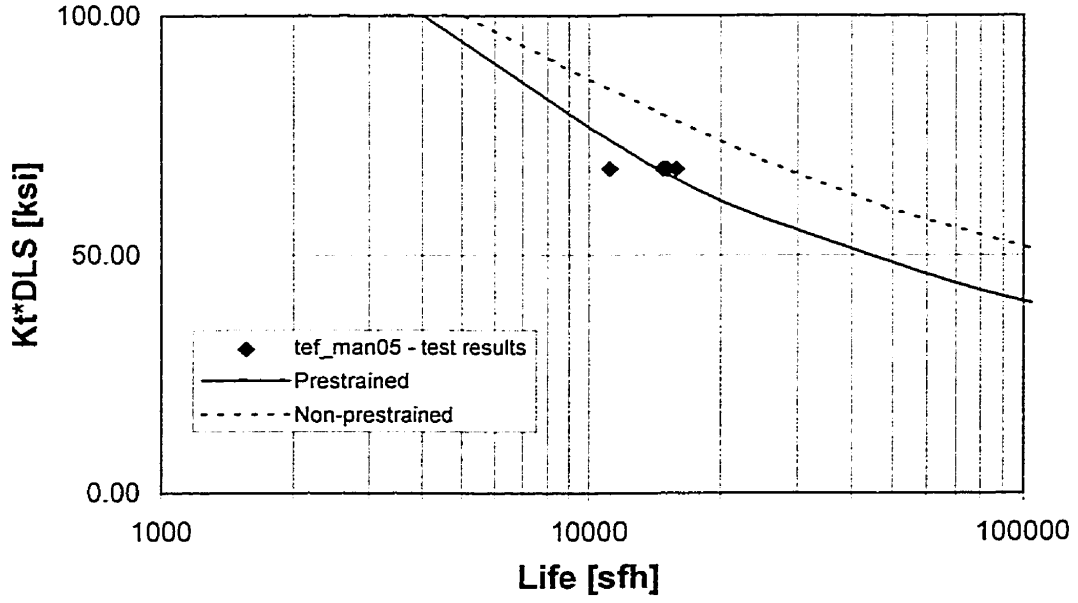

Figure 8-2: Low K_t Coupon - Prestrain and Non-prestrain LS Predictions

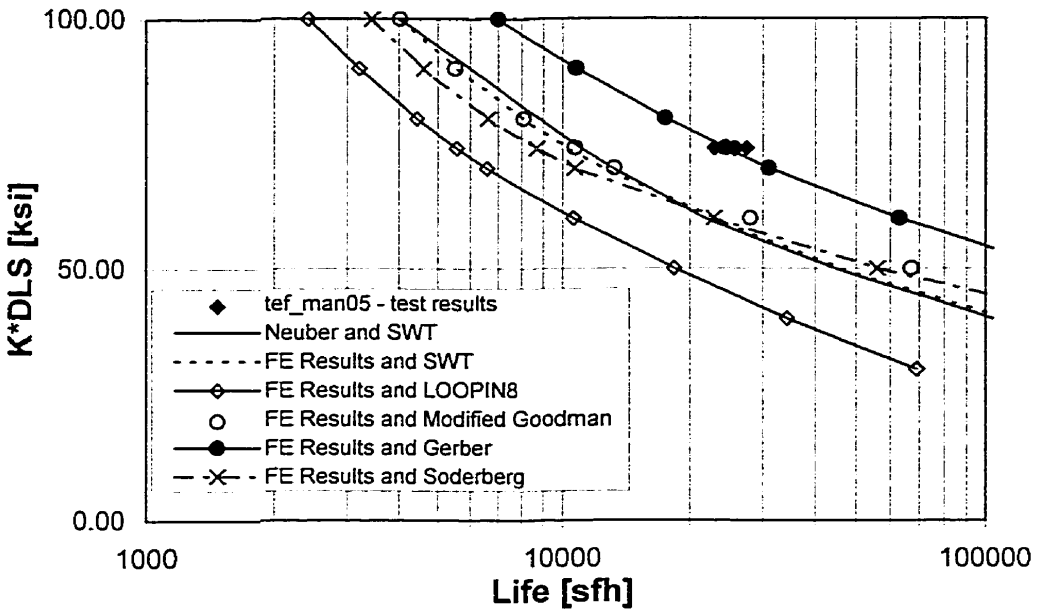

Figure 8-3: Equivalent Strain Equation Study - High K_t Coupon

Appendix A - Coupon Test Program

1. Low K_t Coupon

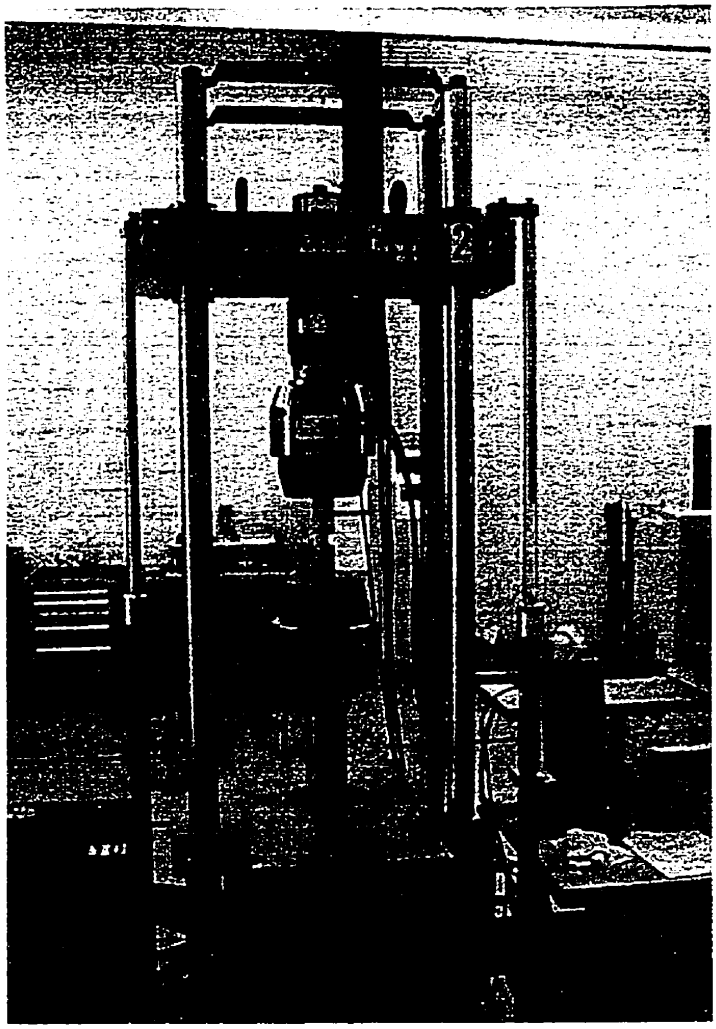

Component	Model No.	Serial No.	Capacity	Calibration
LVDT	N/A	602	N/A	12 March 1997
Load Cell	661.23A-04	1392	250 kN / 55 kips	12 March 1997
Hydraulic Grips	641.36	449	250 kN / 55 kips	N/A
Load Frame	311.11	446	250 kN / 55 kips	N/A

Schematic and Calibration Information for 55 kip Load Frame

COUPON TEST SET-UP - LOW K_t
Load Frame #2

- **Test Specimens**

Specimens for the trailing edge flap study were used. The coupon is called "Low K_t", and is made from aluminum 7050-T7451.

- **Test Procedure**

Note : After 5 specimens, remove the shims from hydraulic grips and grit blast. Then re-install in their previous locations (marked).

1. Start TestStar and open appropriate configuration file (*.TCC).
- for Low K_t: TEF_A1.TCC

2. Start hydraulic system.
- Reset the POD (if errors still there, turn APC control switch "on"), verify that CLC mode is selected.
- Put HPS on "low", then "high".
- Put HSM on "low" and extend actuator slightly to ensure it is free.
- Put HSM on "high".

3. Check tuning values in "CLC" and "Force Sg" modes.
The following values should be used :

- CLC, for both titanium and aluminum : P = 30 (master), P = 6 (limit)
- Force Sg, for aluminum : P = 7.50, I = 0.9, D = 0.02, F = 0.04

Note : these values should be tuned for a specific coupon and/or spectrum.

4. Check input signals range and limits
- A) Load transducer

for man05:	range =	10000 lbf
	upper limit =	10000 lbf
	lower limit =	-5500 lbf
for sum05:	range =	25000 lbf
	upper limit =	11000 lbf
	lower limit =	-5500 lbf

- B) Displacement

range = 5 inches

5. Zero out load transducer and lock zero.

- on POD, switch from present mode to the "Displ Pod" mode
- TestStar window :
  - > Adjust
  - > Input Signals
  - > Force
  - > Check and record shunt calibration values
  - > Unlock zero
  - > Autozero
  - > Lock zero
- on POD, switch from "Displ Pod" to "CLC"

6. Install specimen in hydraulic grips

- make sure that the "CLC" mode is selected, make sure APC set to OFF.
- place crosshead 47-48 inches above the base, corresponding to a post length of 47-48 inches.
- place specimen (selected in random order) in bottom grip and center it between the two screws that are needed to maintain the inserts. The specimen should be placed with the reference hole at the top right position.
- tighten specimen slightly in bottom grip.
- extend actuator slowly with the shim on top of the specimen so that the shim just enters the top grip inserts.
- extend hydraulic cylinder for specimen to be the closer to its final position. Use the distance from bottom grip to notch as a rough estimate of how far to raise actuator.
- turn APC to OFF.
- use square and insert built for this purpose to align specimen. Tighten bottom screws first to align the square to the actuator. Apply hydraulic pressure to bottom grip.
- remove the square from the actuator once alignment is complete.
- extend actuator until shim has bottomed out in top grip (Do not exceed -5 to -8 lbf of compressive force when doing so). Turn APC to OFF, then apply hydraulic pressure to top grip.

7. Check on any load change (with hydraulic pressure applied to grips, load should be between 30 and 40 lbf)

8. Zero out displacement transducer and lock zero.

- on POD, switch from "CLC" to "Force POD"
- TestStar window :
  - > Adjust
  - > Input Signals
  - > Displacement
  - > Switch range from 5.0 in to 0.5 in (configuration should be saved with 5.0 in range to allow installation of specimen)
  - > Unlock zero
  - > Autozero

> Lock zero

- on POD, switch from "Force POD" to "CLC" and make sure APC set to OFF

9. Start TestWare-SX and open appropriate template (WINGTST.000)

Select desired procedure :

- WINGTST Default Procedure
- TEF_ACT Mean05 haversine Al
- TEF_ACT Sum05 haversine Al

10. Change data file name for each specimen

11. For the first specimen in a series, create a new SAC file

NOTES:

1. Run man05 with 300% rate multiplier, and sum05 with 200% rate multiplier.
2. To remove coupon, set displacement range to 5".

TestWare-SX Procedure File for tef_man05 Sequence - Low K_t Coupon

Procedure Name = TEF_ACT mean05 haversine AL
File Specification = C:\TS2\TWSX\WINGTST.010
Software Version = 3.0B
Printout Date = 03-10-1998 12:04:51 PM

Data File Options
  File Format = Excel Text File
  Log Events = Yes
  Include Procedure Description = No

Recovery Options
  Autosave disabled.

Ramp to mean : Step
  Step Done Trigger 1 = ramp up

  ramp up : Monotonic Command
    Start Trigger = Step Start
    End Trigger = <none>
    Segment Shape = Ramp
    Time = 3 (Sec)
    AXIAL
      Control Mode = FORCE SG
      End level = 50 (lbf)

Spectrum Cycling : Step
  Step Done Trigger 1 = Play Spectrum

  Record Peaks/Valleys : Data Acquisition
    Start Trigger = Step Start
    End Trigger = Play Spectrum
    Mode = Peak / Valley
    Buffer Type = Circular
    Master Channel = FORCE
    Data Header = Peaks/Valleys
    Sensitivity = 10 (lbf)
    Buffer Size = 16000

  Play Spectrum : File Playback Command
    Start Trigger = Step Start
    End Trigger = <none>
    File Name... = C:\TS2\TWSX\TE_MAN05.SFP

Passes = 0
Rate Multiplier = 300 (%)
Compensation = SAC
AXIAL
Control Mode = FORCE SG
Level Reference = 0 (lbf)
Level Multiplier = 100 (%)
Table Options
Create new SAC table. = No
Load SAC table from file. = Yes
Use existing SAC table. = No
Additional Options
Save SAC table to file. = No
Default Table Limits = No
Error Tolerance = 90 (lbf)
Upper Table Limit = 10000 (lbf)
Lower Table Limit = -5500 (lbf)
SAC Load File... = C:\TS2\TWSX\TEFM05.SAC
SAC Save File... =

2. High K_t Coupon

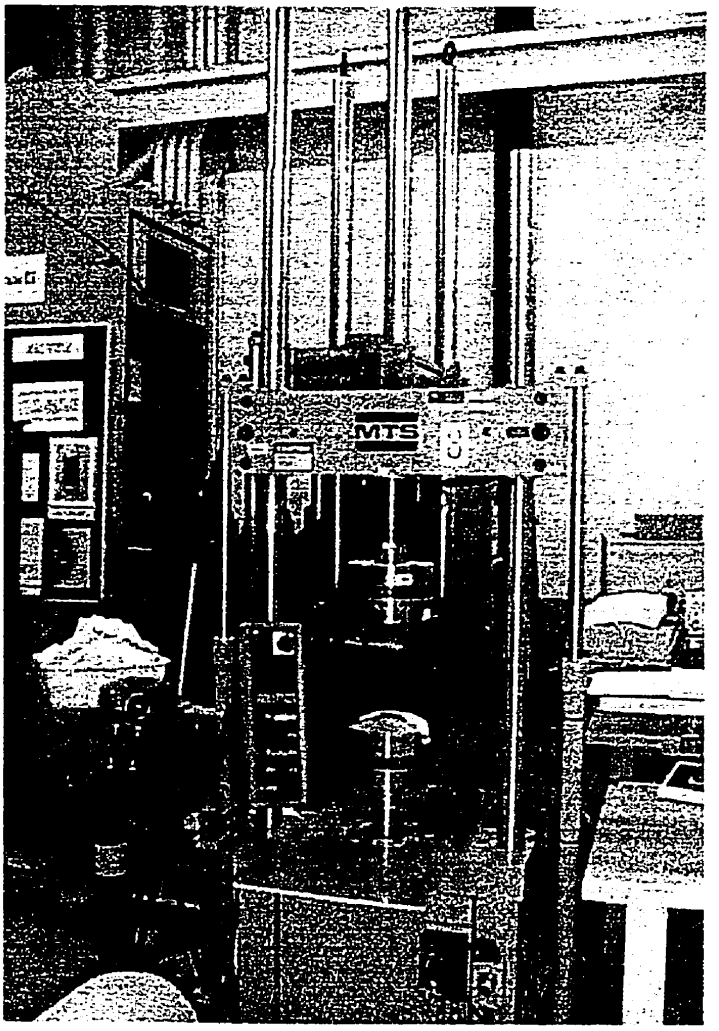

Component	Model No.	Serial No.	Capacity	Calibration
LVDT	N/A	101	N/A	22 January 1998
Load Cell	661.21A-03	4684	100 kN / 22 kips	23 January 1998
Hydraulic Grips	647.10A	0284111	100 kN / 22 kips	N/A
Load Frame	312.21	1323	100 kN / 22 kips	N/A

Schematic and Calibration Information for 22 kip Load Frame

COUPON TEST SET-UP - HIGH K_t
Load Frame #8

- **Test Specimens**

Specimens for the trailing edge flap study were used. The coupon is called "High K_t", and is made from aluminum 7050-T7451.

- **Test Procedure**

1. Start TestStar and open appropriate configuration file (*.TCC).
- for High K_t: TEF_AP.TCC

2. Start hydraulic system.
- Reset the POD (if errors still there, turn APC control switch "on"), verify that CLC mode is selected.
- Put HPS on "low", then "high"
- Put HSM on "low" and extend actuator slightly to ensure it is free
- Put HSM on "high"

3. Check tuning values in "CLC" and "Force Sg" modes.
The following values should be used :
- CLC, for both titanium and aluminum : P = 30 (master), P = 6 (limit)
- Force Sg, for aluminum :P = 7.50, I = 0.9, D = 0.02, F = 0.04

Note : these values should be tuned for a specific coupon and/or spectrum.

4. Check input signals range and limits
- A) Load transducer

for man05:	range =	10000 lbf
	upper limit =	10000 lbf
	lower limit =	-5500 lbf
for sum05:	range =	25000 lbf
	upper limit =	11000 lbf
	lower limit =	-5500 lbf

- B) Displacement

range = 5 inches

5. Zero out load transducer and lock zero.

- on POD, switch from present mode to the "Displ Pod" mode

  TestStar window : > Adjust
  - > Input Signals
  - > Force
  - > Check and record shunt calibration values
  - > Unlock zero
  - > Autozero
  - > Lock zero
- on POD, switch from "Displ Pod" to "CLC"

6. Install specimen in hydraulic grips

- make sure that the "CLC" mode is selected, make sure APC set to OFF.
- place crosshead 38 inches above the base, corresponding to a post length of 38 inches.
- place specimen (selected in random order) in bottom grip against lower stop. The specimen should be installed with the reference hole at the top right position.
- tighten specimen slightly in bottom grip.
- extend actuator slowly so that the specimen just enters the top grip wedges.
- extend hydraulic cylinder for specimen to be the closer to its final position. Use the distance from bottom grip to slot as a rough estimate of how far to raise actuator.
- turn APC to OFF.
- use upper stop to align specimen. Verify alignment with digital protractor. Apply hydraulic pressure to bottom grip.
- extend actuator until specimen has bottomed out in top grip (Do not exceed -5 to -8 lbf of compressive force when doing so). Turn APC to OFF, then apply hydraulic pressure to top grip.

7. Check on any load change (with hydraulic pressure applied to grips, load should be between 10 and 20 lbf)

8. Zero out displacement transducer and lock zero.

- on POD, switch from "CLC" to "Force POD"
- TestStar window :
  - > Adjust
  - > Input Signals
  - > Displacement
  - > Switch range from 5.0 in to 0.5 in (configuration should be saved with 5.0 in range to allow installation of specimen)
  - > Unlock zero
  - > Autozero
  - > Lock zero
- on POD, switch from "Force POD" to "CLC" and make sure APC set to OFF.

9. Start TestWare-SX and open appropriate template (WINGTST.000).
Select desired procedure :

- WINGTST Default Procedure
- TEF_ACT Mean05 haversine Al
- TEF_ACT Sum05 haversine Al

10. Change data file name for each specimen.

11. For the first specimen in a series, create a new SAC file.

NOTES:

1. Run man05 with 300% rate multiplier, and sum05 with 200% rate multiplier.
2. To remove coupon, set displacement range to 5".

TestWare-SX Procedure File for tef_man05 Sequence - High K_t Coupon

Procedure Name = TEF_ACT mean05 haversine AL
File Specification = C:\TS2\TWSX\WINGTST.010
Software Version = 3.1B
Printout Date = 03-10-1998 12:10:20 PM

Data File Options
  File Format = Excel Text File
  Log Events = Yes
  Include Procedure Description = No

Recovery Options
  Autosave disabled.

Ramp to mean : Step
  Step Done Trigger 1 = ramp up

  ramp up : Monotonic Command
    Start Trigger = Step Start
    End Trigger = <none>
    Segment Shape = Ramp
    Time = 3 (Sec)
    Control Channel 1
      Control Mode = Force Segment
      End level = 50 lbf

Spectrum Cycling : Step
  Step Done Trigger 1 = Play Spectrum

  Record Peaks/Valleys : Data Acquisition
    Start Trigger = Step Start
    End Trigger = Play Spectrum
    Mode = Peak / Valley
    Buffer Type = Circular
    Master Channel = Force
    Data Header = Peaks/Valleys
    Sensitivity = 10 lbf
    Buffer Size = 16000

  Play Spectrum : File Playback Command
    Start Trigger = Step Start
    End Trigger = <none>
    File Name... = C:\TS2\TWSX\TE_MAN05.SFP

Passes = 0
Rate Multiplier = 200 (%)
Compensation = SAC
Control Channel 1
    Control Mode = Force Segment
    Level Reference = 0 (kip)
    Level Multiplier = 80.44 (%)
    Table Options
        Create new SAC table. = No
        Load SAC table from file. = Yes
        Use existing SAC table. = No
    Additional Options
        Save SAC table to file. = No
        Default Table Limits = No
    Error Tolerance = 90 lbf
    Upper Table Limit = 10000 lbf
    Lower Table Limit = -5500 lbf
    SAC Load File... = C:\TS2\TWSX\TEFM05.SAC
    SAC Save File... =

Appendix B - Format of McCracken Input and Results Files

The McCracken Fatigue Life Prediction Program (McCracken) is available through the Department of Mechanical and Aerospace Engineering at Carleton University. Individuals interested in obtaining the McCracken application are encouraged to submit a written request to the following address:

Department of Mechanical and Aerospace Engineering

Carleton University

1125 Colonel By Drive

Ottawa, Ontario, Canada

K1S 5B6

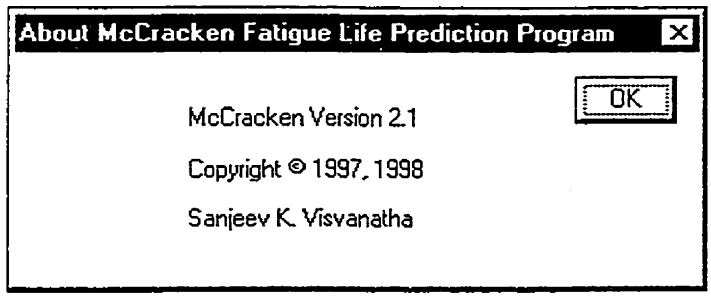

1. Cyclic Stress vs. Stress*Strain Curve

Filename extension: .sed

Format of Data File:

Line Number	Required Data
1	n
2	X_1,Y_1
3	X_2,Y_2
etc.	etc.
n	$X_{(n-1)}$,$Y_{(n-1)}$
n+1	X_n,Y_n

Notation:

Symbol	Definition
n	Number of data pairs (integer)
X_n	Stress*Strain at index "n"
Y_n	Stress at index "n"

Order:

Data pairs arranged in order of increasing values of Stress*Strain, i.e. increasing X_n.

Example of Data File:

12
0,0
0.16,40
0.273,49.8
0.357,54.9
0.454,58.9
0.549,61.3
0.754,64.1
1.08,67
1.42,69.1
1.99,71.1
2.5899,72
4.5999,72.1

2. Strain-Life Curve

Filename extension: .end

Format of Data File:

Line Number	Required Data
1	n
2	X_1, Y_1
3	X_2, Y_2
etc.	etc.
n	$X_{(n-1)}, Y_{(n-1)}$
n+1	X_n, Y_n

Notation:

Symbol	Definition
n	Number of data pairs (integer)
X_n	Strain Amplitude at index "n"
Y_n	Life at index "n"

Order:

Data pairs arranged in order of increasing values of Strain Amplitude, i.e. increasing X_n.

Example of Data File:

11
0.00204,9.00E+05
0.00265,2.55E+05
0.0033,8.55E+04
0.0041,2.34E+04
0.0047,9.10E+03
0.0062,2.30E+03
0.0084,7.80E+02
0.0123,2.52E+02
0.0188,9.00E+01
0.0325,3.00E+01
0.056,1.00E+01

3. Spectrum File

Filename extension: .trunc

Format of Spectrum File:

Line Number	Required Data					
1	A_1	B_1	C_1	D_1	E_1	F_1
2	A_2	B_2	C_2	D_2	E_2	F_2
3	A_3	B_3	C_3	D_3	E_3	F_3
etc.						

Notation:

Symbol	Definition
A	Spectrum flight reference number
B	Blank
C	Gauge strain (με)
D	Nominal weight off wheels occurrence time
E	Angle of attack
F	Dynamic pressure

Column Alignment:

The columns start at the following locations:

Column	Spaces occupied (from leftmost position)
A	1-5
B	6-12
C	13-23
D	24-34
E	35-42
F	43-50

Example of Spectrum File:

```
80152          738.00   1662.75     4.7   125.0
80152          279.00   3190.65     4.9   280.0
80152          689.00   3200.65     9.1   257.0
80152          213.00   3292.25     3.5   375.0
80152          640.00   3297.55     6.0   371.0

                etc.
```

4. Results File

Filename extension: .res

Format of Results File:

Line Number	Information Displayed	
1-9	Load Spectrum --- Load Spectrum File = Reference Strain = Turning Points = Flight Hours per Block = Kt =	
10-17	Material --- Cyclic Stress-Strain Data = Strain-Life Data = Modulus of Elasticity = Cyclic Proportional Limit =	
18-22	Elapsed Time --- Elapsed Time (total seconds) =	
23-27	Kt*DLS vs Life --- Life Kt*DLS	
28	Life(1)	Kt*DLS(1)
etc.	etc.	etc.
28 + n	Life(n)	Kt*DLS(n)

Notation:

Symbol	Definition
n	Total number of K_t*DLS values for which life predictions were made
Life(n)	Life prediction for index "n"
K_t*DLS(n)	K_t*DLS for index "n"

Order:

K_t*DLS vs. Life data is arranged in order of decreasing K_t*DLS. The first data pair will be for the coupon DLS.

4. Results File - continued

Example of Results File:

```
Load Spectrum
-------------

Load Spectrum File = C:\McCracken\Load Spectrums\wflug_mean00000500.trunc
Reference Strain = 2083.000000
Turning Points = 33682
Flight Hours per Block = 326.000000
Kt = 1.390000

Material
--------

Cyclic Stress-Strain Data = C:\McCracken\Material\Aluminum from CI89 - NP.sed
Strain-Life Data = C:\McCracken\Material\Aluminum from CI89 - P.end
Modulus of Elasticity = 10000.000000
Cyclic Proportional Limit = 40.000000

Elapsed Time
------------

Elapsed Time (total seconds) = 65.000000

Kt*DLS vs Life
--------------

Life
Kt*DLS
14499.300363    57.685000
3088.743874     100.000000
4263.657052     90.000000
5650.064118     80.000000
7850.674271     70.000000
12622.446882    60.000000
24444.551408    50.000000
56113.146576    40.000000
```

IMAGE EVALUATION
TEST TARGET (QA–3)

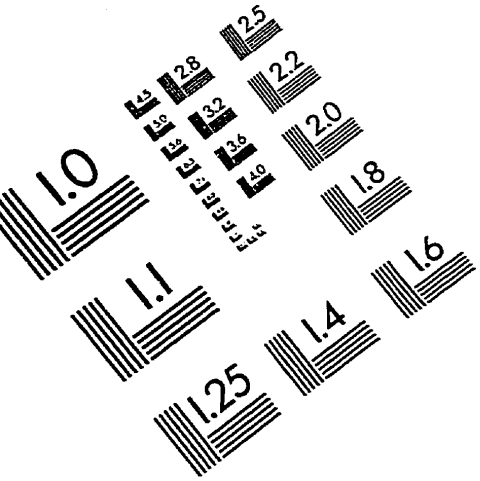

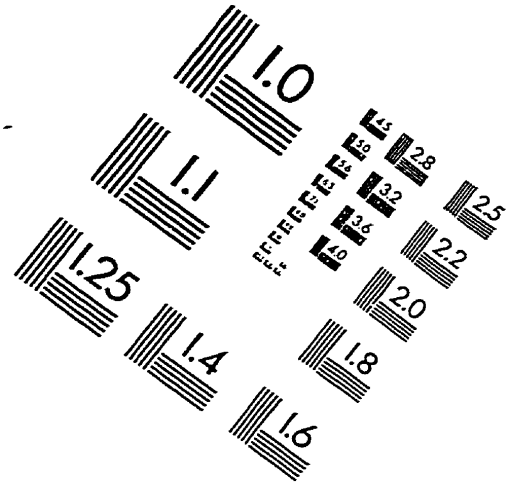

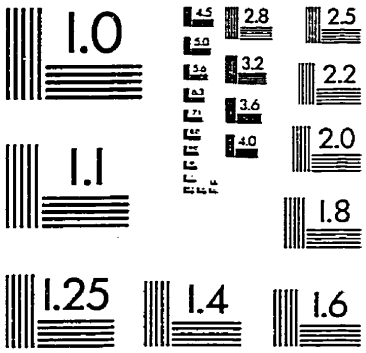

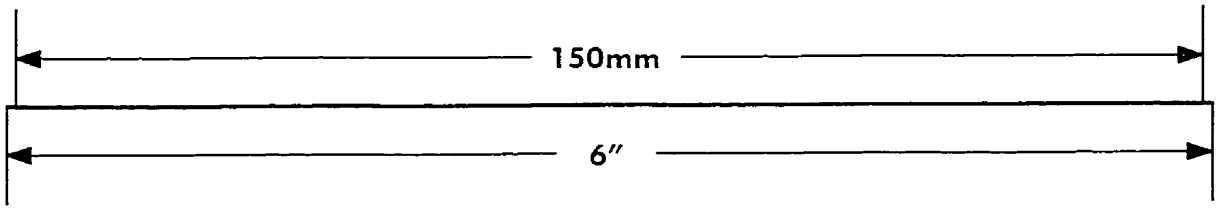

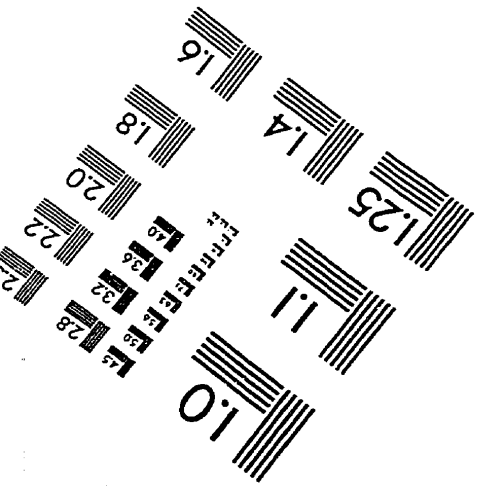

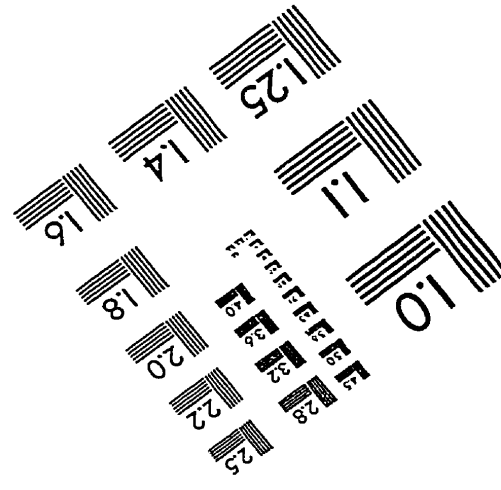

APPLIED IMAGE, Inc
1653 East Main Street
Rochester, NY 14609 USA
Phone: 716/482-0300
Fax: 716/288-5989